

University of Naples Federico II



**Ph.D. Program in
Biomorphological and Surgical Sciences**

XXXIII Cycle
(Years 2018-2021)

Program Coordinator: Prof. Alberto Cuocolo

Ph.D. Thesis

**Integrated Methodologies and Technologies
for the Design of Advanced Biomedical Devices**

Tutor

Prof. Giovanni Improta
Prof. Massimo Martorelli

Ph.D. Student

Dr. Ida Papallo

Contents

Chapter 1: Additive manufacturing and reverse engineering: current trends and future challenges in the design of biomedical devices	1
1.1. Introduction	5
1.2. Additive manufacturing processes: classification	15
1.3. Design for Additive Manufacturing: basic concepts	
1.4. An introduction to the STL file format	21
1.5. Biomedical Applications	23
1.6. The reverse engineering approach in biomedical field	36
1.7. Future challenges in biomedical field	44
1.8. References	44
Chapter 2: An integrated design of 3D additively manufactured hybrid structures for cranioplasty	57
2.1. Introduction	57
2.2. Materials and Methods	61
2.3. Results and Discussion	67
2.4. Conclusions	75
2.5. References	76
Chapter 3: An approach towards the design of technical solutions in skull base reconstruction after endoscopic endonasal surgery	84
3.1. Introduction	84
3.2. Materials and Methods	85
3.3. Results and Discussion	87
3.4. Conclusions	94
3.5. References	94
Chapter 4: Design strategies for the development of customized prosthetic devices with tailored properties for skull base reconstruction after extended endoscopic endonasal surgery	100
4.1. Introduction	100
4.2. Materials and Methods	100
4.3. Results and Discussion	104
4.4. Conclusions	114
4.5. References	114
Chapter 5: Design of solid-lattice hybrid structures with optimized properties for biomedical applications	116
5.1. Introduction	116
5.2. Materials and Methods	117
5.3. Results and Discussion	119
5.4. Conclusions	125
5.5. References	126

Chapter 1

Additive manufacturing and reverse engineering: current trends and future challenges in the design of biomedical devices

1.1. Introduction

Over the past years, additive manufacturing has emerged as a cost-effective and on-demand modality for the development of geometrically complex objects [1].

The ability to design and to print virtually any object shape using a wide range of materials, such as polymers, metals, ceramics and bioinks, has allowed the possibility to adopt such technology for biomedical applications in research and clinical settings [1].

Current advances in tissue engineering, therapeutic delivery, fabrication of medical devices and operative management planning ensure that additive manufacturing will continue to play an increasingly important role in the future of healthcare [1].

Traditional manufacturing consists of formative (molds) or subtractive (machining) techniques which require multiple steps and costly infrastructure, thus limiting capability for timely implementation of potential modifications to the final product [2]. In addition, these traditional fabrication methods do not allow for complex geometries that are generally required in biomedical applications [1,2].

Over the past four decades, 3D printing, or additive manufacturing, has emerged as a robust tool for the development of devices with complex geometries in a cost-effective and timely manner [1–4].

Developed in the 1980s, the basic concept of 3D printing involves a layer-by-layer material deposition in the three-dimensional space through a computer-generated model [1,5].

Such approach allows for the development of complex designs that would be very difficult or impossible to produce using conventional manufacturing methods [1,2].

The role of additive manufacturing is becoming increasingly important in healthcare, with a special focus on therapeutic delivery [1,6-8], surgical planning [1,9], implant design [1,10] and tissue engineering [1,11-13].

Since the 1980s, several techniques for additive manufacturing have been developed to process different kinds of materials [1].

Currently, there are different techniques for additive manufacturing as outlined by the ISO/ASTM 52900 standard [1,14], and some comparisons among the techniques are summarized in Table 1.1 [1].

Printing Technique	Material	Resolution	Biomedical Applications	Advantage	Disadvantage
Binder Jetting	Sand Metal powder	50–400 μm	Degradable (Fe-based alloys) metallic implants ^[15] . Generally used for hard, mineralized tissues	Low cost, fast, color printing, no support structure needed, large objects	Low strength, requires post-processing, powders pose a respiratory hazard
Directed Energy Deposition	Metal Nylon	250–500 μm	Limited use in medical applications	Fast, composite materials, can patch defects on existing objects	Expensive, slow, low resolution, requires post-process machining
Material Extrusion (FDM ¹)	Hydrogels Thermoplastics Ceramics Bioinks	100–200 μm	Bioprinting of scaffolds for cell culture, tissue and organ development (soft tissues) ^[16] Production of rigid and soft anatomical models for surgical planning	Color, low cost, accessible, composite materials, open source designs	Slow, anisotropy, lower resolution, nozzles impart high shear forces on cells
Material Jetting/Inkjet (MJ ² , DOD ³)	Photopolymer Bioinks	20–100 μm	Bioprinting of scaffolds for cell culture, tissue and organ development (soft tissues)	Good resolution and cell viability	Slow, material waste
Powder Bed Fusion (SLS ⁴ , DMLS ⁵ /SLM ⁶ , EBM ⁷)	Thermoplastics Metal Powder Ceramics	100–200 μm	Metallic implants; dental, craniofacial and orthopedic ^[17] Temporary and degradable rigid implants ^[18]	Strong, fast, no solvents required	Most expensive, medium resolution, post-processing required
Sheet Lamination	Paper Ceramics Metal	~1 mm	Macroscopic anatomical models	Low cost, composite materials, no support structure needed	Slow, lots of material wasted, delamination
Stereolithography (SLA ⁸ , DLP ⁹)	Photopolymer Bio-resin	1.2–200 μm	Bioprinting of scaffolds for cell culture, tissue and organ development, can be used for both soft and hard tissues ^[19]	High resolution, fast, very good cell viability, nozzle free	Raw material toxicity, limited material selection, possible harm to DNA by UV
Spheroid assembly	Bioink Organoids	100–200 μm	Tissue and organ development, soft tissues ^[20]	Biologically active models, scaffold free, freeform fabrication	Fragile raw material, requires subsequent spheroid fusion

¹Fused deposition modelling; ²Material jetting; ³Drop-on-demand; ⁴Selective laser sintering; ⁵Direct metal laser sintering; ⁶Selective laser melting; ⁷Electron beam melting; ⁸Stereolithography; ⁹Digital light processing.

Table 1.1. Additive Manufacturing technologies: materials, resolutions, biomedical applications, advantages and disadvantages [1].

There are some issues related to additive manufacturing technologies (Figure 1.1) [21], especially concerning poor quality, low productivity and uncertainty of the mechanical properties of the final part [21,22].

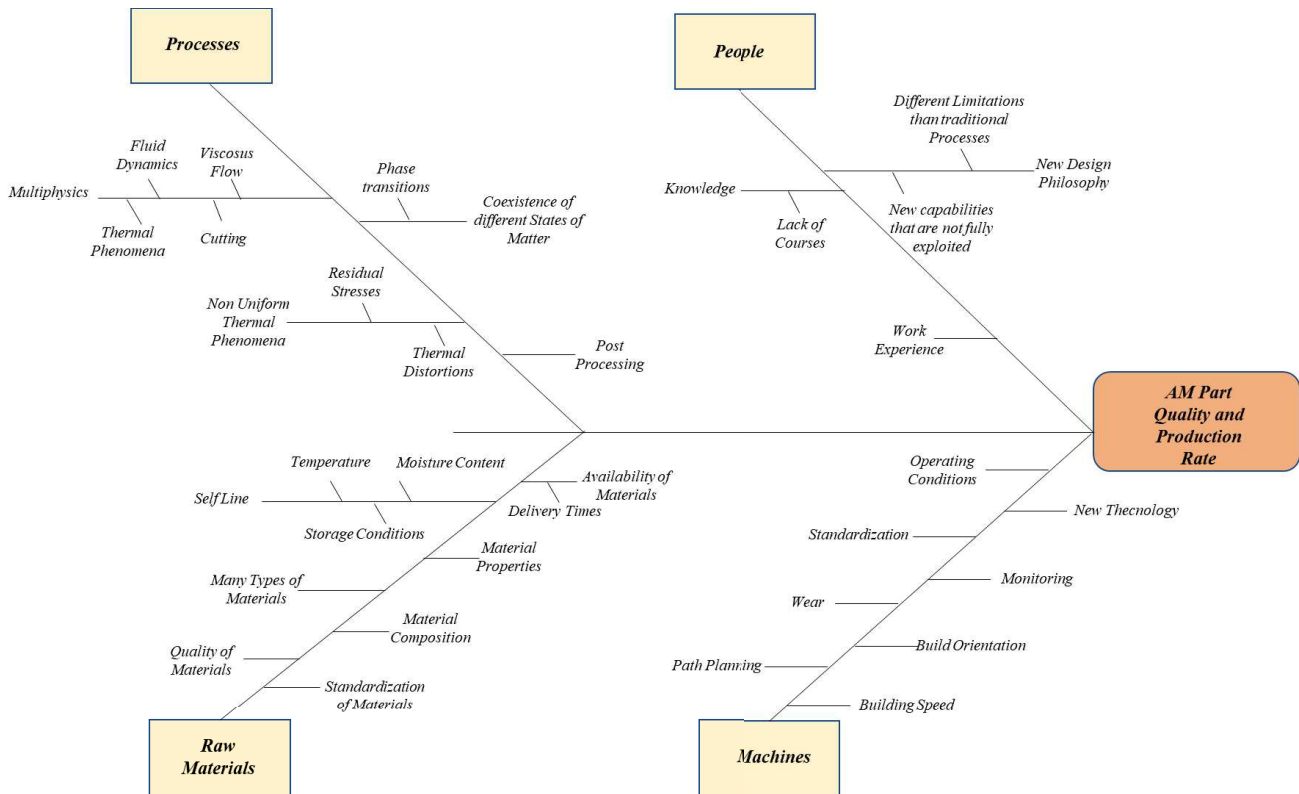


Figure 1.1. Additive manufacturing issues [21].

According to the general principles, process categories and feedstock (ISO 17296-2), a classification [21,23,24] is summarized in Table 1.2 [21].

Additive manufacturing Process Group	Typical commercial names
Vat Photopolymerization	Stereolithography, Digital Light Processing, Solid Group Curing, Projection Stereolithography
Powder Bed Fusion	Electron Beam Melting, Electron Beam Additive Manufacturing, Selective Laser Sintering, Selective Heat Sintering, Direct Metal Laser Sintering, Selective Laser Melting, Laser Beam Melting
Direct Energy Deposition	Laser Metal Deposition, Direct Metal Deposition, Direct Laser Deposition, Laser Engineered Net Shaping, Electron-Beam Freeform Fabrication, Weld-based Additive Manufacturing
Binder Jetting	Powder Bed and inkjet Head, Plaster-based 3D Printing
Material Extrusion	Fused Deposition Modelling, Fused Filament Fabrication
Material Jetting	Multi-Jet Modelling
Sheet Lamination	Laminated Object Manufacturing, Ultrasonic Consolidation

Table 1.2. Additive manufacturing processes: classification [21].

1.2. Additive Manufacturing processes: classification

1.2.1 Vat Photopolymerization processes

The parts produced by Vat Photopolymerization (VP) generally possess high dimensional accuracy and surface finish in comparison to the majority of other additive manufacturing techniques. In addition, the building time represents an advantage of the VP technologies employing mask projection, where an entire part cross section may be projected [21].

However, the use of photopolymers with impact strength and durability which are lower than those of injection molded thermoplastics may be considered the main drawback of the VP technologies [21,25].

Consequently, the main issue of such processes is related to the mechanical properties of the manufactured devices and the process optimization may lead to several improvements in this field [21].

- *Stereolithography*

Stereolithography (SL) was developed by 3D Systems, Inc. This technology was the first and most widely used process of “rapid prototyping”. For this reason, in the past the two terms were employed synonymously [21,45]. It is a liquid-based process in which an ultraviolet laser makes contact with the resin. Thus, the process is based on the curing or solidification of a photosensitive polymer.

The starting point is the creation of a CAD model. Successively, an STL file is generated. The thickness of each layer and the resolution are strongly related to the employed equipment. A platform is built to anchor the piece and supporting the overhanging structures [45]. Then the application of UV laser to the resin allows for the solidification of specific locations of each layer. Once the layer is finished the platform is lowered. When the process is done, the excess of material may be removed and reused [45-48]. A further version of this process (microstereolithography) has also been developed with a higher resolution. A layer thickness of less than 10 μm may be obtained using this process [49].

Figure 1.2 [45] reports the basic parts of a stereolithography machine.

The photopolymerization represents the basic principle of such process. It is the process where a liquid monomer or a polymer is converted into a solidified polymer by the application of UV light acting as a catalyst for the reactions (ultraviolet curing). Powders may be also suspended in liquid like ceramics [21,45,50]. With regard to the final piece, many errors may occur as an effect of the stereolithography process. As an example, overcuring is frequent, occurring to overhang parts as there is no fusing with a bottom layer. Scanned line shape is another drawback especially related to the scanning process. Moreover, as the resin generally has a high-viscosity the layer thickness is often variable, thus introducing an error in the border position control [45]. Another error may be due to the fact that the part could require a surface finished process which is normally done by hand [45,51]. Such errors may be clearly minimized benefiting from an equipment of high quality. It is also possible to use different kinds of materials during the building process (multiple material stereolithography).

In order to process different kinds of materials, the employed resin should be completely drained and replaced with another material once the process reaches the layer where the change has to take place. A scheduling process must be suitably specified in the software [45,52].

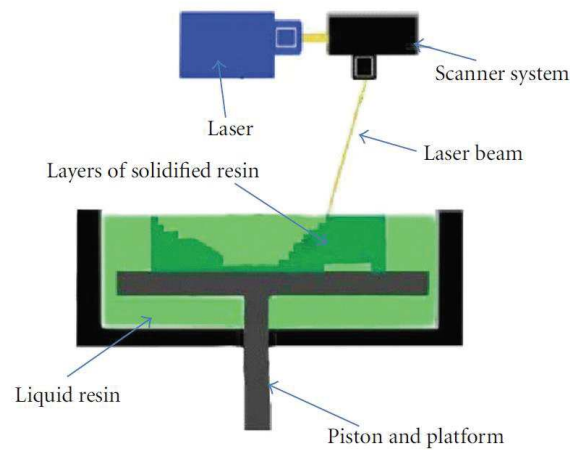


Figure 1.2. A schematic representation of stereolithography [45].

1.2.2 Powder bed fusion

Four different fusion mechanisms are reported for the powder bed fusion (PBF) process group. In brief, the powder particles are fused together using solid-state sintering, chemically induced sintering, liquid-phase sintering or full melting [21,26,27]. Basically, the PBF processes may be divided into three subcategories with the aim to address the difference in the process mechanism (i.e., sintering and full melting), which are employed by the most commercially available machines, as well as the difference in terms of the energy source (i.e., laser or electron beam).

The selective laser sintering (SLS), selective laser melting (SLM) and electron beam melting (EBM) process groups are the three PBF subcategories reported in the literature [21].

The high residual stresses related to the PBF additive manufacturing processes, especially in the case of metal manufacturing, lead to the part warping. Accordingly, in order to minimize this effect, some strategies, involving the use of internal cooling channels, an appropriate selection of the part orientation and the location of the supports, must be considered [21].

Moreover, the effects of the thermal history of the part (i.e., residual stresses, thermal distortions) must also be taken into consideration [21].

The optimization of the PBF processes has to take into account the modelling of thermal and thermo-mechanical phenomena. In particular, the possibility to combine the laser power, spot size and scan speed play a crucial role in the determination of the fusion depth, whilst the melt pool dimensions directly influence the residual stresses of the parts [21]. The laser absorption characteristics, powder bed density and powder bed thermal conductivity are strongly influenced by powder shape, size and distribution [21]. As consequence, it is important to consider such parameters. In addition, the bed temperature and the selection of the laser power play a fundamental role in the dimensional accuracy, shrinkage, density and curling of the manufactured device, as well as in the recyclability of the unused powder. Thus, all the above parameters must be taken into account in the thermal modelling of PBF processes [21,25]. The different subcategories of the PBF family are briefly described below.

PBF family comprises distinct additive manufacturing techniques such as SLM, SLS and EBM [75]. In SLS the laser fuses the powder material, in SLM a high power-density laser melts the powder, whereas EBM process needs maintenance of vacuum in processing chamber to develop FGM components [52-75]. A schematic representation of EBM method is shown in Figure 1.3 [75].

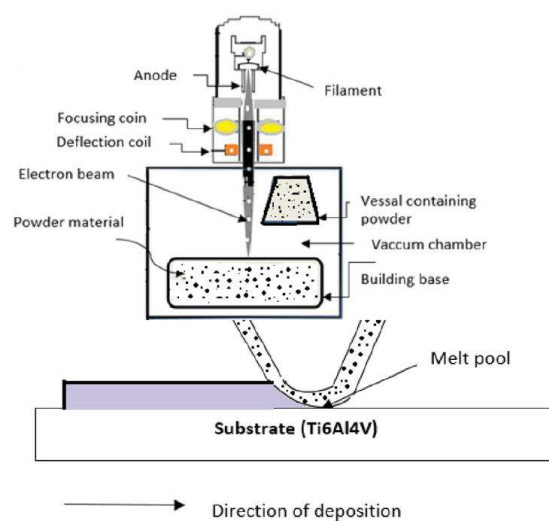


Figure 1.3. A schematic representation of EBM process [75].

In this scenario, surface roughness, mechanical properties, chemical composition and microstructure of Ti alloy implant manufactured by SLS technique were also studied [21,75]. As an example, the obtained results demonstrated that this technology represents an effective process for manufacturing dental implants with functionally graded materials, exhibiting interesting characteristics which are close to those of natural bone. SLS technique has been also used to develop functionally graded scaffolds with improved properties [21,75].

- *Selective laser sintering*

Many studies have been focused on the modelling of the SLS process [21]. Mechanical properties and microstructure have been properly modelled using a numerical approach [21,28,31,32] and an empirical one [3]. According to a previous study [34], the laser power, laser scan speed and laser scan spacing affect the microstructure, physical and mechanical properties of the parts manufactured by SLS. Such parameters are directly related to the amount of energy on the powder surface of the manufactured part [21].

SLS is a three-dimensional printing process in which a laser beam is employed to sinter the powdered material. The chamber is heated to almost the melting point of the material. The powder is fused at a specific location for each layer [45].

The particles lie loosely in a bed. The bed is controlled by a piston, which is lowered the same amount of the layer thickness each time a layer is finished [21,45]. A wide range of materials may be processed, involving polymers, metals, combination of metals, combinations of polymers and metals, and combinations of ceramics and metals [21, 45,49, 55,56]. With regard to polymers, acrylic styrene and polyamide (nylon) are used, also showing almost the same mechanical properties as the injected parts [45,55,57]. Polymer-based composites may be also used (e.g., fiberglass reinforced polyamide). They may be also reinforced with metals such as copper. Concerning the use of metals, a binder is necessary. It may be a polymer binder, which may be later removed by heating or a mix of metals with great differences in terms of melting point [45,55, 57, 58]. Parts of alumina with high mechanical

strength may be built using polyvinyl alcohol as an organic binder [45,47]. The great advantage of this technological approach consists in the wide range of materials that can be processed. The unused powder may be suitably recycled.

Among the disadvantages, it is worth noting that the size of the material particles limits the accuracy, the oxidation must be avoided by performing the process in an inert gas atmosphere and the process has to occur at a constant temperature, which is near the melting point. Such process is often called direct metal laser sintering [45].

- *Selective laser melting*

SLM is similar to SLS, as they “start” from the same concept, however differing in technical details. With regard to the manufacturing of the part, in the SLM process powder melting occurs instead of sintering [21]. Works on SLM modelling are characterized by a similar distribution to those of the SLS process. In particular, the surface roughness of the obtained devices has been modelled in many studies [21,35,36] using analytical and numerical approaches. In further investigations [21,29,30,37–38], topology and dimensional accuracy issues have been modelled using the numerical approach. In a previous study [21,39], the mechanical properties and microstructure have been modelled analytically, whereas in further researches they were numerically evaluated [21,36,40].

- *Electron beam melting*

EBM or EBAM (Electron beam additive manufacturing) present several advantages such high energy efficiency, moderate operation cost, high scan speed [21]. Anyway, great efforts have been put to improve the process stability, part defects and quality variations [21,41].

EBM is similar to SLS. Even though it is a relatively new process, it is growing rapidly [45].

In this process, an electron laser beam powered by a high voltage (e.g., 30 - 60 kV) melts the powder [21,45].

The process occurs in a high vacuum chamber avoiding the oxidation issues as it is employed for manufacturing metal parts. EBM may also process a wide range of metals [45].

A further use of this technological approach can be the manufacturing in outer space [45,59,60], as the process is all performed in a high vacuum chamber [45].

1.2.3 Directed energy deposition

The directed energy deposition processes (DED) is characterized by a simultaneous material deposition and melting [21]. In particular, a focused thermal energy is used to melt a substrate, which is heated by the power source (i.e., mainly laser beam), while there is a simultaneous deposition of material which is also melted [21,25]. The material may be in the form of wire or powder. Most of the DED machines possess a great flexibility in terms of selection of the process parameters, and the effects on many of them are strongly interrelated (e.g., beam power, traverse speed, and powder feed rate). Furthermore, they clearly affect the melt pool characteristics as well as the thermal history determining the residual stresses, the warping and the surface roughness of the manufactured parts [21,25]. In addition, it has been demonstrated how the droplet kinematics plays a fundamental role in the process. The above reported concepts clearly stress the importance of modelling the thermal history, especially focusing on laser power, scanning speed and melt pool characteristics [21]. Many studies can be considered for the optimization of the process parameters, with the aim to minimize the need of expensive and time consuming experimental trial-and-error approaches [21]. Another important feature is represented by the thermo-mechanical effects and the fluid dynamics [21].

- Laser Engineered Net Shaping

In the laser engineered net shaping, a device is manufactured by melting metal powder which is injected into a specific location. A high-powered laser beam is employed in this process [45]. The material is cooled down, thus solidifying. The process is carried out in a closed chamber with an argon atmosphere [45].

Such technological approach allows the use of a wide range of metals and their combination (e.g., stainless steel, nickel based alloys, titanium-6 aluminium-4 vanadium, tooling steel, copper alloys). Alumina can be also employed [45]. This process can be used to repair parts that by other technological approaches is impossible or more expensive to do. The residual stresses by uneven heating and cooling processes may represent a drawback playing a significant role in high precision processes like the repair of turbine blades [45,47, 49, 61–62].

Figure 1.4 [45] reports a schematic representation of the laser engineered net shaping.

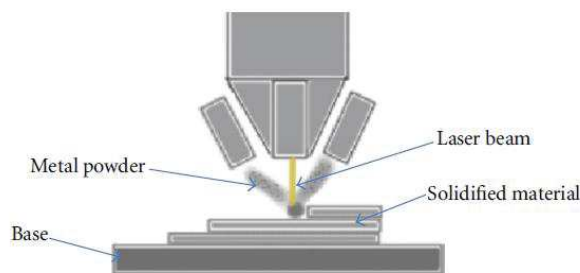


Figure 1.4. A schematic representation of the laser engineered net shaping [45].

1.2.4 Binder jetting

Devices manufactured by binder jetting (BJ), with plaster-based powder and water-based binder processes, generally possess low stiffness and strength. The use of “infiltrants” may overcome this drawback, improving the material properties [21].

A further strategy involves the use of a poly-methyl methacrylate powder and a liquid binder which causes a curing reaction, at room temperature [21]. In this case, after the printing process has been completed, the part must remain in the build chamber for some hours, the aim being to complete the curing process. A series of post processes is required for parts manufactured by BJ. In general, furnace cycles are needed after the printing of a metal part, allowing for the removal of the binder polymer and the increase of the density [21]. Extra metal ingots can be added to achieve this goal. The surface roughness and dimensional accuracy of the manufactured parts must be improved, as they generally possess poorer accuracies and surface finishes in comparison to those fabricated by

material jetting process [21,25]. These problems may be ascribed to the inherent characteristics of the process. Anyway, modelling and process optimization strategies may lead to the improvement of these issues [21].

1.2.5 Material extrusion

Fused deposition modelling (FDM) is the commercial name of the material extrusion process. Many issues related to the quality of the manufactured parts have been frequently analyzed. The distortions of the part are determined by the cooling process profile and, consequently, the material warping may be the effect of a nonlinear cooling. In addition, the development of porous devices is possible and it is also related to the cooling profile [21].

The major role is played by the differences in temperature among the building platform, chamber and the different layers of the device. The success of the bonding between the filament and the layer on which it is deposited and, hence, the mechanical properties of the manufactured device are also related to the temperature of the extruder [21,11]. A further important issue is the anisotropy of the material properties of the parts. This can be ascribed to the crisscrossing manner employed by the material extruder during the filament deposition process [21,44].

- *Fused Deposition Modeling*

In the fused deposition modeling (FDM) a thin filament of a thermoplastic material feeds a machine where a print head can melt and extrude it. The great advantage of the FDM is represented by the potential to process a wide range of materials such as polycarbonate (PC), acrylonitrile butadiene styrene (ABS), polyphenylsulfone (PPSF), PC-ABS blends, PC-ISO as a medical grade PC [45], and in general thermoplastic polymers and micro/nanocomposite materials with a thermoplastic matrix. Further advantages of this process include no resins to cure, no chemical post-processing required, less expensive machine, and materials resulting in a more cost effective process [45-47]. Among the disadvantages, it is worth remembering that the resolution on the z axis is low in comparison to other

additive manufacturing process. Thus, if a smooth surface is required for a specific application, a finishing process is needed. The process may be often slow, especially when large and complex devices must be built [45]. A fully dense mode and a sparse mode may be considered to save time, however reducing the mechanical properties [45,54].

The potential to process a wide range of materials, lower machine and equipment cost, ease to use, durable and inexpensive raw material represent the merits [63-75]. On the other hand, the quality of printed devices and their mechanical strength are lower than those manufactured by SLA or SLS. These represent the major drawback of this technology [75-89]. A schematic representation of FDM technique is shown in Figure 1.5 [75]. Such technological approach is one of the additive manufacturing process employed for the fabrication of FGMs. In this technique the material is heated, injected through a nozzle tip and deposited on a base in layers to fabricate the desired component [75].

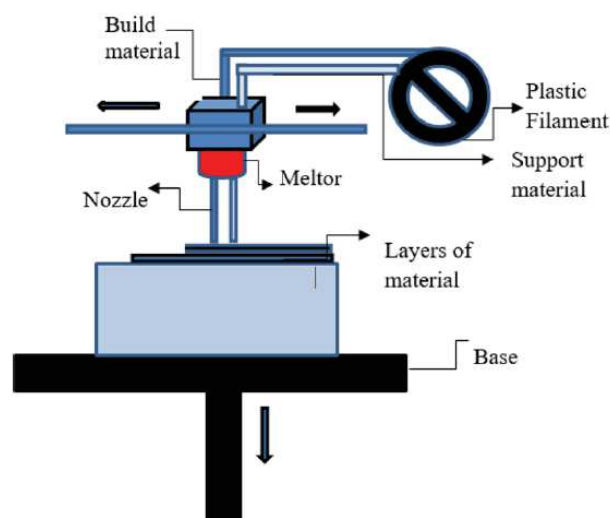


Figure 1.5. A schematic representation of FDM process [75].

1.2.6 Material jetting

There are some technical problems related to material jetting. Droplet velocity and size represent the most important factors as they play a crucial role in the deposition characteristics [21]. Furthermore, the satellite droplets breaking off from the main droplet are characterized by not well defined

boundaries [21,42], along with the droplet splashing on impact, and have to be limited in order to improve the quality of the parts fabricated by material jetting [21,43].

For this reason, the process temperature and fluid dynamics have to be properly considered in the optimization of the material jetting process.

1.3. Design for Additive Manufacturing: basic concepts

Several materials, digital and CAD/CAM technologies have been employed in different applications [90-137]. Design for additive manufacturing (DfAM) is a term derived from the term design for manufacturing (DfM), which represents the process of designing a part or a product for easy manufacturing [138]. DfAM refers to a category specialized in components fabricated using additive manufacturing techniques. In comparison to other manufacturing technologies [138], additive manufacturing is characterized by relatively few fabrication constraints, allowing for a more optimization driven design process [138]. System design, part design and process design may be considered three important categories in the field of DfAM research [138].

If compared to existing categorizations, the above reported categories are mainly focused on the design process, also dividing up the research based on how and when the research could be useful for an engineer designing a product or component for additive manufacturing [138].

System design research is focused on what should be fabricated using additive manufacturing and what the component boundaries should look like [138].

Part design research concerns on how a single part should best be designed, and such category is considered the most important from a geometrical perspective [138].

Process design research focuses on how design and other preparations of the device for the fabrication process are best performed. This category involves steps necessary for the design work without including the manufacturing itself [138].

The above reported categories may be seen as chronological steps where the formulations of goals is reported for each step. Anyway, even though the process design step is the last step, the system and

part design categories involve several process-specific details and, hence, process features must not be completely left to the end of the design process [138].

A classification of the major research categories in DfAM is shown in Figure 1.6.

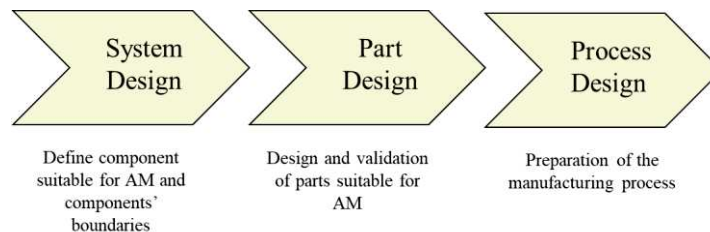


Figure 1.6. Major research categories in DfAM [138].

The reported classification is strongly related to the DfAM process where several activities are connected to each other, the aim being to develop a standardized process. Different design methods for additive manufacturing are reported in the literature and are extensive to a greater or lesser extent [138].

1.3.1 System design

As previously reported, system design is focused on the overview of a component trying to identify when additive manufacturing results an appropriate manufacturing method, what the part boundaries within a device and connecting to other components should look like, and which requirements are considered for the parts [138].

- Selection of components for additive manufacturing

The aim of this step is to define which components would in some sense gain from being fabricated using additive manufacturing. In this context, an identification of the suitable components was proposed by Klahn et al. [138,139]:

- 1- components where additive manufacturing technologies would bring benefits;
- 2- components where additive manufacturing technologies could bring benefit even if risks and expectations must be further evaluated;
- 3- components where no benefits of using additive manufacturing technologies are expected;
- 4- components where additive manufacturing technologies could not be used as a fabrication method.

To support the decision-making process concerning which products or components should be fabricated using additive manufacturing, four points where such advanced technologies provide possibilities to add value to the product in comparison to traditional manufacturing methods can be reported [138]. The integrated design is the first point, where the attention is focused on the reduction of the number of parts in the system. The second point is the availability to individualize products or components. The third point is related to the fact that the manufacturing method allows for a lightweight design, if compared to conventional manufacturing techniques. The fourth point is the potential to develop more efficient designs, taking into account that a more complex part is not more expensive to fabricate than a simple part [138,139].

- *Definition of design problem*

When the identification of a suitable component is done where one or more parts can be fabricated using additive manufacturing, the identification of the boundaries between the different parts is needed [138]. This involves the definition of the interfaces with other components, etc. Additive manufacturing allows for a more integrated design also reducing the number of components in a system, when compared to conventional manufacturing techniques. Rodrigue and Rivette [138,140] developed a methodology for the reduction of the number of parts in an assembly process, the aim being to add value for products when fabricated using additive manufacturing [138].

The method consists of nine steps [138]:

- 1 - Concept design;
- 2 - Concept assembly;
- 3 - Determination of candidates in the assembly that could be eliminated;
- 4 - Determination of the acceptability of the new design;
- 5 - Development of new design alternatives with the reduced assembly;
- 6 - Determination of functions and characteristics which could be optimized;
- 7 - Optimization of the functions;
- 8 - Optimization of the characteristics;
- 9 – Material selection for the parts in the reduced assembly.

- *Definition of material and constraints*

The aim of the current step is the identification of constraints and requirements for the part to be fabricated. With regard to this step, the same methods for analyzing the design problem may be employed as in ordinary design problems. The selection of material and hard fabrication constraints links this step to the additive manufacturing [138]. This is related to the additive manufacturing method as well as to which machine may be eventually employed for the fabrication of the component. The constraints for additive manufacturing depend on the selected method [138]. The maximum build size represents one general hard constraint as it is fixed for each machine. Some additive manufacturing techniques (e.g., direct energy deposition) do not present such build size problem, whereas other additive manufacturing technologies (e.g. powder bed fusion) are characterized by an extremely strict build size [138].

1.3.2 Part design

- *Initial design: creation*

The goal of the initial design is the definition of an idea of what the part should look like. Several methods may be used according to the considered part and the identified requirements. Topology

optimization (TO) is a method often employed in the case of structural components and represents an efficient methodology to create a design which is also optimal for structural applications [138].

Recently, many efforts have been devoted to the development of novel TO formulations, also including different kinds of additive manufacturing constraints. Benefiting from the employed algorithms, it results possible to directly use the TO design for additive manufacturing or to develop a design which does not require as much redesign between the manufacturing and TO [138].

Anyway, in this context the research is mainly focused on different formulations related to the optimization problems [138].

- *Initial design: interpretation*

The interpretation and adaption strategies are fundamental to understand the manufacturability of the initial design using additive manufacturing techniques. In this scenario, the attention must be focused on design rules and potential limitations [138].

The design rules are clearly related to the additive manufacturing technique, the selected material, the kind of machine and the settings for the employed machine.

This is a very complex area characterized by a lot of on going research [138]. With regard to the creation of the best design for additive manufacturing, restrictions and features that result impossible using other fabrication methods have to be considered. One feature is represented by lattice, cellular or grid structures reducing the weight of the device, however preserving good mechanical performances [138]. Using conventional fabrication methods, it is difficult to develop these structures integrated in components, whilst it results possible when using additive manufacturing techniques. As reported in the literature, lattice structures may be divided into three categories: periodic, disordered and pseudo-periodic [138]. The periodic structures show a standard cell which is evenly distributed over the design, whereas the disordered ones are randomly distributed structures spread over a design. The pseudo-periodic structures are based on a standard cell which is adapted to the design shape [138]. The periodic and pseudo-periodic lattice structures may be homogeneous and

heterogeneous. Concerning the homogeneous structures, the standard cells possess the same size everywhere in the design. In heterogeneous structures the standard cell may vary in size [138].

Two approaches for designing lattice structures are reported in the literature [138,141]. A first approach is based on a parametric optimization; in this case, a standard cell density is optimized by means of a parametric optimization [138]. A second approach involves a variable density topology optimization to design a lattice. The parametric design optimization may combine a CAD model with a finite element (FE) model. A method for the development of lattice structures from TO is also reported by Robbins et al., 2016 [138,142]. This method employs several strategies of topology optimization using different densities which, in the final step, involve graded density lattice structures. Many technical problems and challenges using additively manufactured lattice structures are described by Wang et al. (2013) [138,143]. These studies also stress the fact that the relatively rough surfaces of additively manufactured components have a great impact on thin lattice structures and the removal of unused powder from the structure, especially if powder bed fusion technologies are employed. With regard to laser methods, the removal of powder is easier in comparison to that of pre-sintered powder from electron beam manufacturing [138]. A further problem in the combination of lattice structures with additive manufacturing is represented by the small and many surfaces occurring within the lattice structure. These features are obviously difficult to represent with the STL file format due to the small scale of the lattice structure. Furthermore, a little error in the data file may significantly affect the structural strength of the design [138].

- *Design verification*

The design verification is similar to the design process related to other fabrication processes. It involves CAE analyses to verify thermal, structural, aerodynamic and further properties [138]. Concerning CAE analyses for additively manufactured parts, the possibility of creating more complex structures and the anisotropic material behaviour have to be considered [138]. The geometry and build direction influence the surface roughness of additively manufactured parts, making difficult the

simulation from fluid dynamics, thermal and aerodynamic perspectives, which strongly depend on the surface [138]. From a structural point of view, the mechanical properties (i.e., Young’s modulus, yield strength, fatigue strength) of the manufactured parts are fundamental. Such properties clearly depend on the anisotropy and, consequently, are difficult to simulate [138].

1.3.3 Process design

The process design includes the research aiming at describing the design preparation for manufacturing. As reported in the literature [138,144], the process design is divided into three steps: part orientation, slicing scheme and process variable optimization. Different steps such as support generation, path generation and post-processing have also been added into the definition of additive manufacturing process design [138,145]. The choices affect the best design of the component (and the system), and, hence, iterations become necessary [138].

Figure 1.7 shows the steps involved in product development using additive manufacturing [45].

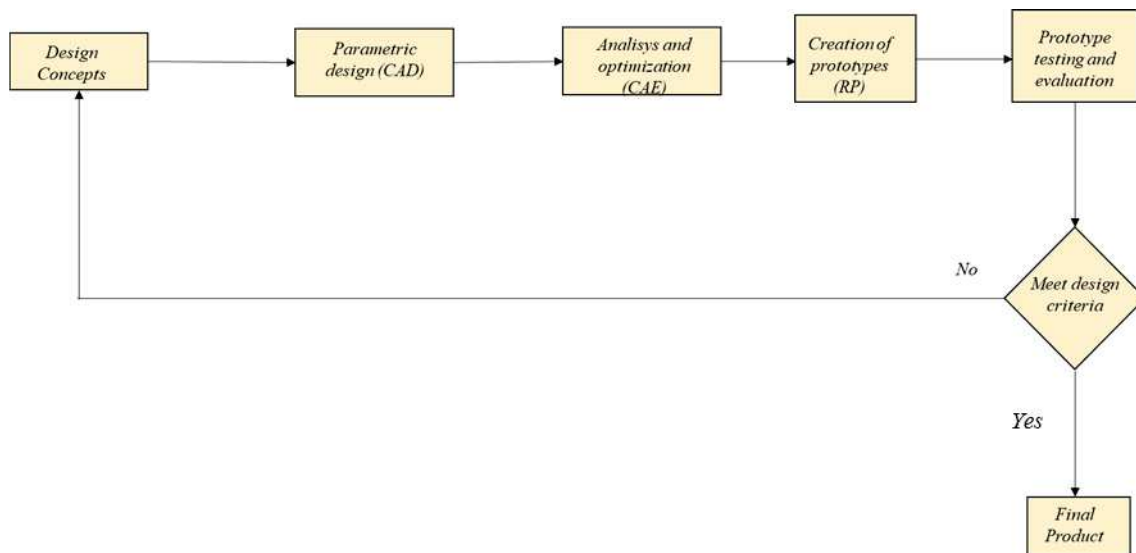


Figure 1.7. Main steps involved in product development cycle [45].

1.4. An introduction to the STL file format

The STL file was created by 3D Systems Inc. First, the stereolithography was developed and the STL file stands for this term. STL is also called Standard Tessellation Language [45].

Even if there are further kinds of files, the STL file represents the standard for every additive manufacturing process [45]. The STL file describes only the surface geometry of a 3D object without any representation of color, texture or further common CAD model attributes.

The continuous geometry in the CAD file can be converted into a header, small triangles, or coordinates triplet list of x, y, and z coordinates and the normal vector to the triangles. Such process is not accurate and the smaller the triangles the closer to reality [45,46,49,53].

The identification of the interior and exterior surfaces may be done using the right-hand rule and the vertices cannot share a point with a line. Further edges are added when the figure is sliced. The slicing process also introduces inaccuracy to the file due to the fact that using the algorithm the continuous contour is replaced by discrete stair steps [45,53]. The strategy employed for a feature having a small radius in relation to the dimension of the part is represented by the creation of separate STL files and their successive combination. This method may be employed to reduce the inaccuracy. The dimension in z direction may be designed with the aim to have a multiple of the value of the layer thickness [51]. Figure 1.8 [45] reports the position of the STL file creation in the data flow of an additive manufacturing process.

The data flow in the STL file creation is reported in Figure 1.9 [45].

Further kinds of files are stereolithography contour (SLC) and SLI from 3D Systems, CLI from EOS, stereolithography contour from Stratasys, Hewlett-Packard graphics language (HPGL) from Hewlett-Packard, and F&S from Fockele and Schwarze and initial graphics exchange specifications (IGES) [45].

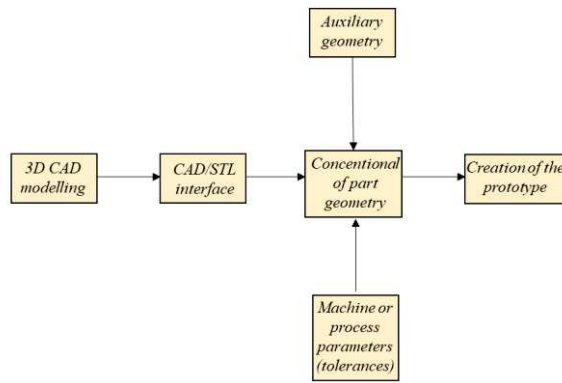


Figure 1.8. Data flow in additive manufacturing [45].

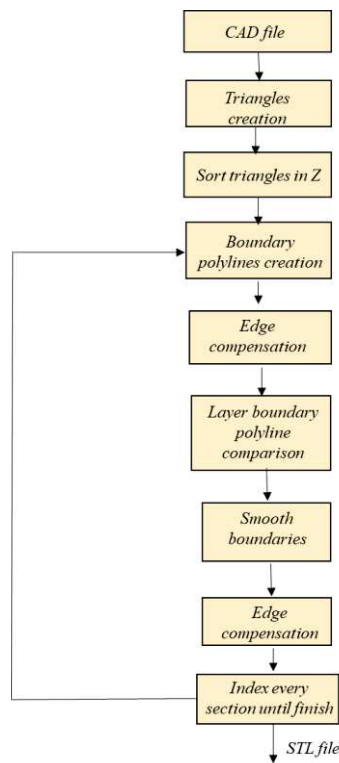


Figure 1.9. Data flow in STL file creation [45].

1.5. Biomedical Applications

Additive manufacturing technologies have a wide range of applications in the biomedical world [45]. They are influencing the practice of medicine by means of the possibilities to make rapid prototypes and high quality bone transplants and models related to damaged bone and tissue defects of the patients for several analyses [45]. 3D printing methods allow to scan and develop physical models of

bone defects from patients, thus providing the possibility to plan surgical procedures and to achieve a better result [45, 64, 65]. Today, customized bone devices can be obtained using additive manufacturing technologies. Taking into account the limitless form or shape of what may be built, doctors may decide to create a porous device with a controlled morphology which is able to promote osteoconductivity or to create a specific metal device depending on the bone to be replaced [45,66]. Characteristics such as pore shape and size, density, and pore interconnectivity result important features that are able to promote tissue ingrowth, also providing appropriate mechanical properties [45]. The mechanical strength of such devices are much higher than others manufactured by other techniques. In addition, this approach may also reduce the possibility of inflammation caused by microdebris which breaks during the procedure [45,63]. Additive manufacturing represents a good tool for dentists as they may easily build a model of the mouth of a patient or to replace the teeth, using stereolithography, selective laser sintering and electron beam melting [45,67–69].

As reported [68], an 83-year-old woman was the first-ever person receiving a transplant jawbone customized for her face using a 3D printer. In this case, the time related to surgery and recovery were less than other patients receiving the same procedure. The shapes of bones strongly vary depending on each person and 3D printing allows for the production of devices which fit better, are secure and may be easily inserted, providing a reduction in terms of the time for the procedure and producing better cosmetic results [45,69, 70].

Stereolithography is also employed to fabricate prosthetic sockets. Such technology may ensure that the form of the socket may adapt better to the patient also being more cost-effective than hand or machined methods. Even though “hard” devices may be produced in the case of bone tissue repair and regeneration, this technological approach also allows to print cells in a 3D array as well as tissues [45]. This technological approach may help patients to recover faster and with a better cosmetic result. Moreover, 3D cell printing technologies may also offer the possibility to print artificial blood vessels which can be employed in the coronary bypass surgery or in other blood vessel procedure or diseases (e.g., cardiovascular defects) [45,71–73].

Thus, the research on “bioprinting organs” will potentially lead to printed organs in the future [74].

Many progresses have been made in 3D printing highlighting the possibility to print biological tissues as well as in the field of molecular electronics [45]. High-resolution processes such as nanolithography and photolithography may also allow to create biochips and biosensors [45,72].

It is well known that additive manufacturing has a great potential in the biomedical sector and is expected to revolutionize healthcare [75]. The biomedical applications of additive manufacturing involves the fabrication of tissues and organs, anatomical models customized prostheses and implants, drug delivery devices in pharmaceutical field [75-77]. The extensive use on additive manufacturing in the biomedical field may be related to many advantages such as customization and personalization of the products, biocompatibility, enhanced productivity, cost effectiveness, accessibility, reduction in production time, easy assembly [75,78]. However, additive manufacturing is still not widely employed in mass production due to low speed [75,79,80]. Anyway, such limitation can be also considered as a merit, since in the biomedical field high precision and customized devices are generally required in less quantity [75]. It is worth remembering that in medicine customized therapies and devices change from one patient to another. For this reason, additive manufacturing technologies are most widely employed in biomedical and clinical applications [75,81,82].

Since many years, researchers have been putting efforts with the aim to map human organs as well as to convert them into 3D virtual designs and to develop novel biocompatible materials [75].

The several steps required for the fabrication of 3D models include image acquisition (i.e., selection of the target area), the evolution of the 3D geometry through medical image processing, material selection and machine for 3D printing of devices, eventual post processing, analysis and final application or implementation (Figure 1.10) [75].

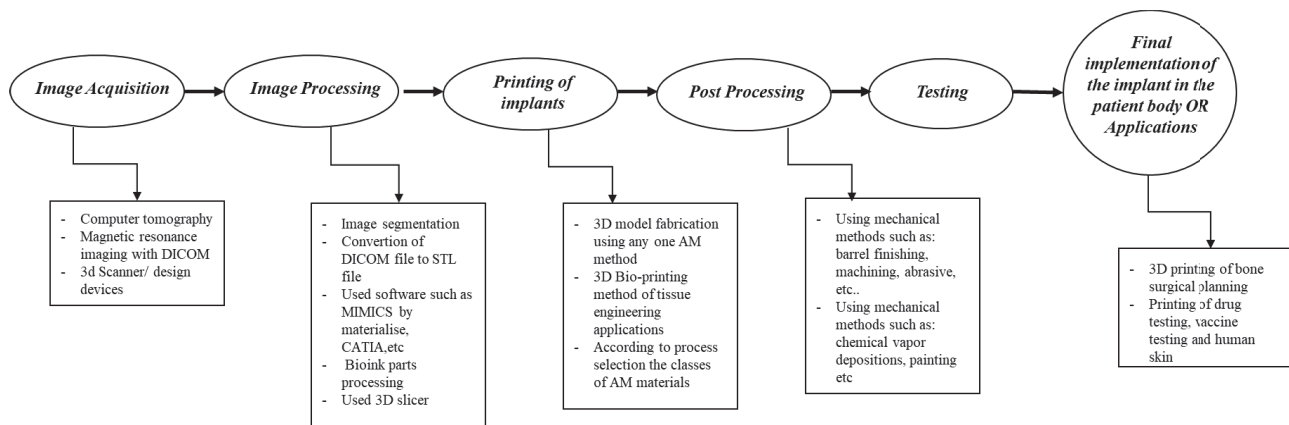


Figure 1.10. Steps involved in the fabrication of 3D biomedical models and devices [75].

The model should help to improve the knowledge and skills of surgeons also leading to a better understanding of diseases, surgical process, costs, application of surgical tools and patient-specific design of implantable devices [83–84]. In the biomedical field, as an example, additive manufacturing technologies are best suited for custom fit mask, new organ development and operation practice [75,85].

1.5.1 Materials, mechanical properties and applications

A wide range of materials may be used for 3D printing in the biomedical field. The selection of material mainly depends on the structural and functional properties required for the final devices (i.e., customized prostheses, prosthetic limbs, surgical tools, scaffolds for tissue engineering) [75]. For generic applications where strength, durability and flexibility represent important features, acrylonitrile butadiene styrene (ABS) and nylon are a good choice [86].

However, polylactic acid (PLA) is a suitable biocompatible and biodegradable polymer in the biomedical field.

An ideal biomaterial must be easy to print, nontoxic and biocompatible, also reproducing living tissues.

Such biomaterials are employed for several biomedical applications [75]. Metals and alloys are used if the application requires high strength devices, such as in the case of orthopedic implants, plates,

screws. Ceramics are appropriate in designing bioactive orthopedic implants. Anyway, polymers are also widely used in the medical field [75,87].

Composite materials are widely considered to develop devices with tailored and improved mechanical properties for biomedical applications. Moreover, the selection of materials for different kinds of biomedical applications strongly depends upon the specific application.

Table 1.3 reports commonly employed materials for different biomedical applications [75].

Type of Metal	Applications
316 L SS; Ti; Ti6Al4V; CoCrMo; Ti6Al4V; Ti6Al7Nb; 316 L SS	Orthopedics: Bone fixation: plate, screw Orthopedics: Artificial joints Otorhinology: Artificial eardrum
Poly glycolic acid (PGA)	Internal fixation, Graft material, Scaffold
Poly lactic glycolic acid (PLGA)	Interference screw, Microspheres & carriers for BMP, Scaffolds, Composite
PolyL-lactic acid (PLLA)	Carrier for BMP, composite with HA, scaffolds
Hydroxyapatite (HA)	Composites, Scaffolds, bone fillers, pastes, coatings, drug delivery
Magnesium (Mg)	Implants, osteosynthesis devices, plates, screws, ligatures, and wires.
Tricalcium Phosphate (TCP)	Bone fillers, injectable pastes, cements
Polycaprolactone (PCL)	Scaffolds and composites with HA fillers
Stainless Steel	Implants, plates, mini-plates, screws, Implants, screws, plates, BMP carriers, orthognathic surgery, mid-facial fracture treatment
Bioglass	Bone defect fillers

Table 1.3. Commonly employed materials for different biomedical applications [75].

Biomimetic materials are also considered in tissue engineering applications. The improvement in the design of scaffolds through conventional method (e.g., salt leaching & phase separation) has been done by many researchers [75].

However, the different process methods such as additive manufacturing, electrospinning etc. have been already employed for the fabrication of 3D biomimetic scaffolds. Consequently, bone tissue engineering plays a crucial role in the treatment of damaged tissues [75]. Some ceramics and

polymers (e.g., polycaprolactone, poly (lactic co-glycolic) acid) are widely employed in bone tissue engineering [75,88-90].

Many researchers experimentally investigated several additive manufacturing techniques using *in vitro* testing for biomedical applications such as medical education, surgical planning etc.

1.5.2 3D printing in biomedical field: applications

Additive manufacturing has a wide range of applications in the biomedical field. Moreover, it is widely used for making 3D reconstructions of skull models, human skull defects, as well as porous Titanium implants manufactured by EBM.

Figure 1.11 reports the application of additive manufacturing printing in the biomedical field [75].

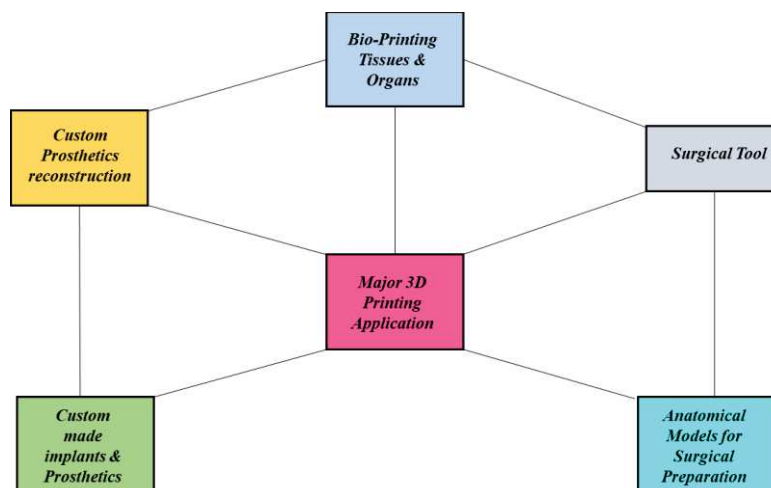


Figure 1.11. Application of additive manufacturing in biomedical field [75].

- *Surgical tools*

Additive manufacturing can be used to develop several dental surgical tools, orthopedic tools and surgical guides [75].

Benefiting from such technological approach, physicians can develop guides which strictly follow the patient's anatomy, also accurately locating surgical instruments. Such devices can be employed in the case of tinny and complex areas along with full safety to patient [75,91].

- *Bioprinting tissues and organs*

Bioprinting is a process involving a computer-guided pipette to layer living cells (bioink), on top of another layer, with the aim to create artificial living tissues [75].

Bioprinting is considered for fulfilling the need of organs and tissues which are suitable for transplantation. Furthermore, such approach is employed for generation and transplantation of some tissues (e.g., heart tissue, cartilaginous structures, bone, tracheal splints, vascular grafts, multilayered skin) [75,92].

These artificial tissue organoids or constructs may be employed in medical research because they reproduce organs on a miniature scale, being economical for transplants of human organs [75].

- *Anatomical models for surgical preparation*

The starting point is the conversion of 2D image (MRI or CT scans) into 3D image. This approach help surgeons in better planning and training [75]. It may be employed to create patient specific implant organ models that surgeons can use to practice on before performing complex surgeries. Anatomical models are widely used in maxillofacial, orthopedic and neurological field [75]. Moreover, such models are widely used for planning treatments in medicine, manufacturing prosthetic devices and assisting diagnosis [75,93].

- *Customized implants and prostheses*

This technological approach is also considered for the development of prosthetic devices that are customized to suit and fit the wearer. The process has been accelerated producing devices able to provide patients the same functionality as produced by traditional techniques.

3D printing is an efficient tool in manufacturing customized implants and prostheses, thus solving many orthopedic problems [75]. The customized devices include maxillofacial, cranial, and orthopedic implants [75,94].

Furthermore, in the biomedical field 3D printing involves several applications: design of scaffolds for tissue regeneration [75,95,96], development of bone replicas [75,97], forensics [75,98], surgical planning [75,99], design of medical instrument [75,100] and design of customized implants [75,101].

- *Tissue engineering*

In order to restore the working of an injured joint, a surgical approach is generally needed [75,102,103].

Several methods (e.g., freeze-drying, gas foaming, electrospinning, emulsification, solvent casting) are usually used to fabricate scaffolds for tissue engineering [75].

As previously reported, the application of 3D printing shows many merits (e.g., low cost, customization and personalization of devices, enhanced collaboration, democratization of design and fabrication). [75,104].

Several kinds of biomaterials are considered to develop scaffolds for tissue using 3D printing technology, and many applications include skin, bone, meniscus, nerve, vascular and cardiovascular tissue [75].

- *Applications in dentistry*

Additive manufacturing is widely employed in dentistry, including maxillofacial and oral surgery, endodontics and orthodontics. Such technology has provided high quality restorations and comfort to dentists [75]. Furthermore, dental restorations and devices fabricated by additive manufacturing should be more robust in production than those manufactured by dental technicians [75].

The different kinds of additive manufacturing techniques (e.g., SLS, FDM) are also used for printing dental pieces and producing bridges, crowns and orthodontic appliances [75,105,106].

Moreover, this may also represents a novel approach helping for surgery simulation/planning, also providing an overview to surgeon before performing the surgery [75,107].

- *Clinical applications in traumatology and orthopedics*

Orthopedics represents a surgical discipline related to biomedical engineering, which is also integrated with orthopedic disciplines (e.g., joint arthroplasty, deformity improvement, trauma surgery). In this scenario, additive manufacturing plays an important role especially for surgeon training, surgical planning, also providing a reduction of the re-operation rate [75]. The main applications in traumatology and orthopedics concern several biomaterials, surgical guides, implants, orthoses [75,108,109].

- *3D printing of biomedical devices*

Commercially available additive manufacturing systems may be divided into different groups. Surgical guides and instruments play a fundamental role in the medical industry [75]. With regard to specific surgical tools such as retractor, hemostats and medical clamps are usually employed and easily manufactured using 3D printing technology [75]. Currently, surgical instruments are generally preferred in dentistry due to high accuracy and customization [75,110,111].

Sports injuries are commonly related to the knee, elbow, and back caused by fascia. Osteoarthritis in knee joint also faced by the old people, and conventional methods are employed for the treatments of such problems [75]. To overcome some drawbacks, a guide may be additively manufactured.

The printing process of ultrasound physiotherapy orthosis may be summarized. As an example, an appropriate device can be employed for scanning of a patient's hand [75]. Successively, the collected data is utilized are used to develop a CAD model. The SLS technology may be employed to manufacture a 3D model. The 3D printed models may consist of two components [75], where the first part may be used for the fixation of the limb and second part for ultrasonic generator. Among the merits of the ultrasound physiotherapy, it is possible to remember restoration, regeneration and anti-inflammatory of nerve fiber. [75,112].

It is well known that additive manufacturing plays an important role in healthcare and further applications include: cardiothoracic surgery [75,113], gastroenterology [75,114], cardiology

[75,115], oral and maxillofacial surgery [75,116], neurosurgery [75,117], orthopedic surgery [75,118], plastic surgery [75,119], otolaryngology [75,120], podiatry [75,121], radiation oncology [75,122], pulmonology [75,123], and vascular surgery [75,124]. Zhang et al. [75,125] designed and fabricated the custom joint prostheses using additive manufacturing, on the basis of the osseous morphological features of resected proximal tibial osteosarcomas.

The custom joint prosthetic reconstruction showed better results for patients with osteosarcoma in the proximal tibia or the proximal tibiofibular joint during limb salvage operations and neoadjuvant chemotherapy [75].

1.5.3 Benefits and challenges of additive manufacturing in biomedical field

Figure 1.12 shows the major benefits of additive manufacturing in the biomedical field [75].

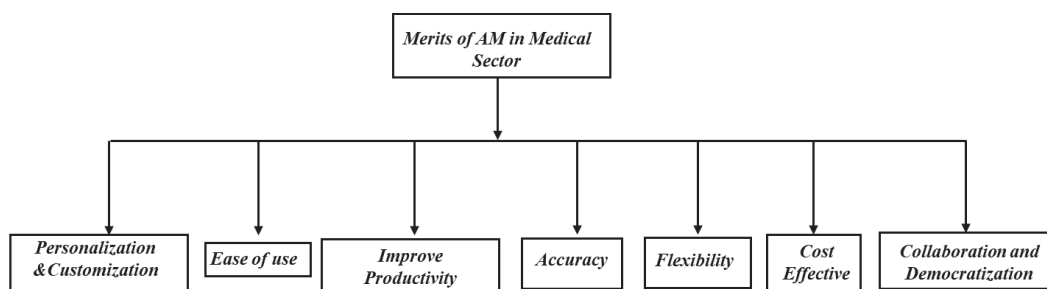


Figure 1.12. Benefits of additive manufacturing in biomedical applications [75].

- Personalization and customization

Personalization means to fulfil the customer’s demand in an efficient and effective manner trying to make the interactions faster and easier, thus providing an increase of the customer-satisfaction [75].

On the other hand, customization refers to the action of modifying something, the aim being to suit/fulfil a specific individual or task.

Customized implants, surgical tools and fixtures clearly influence the time needed for surgery as well as the patient’s recovery time [75,126].

- *Cost effective*

The ability of additive manufacturing technologies to produce product/items economically is well known. The cost of additive manufacturing is less for small dimension devices such as those employed in the case of dental and craniofacial disorders [75]. In addition, it is also possible to print some drug in the dosage form, which may be highly cost effective and easier to deliver to patients [75,126].

- *Improvement in productivity*

Additive manufacturing technology is faster, if compared to conventional fabrication techniques for biomedical devices (e.g., implants, prostheses) which needed milling, forging and a long delivery time [75]. Furthermore, over the past years, speed, resolution and reliability of additive manufacturing technologies have also been improved [75,126].

- *Collaboration and democratization*

As a consequence of the great availability of materials and reduction in the cost, people are increasingly using additive manufacturing machines and their imaginations to develop innovative biomedical devices [75].

- *Accuracy*

Biomedical models fabricated by additive manufacturing technology are characterized by higher accuracy [75,127,128]

- *Flexibility*

Using additive manufacturing technologies, one material may be replaced with another material to enhance the properties of the biomedical devices [75].

- *Ease of use and challenges of additive manufacturing in the biomedical field*

The additively manufactured models are fast and easy to use, as no fixture or tooling is generally needed [75].

The main drawbacks of additive manufacturing technologies in the biomedical field are summarized in Figure 1.13 [75].

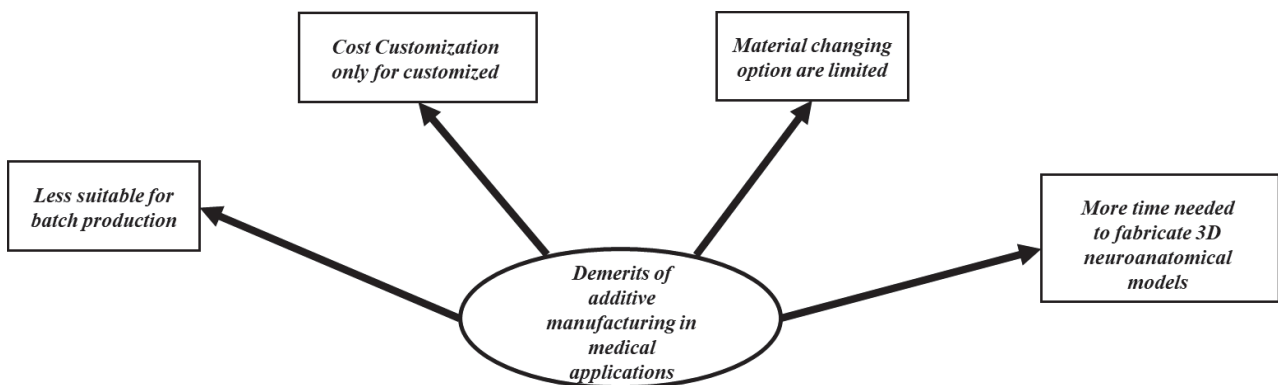


Figure 1.13. Disadvantages of additive manufacturing in biomedical applications [75].

1.5.4 Cost effective in the case of customized parts

Mass customization refers to the ability to develop functional parts which meet the individual customer satisfaction and needs with a reasonable cost [75].

Embedded customization, modular production, and customized product services represent the main steps of mass customization. Mass customization may be considered as a dominant product fabrication strategy [75]. The quick changes are often compulsory to most product manufacturing companies due to a great competition, globalization, rapid technological advances. Additive manufacturing technologies are considered cost effective if the part is produced as per the specific need of customer. Conversely, they are highly expensive and lot of wastage [75]. Customization also provides a help in terms of miniaturization of batch sizes [75,129,130].

1.5.5 Limitation in material changing

Several materials are employed for biomedical applications such as stainless steels, titanium alloys, cobalt alloys, cobalt chrome, titanium etc. The selection of the materials for the fabrication of implants and prostheses is clearly performed focusing on biofunctionality, biocompatibility, corrosion resistance and further functional features. The metallic biomaterials are generally used to replace and to support the parts of the skeleton. Comparing such materials with ceramics and polymers, they exhibit high tensile properties, fracture toughness and fatigue strength [75]. The cobalt alloy are characterized by some attractive properties (e.g., wear resistance, corrosion resistance, heat resistance). Anyway, a limitation of cobalt alloys is related to the difficulties in manufacturing [75,131].

1.5.6 Limitations in neurosurgery

In the neurosurgical field, 3D anatomical models represent a clear drawback in terms of time [75]. To make additive manufacturing machines more appealing and accessible to neurosurgeons, the enhancement in costs, materials, speed and precision are important for CAD software and hardware [75,132].

Furthermore, such technological approach is less appropriate for batch production [75,133], requiring highly skilled person [75,134] and less accurate than other fabrication processes [75,135].

Thus, further research is needed to overcome such drawbacks related to additive manufacturing technologies in the biomedical field.

Figure 1.14 reports the crucial features of smart additive manufacturing technology [75].

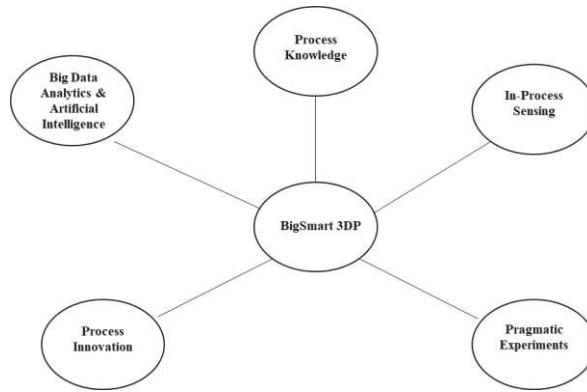


Figure 1.14. Main features of smart additive manufacturing technology [75].

1.6. The reverse engineering approach in biomedical field

Reverse engineering is a process aimed at analyzing an object or system to identify its components and their interrelationships, and to study how it works for redesigning or producing a copy without using the design from which it was originally developed [137]. In the field of geometrical modelling, reverse engineering is used to reconstruct 3D models of an object in several geometrical formats, starting from the available physical models [137]. Taking into account the specific applications and technical requirements related to data processing and accuracy of 3D models to be reconstructed, reverse engineering may be usually divided into 3 groups: (i) industrial reverse engineering, (ii) artistic and architectural reverse engineering, and (iii) medical reverse engineering [137]. Since many years, reverse engineering has been playing a fundamental role in the development of biomedical devices, especially in the design and manufacturing of personalised prostheses, medical training models, surgical tools, orthosis, where data in the form of CT/MRI images and 2D/3D formats are employed for surgical planning [137]. When reverse engineering is considered for biomedical applications and research, it is also called “Medical Reverse Engineering”. In this case, reverse engineering is generally involved in the use of patient data or biomedical objects for the reconstruction of 3D models of anatomical structures and objects which may be interesting for the development of several medical products, as well as for the applications and biomedical research [137]. In addition, the accuracy requirement is strongly related to the specific applications [137]. As

an example, with regard to personalised cranio-maxillofacial implants and training models, the accuracy requirement is usually not high in comparison to the industrial reverse engineering. Concerning the surgical tools and functional devices (e.g., hip, spine and knee implants) the requirement in terms of accuracy is very high [137].

1.6.1 Methods of medical reverse engineering

The final aim of all reverse engineering processes is to obtain 3D data which represent the geometries of the analyzed objects [137]. In general, two kinds of representation of end-use data are considered, especially in the areas of engineering design, 3D geometrical modelling and product development: (i) polygons or triangle mesh and (ii) Non-Uniform Rational B-Spline (NURBS). A polygon or triangle mesh includes vertices, edges and faces for defining the shape of an object [137]. The faces generally consist of triangles, quadrilaterals or further simple convex polygons.

Such kind of data is the simplest way to represent the geometries of the objects. Even if it does not represent an accurate representation of the geometries [137].

NURBS surfaces are the final output of the reverse engineering process that a user would like to obtain for applications characterized by high accuracy requirements. NURBS represent an accurate way for the definition of a free-form curve and surfaces [137]. NURBS are considered useful for several reasons: (i) they provide a mathematical form for standard analytical shapes and free form shapes; (ii) they provide a flexibility in designing a wide range of shapes; (iii) they reduce the consumption of memory when storing shapes; (iv) they may be assessed in a reasonably fast manner using numerically accurate and stable algorithms; (v) they result invariant under affine as well as perspective transformations; (vi) they represent generalizations of non-rational B-splines, non-rational and rational Bézier curves and surfaces [137].

Figure 1.15 shows the fundamental methods of reverse engineering in the biomedical field [137]. It is worth noting that the state of the art of data processing chains for 3D geometrical reconstruction in the biomedical field and the research are emphasised [137].

Four main phases may be individuated: Phase I – reverse engineering inputs; Phase II – data acquisition; Phase III - data processing and analysis; Phase IV – biomedical application/development and research.

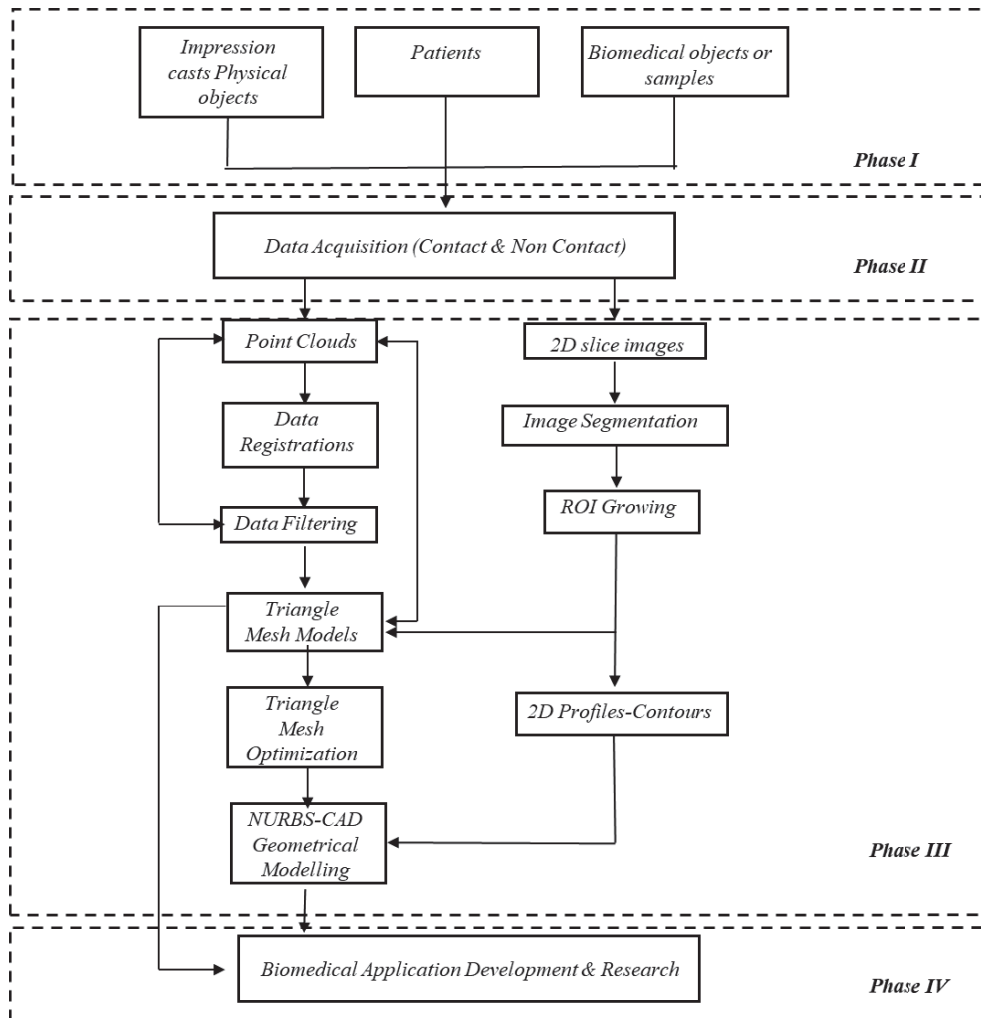


Figure 1.15. Reverse engineering methods in biomedical field: processes and information flows [137].

- *Phase I: reverse engineering inputs*

The interactive nature of the information processing and the possibility to implement the reverse engineering steps are frequently discussed in the literature [137]. The input of reverse engineering is fundamental for data acquisition and, hence, for biomedical applications and research. This can determine the techniques and methods for data acquisition, as well as the processing and analysis of

the data [137]. It defines the required level of accuracy from which the models can be constructed for several biomedical applications [137]. According to the specific applications, several kinds of inputs for reverse engineering can be selected to meet both technical requirements and clinical constraints (Figure 1.16) [137].

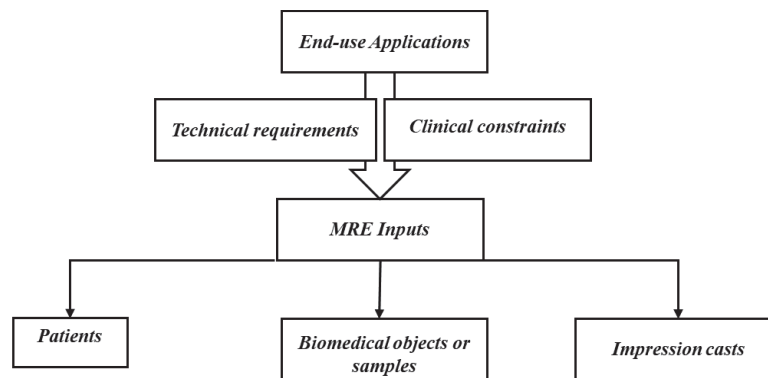


Figure 1.16. Medical reverse engineering (MRE) and end-use applications [137].

In this context, the state of the art involves personalised devices for bone reconstruction, tissue engineering, dental applications and simulations, medical training, surgical tools, orthopedics [137]. Table 1.4 [137] shows the typical end-use applications and the reverse engineering inputs, as well as the related kinds of raw data which are obtained from the data acquisition process.

The reverse engineering inputs may be represented by patients or physical objects as well as biological samples from which the geometrical information of the object may be captured and collected to develop innovative devices as well as to define applications and research [137].

- *Phase II: data acquisition*

There are several methods for data acquisition. Such techniques may be defined into two main groups: contact and non-contact [137]. In order to digitize a surface, contact methods employ sensing devices characterized by mechanical arms, Coordinate Measurement Machines (CMM) and Computer Numerical Control (CNC) machines [137]. With regard to non-contact methods, 2D cross-sectional

images and point clouds representing the geometry of an object can be captured through the projection of energy sources (e.g., sound, light or magnetic fields) on the object. The transmitted or the reflected energy can be then observed [137]. Finally, the geometrical data of an object can be calculated by using triangulation, wave-interference information, time of flight and image processing algorithms. There is no contact between the reverse engineering hardware and the object during the process of data acquisition [137].

Applications	Examples	MRE inputs and data type
Personalised implants	-Implants for bone reconstructions for patients with skull defects due to traffic accidents or bone tumors, -Implants for cosmetic cranio-maxillofacial surgery, -Implants: (i) Implants for bone reconstruction of the mandible, (ii) Dental implants for tooth reconstruction and replacement	- Patients - Data type: CT or MRI images
Dental implants & simulation	-Simulation: Simulation of an implant position on 2D & 3D models, identification of the mandibular canal, calculation of the bone density, & surgical planning, -Drilling guides for dental and spine surgery	- Patients - Impression casts - Data type: CT or MRI images, Point clouds
Surgical tools	-The jigs to assist the process of removing tumors in bone reconstruction surgery	- Patients - Impression casts - Data type: CT or MRI images, Point clouds
Surgical training & simulation	- Medical training models for surgeons and Medical Doctors to enhance surgical skills as well as to learn & practice physical examination, general medical procedures, and clinical skills - Virtual 3D models for medical simulation, biomedical analysis and study	- Patients - Biomedical objects - Impression casts - Data type: CT or MRI images, Point clouds
Vision science & Optometry	- Development of the contact lens - Simulation and study of the contact lens and eye shape	- Patients - Impression casts - Data type: CT or MRI images, Point clouds
Orthopeadics	- Development of hip and knee implants as well as the surgical tools such as orthopedic plates, fixation tools and screws - 3D models for biomedical analysis and study	- Patients - Impression casts - Data type: CT or MRI images, Point clouds
Ergonomics, Orthosis & Prosthesis	- Design & manufacturing of personalised orthosis and ergonomic products such as chairs and car seats, shoes, and sport products - Design & manufacturing of personalised prosthesis	- Patients - Biomedical objects - Impression casts - Data type: CT or MRI images, Point clouds
Tissue Engineering	Design & manufacturing of tissue engineering scaffolds 3D modeling of bone structures for biomedical analysis and study	- Patients - Biomedical objects - Data type: CT or MRI images, Point clouds

Table 1.4. Typical applications, examples, inputs and data type of medical reverse engineering (MRE) [137].

As a wide range of biomedical applications concern biomedical devices or anatomical structures with complex geometries and shapes, the contact methods are less employed in comparison to the non-contact techniques for data acquisition [137]. Moreover, if the considered applications require a high accuracy, the contact techniques must be used.

The advantages and disadvantages of the contact and non-contact techniques are reported in Table 1.5 [137].

Technique	Advantages	Disadvantages
Contact	(i) High accuracy; (ii) Low-costs; (iii) Ability to measure deep slots and pockets; (iv) Insensitivity to colour or transparency.	(i) Slow data collection; and (ii) Distortion of soft objects by the probe.
Non-contact	(i) No physical contact; (ii) Fast digitizing of substantial volumes; (iii) Good accuracy and resolution for common applications; (iv) Ability to detect colours; (v) Ability to scan highly detailed objects where mechanical touch probes may be too large to accomplish the task	(i) Possible limitations for coloured or transparent or reflective surfaces; (ii) lower accuracy.

Table 1.5. Contact and non-contact techniques: advantages and disadvantages [137].

Based on the end-use applications and required accuracy, the selection of the relevant data acquisition techniques may be done [137].

The outputs of the data acquisition process are point clouds and 2D slice images. These outputs are the inputs for the data processing steps [137].

If the laser and structured light are employed, the output of the data acquisition process is in the form of point clouds. If MRI and CT techniques are considered, the output is in the form of 2D slice images [137].

- *Phase III: data processing*

According to the two kinds of raw data obtained from the data acquisition process, several approaches may be considered for data processing to develop the 3D models of biomedical devices or anatomical structures [137].

- *Point clouds as the input for data processing*

The object is generally scanned in different views, thus properly capturing the area of interest or the entire geometry [137]. In this scenario, data registration is clearly needed for combining, aligning or merging the point clouds from multiple scans [137]. Furthermore, an amount of error is introduced into the scan data, and the placement of some points may occur in undesirable regions. This may be ascribed to the complex shapes, which may lead to scan points more than once during the scanning process [137]. In addition, the aligned scan data can generally contain overlapping points.

Accordingly, data optimisation is properly required. In this stage, the following common operations are employed: (i) reduction of noise and point redundancy; (ii) point sampling. The sampling function is employed for the minimization of the number of points in the point cloud data [137]. Successively, the optimized point cloud data can be triangulated for creating 3D triangle mesh or polygon models. The optimization of 3D triangle mesh models can be then performed. Such models can be manipulated and converted into 3D NURBS CAD models, also meeting the requirements related to the applications [137].

- *Slice images as the input for data processing*

Concerning CT and MRI, the images are usually stored in the form of DICOM format. Anyway, with regard to the applications that employ MicroCT systems, several data formats (e.g., BMP, PNG) can be used [137]. Dedicated image processing tools and packages are available for image processing for 3D data reconstruction of the soft and tissues as well as objects of interest [137]. 3D In the case of 3D reconstruction from 2D slice images, there are two basic steps: (i) image segmentation, and (ii) region of interest growing. Segmentation by threshold methods is employed to define the region of interest which presents the object for the reconstruction. This approach is based on the grey-scale value of the image pixels [137]. A lower threshold or a lower and a higher threshold may be considered the basis. The capacity of splitting the segmentation into separate objects is provided by the region growing technique; such approach may be considered useful for the separation of

anatomical structures, in the case of soft tissues and bone [137]. The outputs of the image segmentation and region of interest growing are represented by 3D triangle mesh models or 2D contours of the region of interest or anatomical structures. Like in the case of point clouds as the input for data processing, the optimization, manipulation, control or conversion of 3D triangle mesh models into 3D NURBS CAD models can be performed to meet the requirements according to the applications [137].

- *Phase IV: biomedical applications/development & research*

The obtained 3D triangle mesh models may be directly employed for different applications such as additive manufacturing, surgical planning, and structure or biomechanical analysis [137]. With regard to applications which require high accuracy for further geometrical modeling and design, such triangle mesh models are considered as the reference to develop CAD entities (e.g., points, curves and primitives) and to construct NURBS CAD models which may be employed as the reference for the development of biomedical devices and for research activities where CAD/CAM/CNC/CAE systems are used [137]. Even though the benefits related to the applications of the reverse engineering approach in designing and manufacturing biomodels, personalised devices and surgical tools have been frequently reported, the number of clinical cases result still limited and the technological approach has not been widely considered for treatment and diagnosis as a consequence of difficulties in terms of technology transfer to hospitals [137]. These difficulties may be generally ascribed to the design complexity, challenges about multidisciplinary collaborations and communications, high cost of technologies and investment [137].

Clinical and technical constraints must be properly defined in order to develop applications. Furthermore, an appropriate selection of the hardware and software for implementation is also fundamental [137]. Commercially available hardware for applications of medical reverse engineering are CT or MRI systems, non-contact scanners based on structured light and laser source, and further

dedicated instruments. According to the level of accuracy required for the applications, the systems is suitably selected.

Anyway, no single software may fulfil and fully satisfy the requirements in data processing and geometrical modelling [137]. Thus, the software selection is also dependent on the end-use application, also according to the data exchange among the packages and the complexity of the processes of geometrical modelling [137]. In this context, typical tools and software are fundamental to implement the applications of medical reverse engineering (e.g., medical image processing, additive manufacturing, simulation and finite element analysis, freeform modelling, CAD/CAM methods) [137].

1.7. Future challenges in biomedical field

Although additive manufacturing technology plays an important role in the biomedical field and provides a great number of advantages (cost savings, customization, optimization of product design, shorter supply chain, ability to develop devices with complex geometry) some applications (e.g., organ printing) still represent a great challenge [75].

Furthermore, over the past years, many efforts have been made to develop innovative materials for reproducing human organs and tissues as well as to improve the dimensional accuracy and the mechanical properties of additively manufactured devices [75].

Moreover, further efforts have been devoted to the reduction of the high cost of printers, and to the development of high performance bioprinters [75]. For this reason, more research is still needed in the field of materials, optimization of process techniques and applications of additive manufacturing [75].

1.8. References

[1] Ahangar P, Cooke ME, Weber MH, Rosenzweig DH. Current Biomedical Applications of 3D Printing and Additive Manufacturing. *Applied Sciences*. 2019; 9(8):1713.

- [2] Zadpoor, A.A. Design for Additive Bio-Manufacturing: From Patient-Specific Medical Devices to Rationally Designed Meta-Biomaterials. *Int. J. Mol. Sci.* 2017, 18, 1607.
- [3] Hu, Q.; Sun, X.Z.; Parmenter, C.D.J.; Fay, M.W.; Smith, E.F.; Rance, G.A.; He, Y.; Zhang, F.; Liu, Y.; Irvine, D.; et al. Additive manufacture of complex 3D Au-containing nanocomposites by simultaneous two-photon polymerisation and photoreduction. *Sci. Rep.* 2017, 7, 17150.
- [4] McHugh, K.J.; Nguyen, T.D.; Linehan, A.R.; Yang, D.; Behrens, A.M.; Rose, S.; Tochka, Z.L.; Tzeng, S.Y.; Norman, J.J.; Anselmo, A.C.; et al. Fabrication of fillable microparticles and other complex 3D microstructures. *Science* 2017, 357, 1138–1142.
- [5] Hull, C.W. Apparatus for Production of Three-Dimensional Objects by Stereolithography. U.S. Patent 4,575,330, 11 March 1986.
- [6] Norman, J.; Madurawe, R.D.; Moore, C.M.; Khan, M.A.; Khairuzzaman, A. A new chapter in pharmaceutical manufacturing: 3D-printed drug products. *Adv. Drug Deliv. Rev.* 2017, 108, 39–50.
- [7] Ahangar, P.; Akoury, E.; Ramirez Garcia Luna, A.; Nour, A.; Weber, M.; Rosenzweig, D. Nanoporous 3D-Printed Scaffolds for Local Doxorubicin Delivery in Bone Metastases Secondary to Prostate Cancer. *Materials* 2018, 11, 1485.
- [8] Akoury, E.; Weber, M.H.; Rosenzweig, D.H. 3D-Printed nanoporous scaffolds impregnated with zoledronate for the treatment of spinal bone metastases. *MRS Adv.* 2019, 156, 1–7.
- [9] Coelho, G.; Chaves, T.M.F.; Goes, A.F.; Del Massa, E.C.; Moraes, O.; Yoshida, M. Multimaterial 3D printing preoperative planning for frontoethmoidal meningoencephalocele surgery. *Child's Nerv. Syst.* 2018, 34, 749–756.
- [10] Arabnejad, S.; Johnston, B.; Tanzer, M.; Pasini, D. Fully porous 3D printed titanium femoral stem to reduce stress-shielding following total hip arthroplasty. *J. Orthop. Res.* 2017, 35, 1774–1783.
- [11] Yang, C.; Wang, X.; Ma, B.; Zhu, H.; Huan, Z.; Ma, N.; Wu, C.; Chang, J. 3D-Printed Bioactive Ca₃SiO₅ Bone Cement Scaffolds with Nano Surface Structure for Bone Regeneration. *ACS Appl. Mater. Interfaces* 2017, 9, 5757–5767.

- [12] Rosenzweig, D.H.; Carelli, E.; Ste_en, T.; Jarzem, P.; Haglund, L. 3D-Printed ABS and PLA Sca_olds for Cartilage and Nucleus Pulposus Tissue Regeneration. *Int. J. Mol. Sci.* 2015, 16, 15118–15135.
- [13] Fairag, R.; Rosenzweig, D.; Ramirez Garcialuna, J.L.; Weber, M.H.; Haglund, L. 3D-Printed Polylactic Acid (PLA) Sca_olds Promote Bone-like Matrix Deposition In-vitro. *ACS Appl. Mater. Interfaces* 2019.
- [14] ISO. ISO/ASTM-52900:2015 (ASTM F2792) Additive Manufacturing—General Principles—Terminology; ISO:Geneva, Switzerland, 2015
- [15] Hong, D.; Chou, D.T.; Velikokhatnyi, O.I.; Roy, A.; Lee, B.; Swink, I.; Issaev, I.; Kuhn, H.A.; Kumta, P.N. Binder-jetting 3D printing and alloy development of new biodegradable Fe-Mn-Ca/Mg alloys. *Acta Biomater.* 2016, 45, 375–386.
- [16] Malda, J.; Visser, J.; Melchels, F.P.; Jüngst, T.; Hennink, W.E.; Dhert, W.J.; Groll, J.; Huttmacher, D.W. 25th anniversary article: Engineering hydrogels for biofabrication. *Adv. Mater.* 2013, 25, 5011–5028.
- [17] Burton, H.E.; Eisenstein, N.M.; Lawless, B.M.; Jamshidi, P.; Segarra, M.A.; Addison, O.; Shepherd, D.E.T.; Attallah, M.M.; Grover, L.M.; Cox, S.C. The design of additively manufactured lattices to increase the functionality of medical implants. *Mater. Sci. Eng. C Mater. Biol. Appl.* 2019, 94, 901–908.
- [18] Rahman, Z.; Barakh Ali, S.F.; Ozkan, T.; Charoo, N.A.; Reddy, I.K.; Khan, M.A. Additive Manufacturing with 3D Printing: Progress from Bench to Bedside. *AAPS J.* 2018, 20, 101.
- [19] Castilho, M.D.; Malda, J.; Levato, R.; Alcalá-Orozco, C.R.; Melchels, F.P.W.; Gawlitta, D.; Hooper, G.J.; Woodfield, T.B.F.; Costa, P.F.; Lim, K.S.; et al. Bio-resin for high resolution lithography-based biofabrication of complex cell-laden constructs. *Biofabrication* 2018, 10, 034101.
- [20] Mironov, V.; Visconti, R.P.; Kasyanov, V.; Forgacs, G.; Drake, C.J.; Markwald, R.R. Organ printing: Tissue spheroids as building blocks. *Biomaterials* 2009, 30, 2164–2174.

- [21] Stavropoulos P, Foteinopoulos P (2018) Modelling of additive manufacturing processes: a review and classification. *Manuf Rev* 5:7–33.
- [22] H. Bikas, P. Stavropoulos, G. Chryssolouris, *Int. J. Adv. Manuf. Technol.* 83 (2016) 389–405
- [23] G.N. Levy, *Phys. Procedia* 5 (2010) 65–80.
- [24] M.D. Monzón, Z. Ortega, A. Martínez, F. Ortega, *Int. J. Adv. Manuf. Technol.* 76 (2015) 1111–1121.
- [25] I. Gibson, D. Rosen, B. Stucker, *Additive manufacturing technologies: 3D printing, rapid prototyping, and direct digital manufacturing*, Springer, Berlin, 2014.
- [26] J.P. Kruth, P. Mercelis, J. Van Vaerenbergh, L. Froyen, M. Rombouts, *Rapid Prototyp. J.* 11 (2005) 26–36.
- [27] J.P. Kruth, G. Levy, F. Klocke, T.H.C. Childs, *CIRP Ann.- Manuf. Technol.* 56 (2007) 730–759.
- [28] F.R. Liu, Q. Zhang, W.P. Zhou, J.J. Zhao, J.M. Chen, *J. Mater. Process. Technol.* 212 (2012) 2058–2065.
- [29] P. Mercelis, J.P. Kruth, *Rapid Prototyp. J.* 12 (2006) 254–265.
- [30] M.P. Mughal, H. Fawad, R. Mufti, *Acta Mech.* 183 (2006) 61–79.
- [31] F.R. Liu, C. He, J.M. Chen, *Int. J. Mach. Tools Manuf.* 65 (2013) 22–28.
- [32] R. Ganeriwala, T.I. Zohdi, in: D.M.H. Dornfeld (Ed.), *Proceedings of the 6th CIRP International Conference on High Performance Cutting*, Elsevier, Vol. 14, 2014, pp. 299–304.
- [33] A. Wegner, G. Witt, *Phys. Procedia* 39 (2012) 480–490.
- [34] Y. Khalil, A. Kowalski, N. Hopkinson, *Manuf. Rev.* 3 (2016) 15.
- [35] G. Strano, L. Hao, R.M. Everson, K.E. Evans, *J. Mater. Process. Technol.* 213 (2013) 589–597.
- [36] C. Qiu, C. Panwisawas, M. Ward, H.C. Basoalto, J.W. Brooks, M.M. Attallah, *Acta Mater.* 96 (2015) 72–79.
- [37] A.V. Gusarov, I. Yadroitsev, P. Bertrand, I. Smurov, *Appl. Surf. Sci.* 254 (2007) 975–979.
- [38] F.J. Gürtler, M. Karg, K.H. Leitz, M. Schmidt, *Phys. Procedia* 41 (2013) 881–886.

- [39] M. Shiomi, K. Osakada, K. Nakamura, T. Yamashita, F. Abe, *CIRP Annals - Manuf. Technol.* 53 (2004) 195–198.
- [40] M. Smith, Z. Guan, W.J. Cantwell, *Int. J. Mech. Sci.* 67 (2013) 28–41.
- [41] X. Gong, T. Anderson, K. Chou, in: *Proceedings of the ASME/ISCIE 2012 International Symposium on Flexible Automation*, American Society of Mechanical Engineers, St. Louis, 2012, pp. 507–515.
- [42] M. Bussmann, S. Chandra, J. Mostaghimi, “Modeling the splash of a droplet impacting a solid surface” *Phys. Fluids* 12 (2000) 3121–3132.
- [43] W. Zhou, D. Loney, F.L. Degertekin, D.W. Rosen, A.G. Fedorov, “What controls dynamics of droplet shape evolution upon impingement on a solid surface?” *AIChE Journal*, Vol. 59 No. 1, pp. 3071-3082, 2013.
- [44] S.H. Ahn, M. Montero, D. Odell, S. Roundy, P.K. Wright, “Anisotropic material properties of fused deposition modelling ABS”. *Rapid Prototy. J.* 8 (2002) 248–257.
- [45] K. V. Wong and A. Hernandez, “A Review of Additive Manufacturing”. *International Scholarly Research Network ISRN Mechanical Engineering*, Volume 2012, Article ID 208760.
- [46] R. Noorani, *Rapid Prototyping—Principles and Applications*, John Wiley & Sons, 2006.
- [47] K. Cooper, *Rapid Prototyping Technology*, Marcel Dekker, 2001.
- [48] P. P. Kruth, “Material increment manufacturing by rapid prototyping techniques”, *CIRP Annals—Manufacturing Technology*, vol. 40, no. 2, pp. 603–614, 1991.
- [49] J.W. Halloran, V. Tomeckova, S. Gentry et al., “Photopolymerization of powder suspensions for shaping ceramics,” *Journal of the European Ceramic Society*, vol. 31, no. 14, pp. 2613–2619, 2011.
- [50] D. T. Pham and C. Ji, “Design for stereolithography,” *Proceedings of the Institution of Mechanical Engineers*, vol. 214, no. 5, pp. 635–640, 2000.
- [51] H. Kim, C. Jae-Won, and R. Wicker, “Scheduling and process planning for multiple material stereolithography,” *Rapid Prototyping Journal*, vol. 16, no. 4, pp. 232–240, 2010.

- [52] M. Szilvoei-Nagy and G. M'aty'asi, "Analysis of STL files," *Mathematical and Computer Modelling*, vol. 38, no. 7–9, pp. 945–960, 2003.
- [53] C. Iancu, D. Iancu, and A. Stamcioiu, "From Cad model to 3D print via "STL" file format" , *Fiability & Durability*,1(5), 73–81, 2010.
- [54] S. Morvan, R. Hochsmann, and M. Sakamoto, "ProMetal RCT(TM) process for fabrication of complex sand molds and sand cores", *Rapid Prototyping*, vol. 11, no. 2, pp. 1–7, 2005.
- [55] T. Hwa-Hsing, C. Ming-Lu, and Y. Hsiao-Chuan, "Slurry based selective laser sintering of polymer-coated ceramic powders to fabricate high strength alumina parts", *Journal of the European Ceramic Society*, vol. 31, no. 8, pp. 1383–1388, 2011.
- [56] G. V. Salmoria, R. A. Paggi, A. Lago, and V. E. Beal, "Microstructural and mechanical characterization of PA12/ MWCNTs nanocomposite manufactured by selective laser sintering," *Polymer Testing*, vol. 30, no. 6, pp. 611–615, 2011.
- [57] D. Slavko and K. Matic, "Selective laser sintering of composite materials technologies," *Annals of DAAAM & Proceedings*, p. p1527, 2010.
- [58] Technology Gateway, "NASA— EBF3—electron beam form fabrication," 2009, <http://www.youtube.com/watch?v=WrWHwHuWrzk>.
- [59] L. Murr, S. Gaytan, D. Ramirez et al., "Metal fabrication by additive manufacturing using laser and electron beam melting technologies," *Journal of Materials Science & Technology*, vol. 28, no. 1, pp. 1–14, 2012.
- [60] C. Semetay, *Laser engineered net shaping (LENS) modeling using welding simulation concepts* [ProQuest Dissertations and Theses], Lehigh University, 2007.
- [61] Y. Xiong, *Investigation of the laser engineered net shaping process for nanostructured cermets* [ProQuest Dissertations and Theses], University of California, 2009.
- [62] Y. S. Liao, H. C. Li, and Y. Y. Chiu, "Study of laminated object manufacturing with separately applied heating and pressing," *International Journal of Advanced Manufacturing Technology*, vol. 27, no. 7-8, pp. 703–707, 2006.

- [63] I. Gibson, T. Kvan, and W. Ling, "Rapid prototyping for architectural models," *Rapid Prototyping Journal*, vol. 8, no. 2, pp. 91–99, 2002
- [64] W. J. James, M. A. Slabbekoorn, W. A. Edgin, and C. K. Hardin, "Correction of congenital malar hypoplasia using stereolithography for presurgical planning," *Journal of Oral and Maxillofacial Surgery*, vol. 56, no. 4, pp. 512–517, 1998.
- [65] Chaput, Christophe, and J. B. Lafon, "Ceramic industry," vol. 161, no. 9, pp. 15–16, 2011.
- [66] R. Makovec, "Digital technologies in dental laboratories," *Annals of DAAAM & Proceedings*, p. p1579, 2010.
- [67] R. van Noort, "The future of dental devices is digital," *Dental Materials*, vol. 28, no. 1, pp. 3–12, 2012.
- [68] A. Moscaritolo, "Woman receives 3D printer? created transplant Jaw," *PC Magazine Online*, 2012, <http://www.pcmag.com/article2/0,2817,2399887,00.asp>.
- [69] S. J. Hollister, "Porous scaffold design for tissue engineering," *Nature Materials*, vol. 4, no. 7, pp. 518–524, 2005.
- [70] M. A. Stoodley, J. R. Abbott, and D. A. Simpson, "Titanium cranioplasty using 3-D computer modelling of skull defects," *Journal of Clinical Neuroscience*, vol. 3, no. 2, pp. 149–155, 1996.
- [71] M. Conner, "3-D medical printer to print body parts," *EDN*, vol. 55, no. 3, p. 9, 2010.
- [72] L. Zhao, V. Lee, S. Yoo, G. Dai, and X. Intes, "The integration of 3-D cell printing and mesoscopic fluorescence molecular tomography of vascular constructs within thick hydrogel scaffolds," *Biomaterials*, vol. 33, no. 21, pp. 5325–5332, 2012.
- [73] "A step forward for artificial blood vessels," *Expert Review of Cardiovascular Therapy* 5.5, 817+, Academic OneFile, 2007.
- [74] J. Thilmany, "Printed life: the 3-D printing of living organs for transplant isn't far-fetched, it's almost here," *Mechanical Engineering-CIME*, 44+, Academic OneFile, 2012.
- [75] The role of additive manufacturing for biomedical applications: A critical review. Rakesh Kumar, Manoj Kumar, Jasgurpreet Singh Chohan

- [76] Schubert C, Van Langeveld MC, Donoso LA. Innovations in 3D printing: a 3D overview from optics to organs. *Br J Ophthalmol* 2014;98:159–61.
- [77] Sidhu HS, Kumar S, Kumar R, Kumar S. Experimental investigation on design and analysis of prosthetic leg. *Journal of Xidian University* 2020;15(5):4486–501.
- [78] Banks J. Adding value in additive manufacturing: researchers in the United Kingdom and Europe look to 3D printing for customization. *IEEE Pulse* 2013;6: 22–6.
- [79] Lee AY, AN J, Chua CK. Two-way 4D printing: a review on the reversibility of 3D-printed shape memory materials. *Engineering* 2017;3:663–74.
- [80] Pop MA, Croitoru C, Bedo T, Geaman V, et al. Structural changes during 3D printing of bioderived and synthetic thermoplastic materials. *J Appl Polym Sci Symp* 2019;136:473–82.
- [81] Lin YH, Chuang TY, Chiang WH, et al. The synergistic effects of graphene-contained 3D-printed calcium silicate/poly- ϵ -caprolactone scaffolds promote FGFR-induced osteogenic/angiogenic differentiation of mesenchymal stem cells. *Mater Sci Eng C Mater Biol Appl* 2019;104:180–7.
- [82] Huang KH, Chen YW, Wang CY, et al. Enhanced capability of BMP-2-loaded mesoporous calcium silicate scaffolds to induce odontogenic differentiation of human dental pulp cells. *Endod* 2018;44:1677–85.
- [83] Jones DB, Sung R, Weinberg C, Korelitz T, Andrews R. Three dimensional modeling may improve surgical education and clinical practice. *Surg Innov* 2016; 23:189–95.
- [84] Diment LE, Ompson MS, Bergmann JHM. Clinical efficacy and effectiveness of 3D printing: a systematic review. *BMJ Open* 2017;7:122–32.
- [85] Kumar L, Haleem A, Tanveer Q, Javaid M, Shuaib M, Kumar V. Rapid manufacturing: classification and recent development. *Int J Adv Eng Res Sci (IJAERS)* 2017;4:29–40.
- [86] Dominguez R, Ku-Herrera JJ, Hernandez-Perez A. An assessment of the effect of printing orientation, density, and filler pattern on the compressive performance of 3D printed ABS structures by fuse deposition. *Int J Adv Manuf Technol.* 2017: 1–11.

- [87] Culmone C, Smit G, Breedveld P. Additive manufacturing of medical instruments: a state-of-the-Art review. *Addit Manuf* 2019;27. <https://doi.org/10.1016/j.addma.2019.03.015>.
- [88] Loh QL, Choong C. Three-dimensional scaffolds for tissue engineering applications: role of porosity and pore size. *Tissue Eng B Rev* 2013;19(6): 485–502.
- [89] Jiang G, Li Q, Wang C, et al. Fabrication of graded porous titanium–magnesium composite for load-bearing biomedical applications. *Mater Des* 2015;67:354–9.
- [90] Gentile P, Chiono V, Carmagnola I, Hatton P, et al. An overview of poly (lactic-co-glycolic) acid (PLGA)-based biomaterials for bone tissue engineering. *Int J Mol Sci* 2014;15(3):3640–59.
- [91] George M, 'Arnad'ottir A, Gíslason M, et al. New directions in 3D medical modeling: 3D-printing anatomy and functions in neurosurgical planning. *Comput Vision in Healthc Appl* 2017;2:1–8.
- [92] Ventola CL. Medical applications for 3D printing: current and projected uses. *P T* 2014;39(10):704–11.
- [93] Wake N, Alexander AE, Christensen AM, et al. Creating patient-specific anatomical models for 3D printing and AR/VR: a supplement for the 2018 Radiological Society of North America (RSNA) hands-on course. *3D Print Med*. 2018;5:17. <https://doi.org/10.1186/s41205-019-0054-y>.
- [94] Dana A. 3D Printing in Medicine. Patient specific in situ 3D printing. 2017. p. 91–113.
- [95] Sodian R, Weber S, Markert M, et al. Stereolithographic models for surgical planning in congenital heart surgery. *Ann Thorac Surg* 2007;83:1854–7.
- [96] Kim BS, Mooney DJ. Development of biocompatible synthetic extracellular matrices for tissue engineering. *Trends Biotechnol* 1998;16:224–30.
- [97] Noorani R. *Rapid prototyping: principles and applications*. Hoboken (NJ): John Wiley and Sons Inc; 2006. ISBN: 978-0-471-73001-73009.
- [98] Liu Q, Leu MC, Schmitt SM. Rapid prototyping in dentistry: technology and application. *Int J Adv Manuf Technol*. 2006;293:317–35.

- [99] Kai CC, Meng CS, Ching LS, Hoe EK, Fah LK. Rapid prototyping assisted surgery planning. *Int J Adv Manuf Technol.* 1998;14:624–30.
- [100] van Noort R. The future of dental devices is digital. *Dent Mater* 2012;28(1):3–12.
- [101] Milovanovic J, Trajanovic M. Medical applications of rapid prototyping. *Mech Eng* 2007;5:79–85.
- [102] Derakhshanfar S, Mbeleck R, Xu K, et al. 3D bioprinting for biomedical devices and tissue engineering: a review of recent trends and advance. *Bioact Mater* 2018; 3:144–56.
- [103] Turnbull G, Clarke J, Picard F, Riches P, Jia L, Han F, et al. 3D bioactive composite scaffolds for bone tissue engineering. *Bioact Mater* 2018;3:278–314.
- [104] Tofail, Syed AM, Koumoulos, et al. Additive manufacturing: scientific and technological challenges, market uptake and opportunities. *Mater Today* 2017: 1–16.
- [105] Oberoi Gunpreet, et al. 3D printing - facets of dentistry. *Front Bioeng Biotechnol* 2017;6:172.
- [106] Hao W, Liu Y, Zhou H, et al. Preparation and characterization of 3D printed continuous carbon fiber reinforced thermosetting composites. *Polym Test* 2018; 65:29–34.
- [107] Javaid M, Haleem A. Current status and applications of additive manufacturing in dentistry: a literature-based review. *J Oral Biol Craniofac Res* 2019;9(3):179–85.
- [108] Cartiaux O, Paul L, Francq BG, Banse X, Docquier PL. Improved accuracy with 3D planning and patient-specific instruments during simulated pelvic bone tumor surgery. *Ann Biomed Eng* 2014;42:205–13.
- [109] Goyanes A, Det-Amornrat U, Wang J, Basit S, et al. 3D scanning and 3D printing as innovative technologies for fabricating personalized topical drug delivery systems. *J Control Release* 2016;234:41–8.
- [110] Wu D, Thames JL, Rosen DW, Schaefer D. Enhancing the product realization process with cloud-based design and manufacturing systems. *Transactions of the ASME. J Comput Inf Sci Eng* 2013;13:55–66.

- [111] Wu D, Rosen DW, Wang L, Schaefer D. Cloud-based design and manufacturing: a new paradigm in digital manufacturing and design innovation. *Comput Des* 2015: 1–14.
- [112] Culmone C, Smit G, Breedveld. Additive manufacturing of medical instruments: a state-of-the-art review. *Accept Manusc* 2019;27:461–73. <https://doi.org/10.1016/j.addma.2019.03.015>.
- [113] Kurenov SN, Ionita C, SAammons D, Demmy TL. Three-dimensional printing to facilitate anatomic study, device development, simulation, and planning in thoracic surgery. *J Thoracic Cardiovasc Surg* 2015;149:973–9.
- [114] Jeon H, Kang K, Park SA. Generation of multilayered 3D structures of HepG2 cells using a bio-printing technique. *Gut Liver* 2017;11:121–8.
- [115] Vukievic M, Mosadegh B, Little JK. Cardiac 3D printing and its future directions. *JACC* 2017;10:171–84. 2017.
- [116] Lino H, Igawa K, Kanno Y. Maxillofacial reconstruction using custom-made artificial bones fabricated by inkjet printing technology. *J Artif Organ* 2009;12: 200–5.
- [117] Randazzo M, Pisapia JM, Singh N, Awani JM. 3D printing in neurosurgery: a systematic review. *Surg Neurol Int* 2016;7:801–9.
- [118] Auricchio F, Marconi S. 3D printing: clinical applications in orthopaedics and traumatology, Effort. *Open Rev* 2016;1:121–7.
- [119] Chae MP, Rozen WM, Mcmenamin PG. Emerging applications of bedside 3D printing in plastic surgery. *Front Surg* 2015;16:10–25.
- [120] Crafts TD, Ellsperman SE, et al. Three-dimensional printing and its applications in otorhinolaryngology-head and neck surgery. *Otolaryngol Head Neck Surg* 2017: 999–1010.
- [121] Williams C, James A, et al. 3D printing in clinical podiatry: a pilot study and review. *J Foot Ankle Res* 2015;8. 5: 41.
- [122] Su S, Moran K, Robar JL. Design and production of 3D printed bolus for electron radiation therapy. *J Appl Clin Med Phys* 2014;15:194–211.

- [123] Guilbert N, Mhanna L, Didier A. Integration of 3D printing and additive manufacturing in the interventional pulmonologist's toolbox. *Respir Med* 2018; 134:139–42.
- [124] Hangge P, Pershad Y, et al. Three-dimensional (3D) printing and its applications for aortic diseases. *Cardiovasc Diagn* 2018;8:19–25.
- [125] Zhang Y, Yang Z, Li X, Chen Y, Zhang S, Du M, et al. Custom prosthetic reconstruction for proximal tibial osteosarcoma with proximal tibiofibular joint involved. *Surg Oncol* 2008;17(2):87–95.
- [126] Ventola CL. Medical Applications for 3D printing: current and projected uses. *Med Appl 3D Print* 2014;39:705–12.
- [127] Mallepre T, Bergers D. Accuracy of medical RP models. *Rapid Prototyp J* 2009; 15:325–32.
- [128] Salmi M, Paloheimo KS, Tuomi J, Wolff J, Mäkitie A. Accuracy of medical models made by additive manufacturing. *J Craniomaxillofac Surg* 2013;41:603–9.
- [129] Ostuzzi F, Rognoli V, Saldien J, Levi M. +TUO project: low-cost 3D printers as helpful tool for small communities with rheumatic diseases. *Rapid Prototyp J* 2015;21:491–505.
- [130] Pine J. Mass customizing products and services. *Plan Rev* 1993;21:6–13.
- [131] Salmi M, Tuomi J, PaloheimoKaija S, et al. Patient specific reconstruction with 3D modeling and DMLS additive manufacturing. *Rapid Prototyp J* 2012;18:209–14.
- [132] Pucci JU, Christophe BR, Sisti JA, Connolly ES. Three-dimensional printing: technologies, applications, and limitations in neurosurgery. *Biotechnol Adv* 2017; 35(5):521–9.
- [133] Kochan A. Rapid prototyping gains speed, volume and precision. *Assem Autom* 2000;20:295–9.
- [134] Gibson I, Cheung LK, et al. The use of rapid prototyping to assist medical applications. *Rapid Prototyp J* 2006;12:45–53.
- [135] Mallepre T, Bergers D. Accuracy of medical RP models. *Rapid Prototyp J* 2009; 15:325–32.
- [136] Galantucci LM, Lavecchia F, Percoco G. Study of compression properties of topologically optimized FDM-made structured parts. *Manuf Technol* 2008;57: 243–6.

- [137] Le, Chi, Jos, Vander Sloten, Le, Tan Hung, Lam, Khanh, Soe, Shwe, Zlatov, Nikolay, Le, Tam Phuoc and Pham, Dinh Trung (2010) *Medical reverse engineering applications and methods*. In: Proceedings of International Conference on Innovations, Recent Trends and Challenges in Mechatronics, Mechanical Engineering and New High-Tech Products Development. INCDMTM, Bucharest, Romania, pp. 186-196.
- [138] Wiberg, A.; Persson, J.; Ölvander, J. “Design for additive manufacturing—A review of available design methods and software”. *Rapid Prototyp. J.* Vol. 25 No. 6, pp. 1080-1094, 2019.
- [139] Klahn, C., Leutenecker, B. and Meboldt, M. (2014), “Design for additive manufacturing - Supporting the substitution of components in series products”, *Procedia CIRP*, Vol. 21, pp. 138-143
- [140] Rodrigue, H. and Rivette, M. (2010), “An assembly-level design for additive manufacturing methodology”, *IDMME– Virtual Concept*, pp. 1-9.
- [141] Zhang, Y. Bernard, A., Gupta, R.K. and Harik, R. (2014), “Efficient design-optimization of variable-density hexagonal cellular structure by additive manufacturing: theory and validation”, *Journal of Manufacturing Science and Engineering*, Vol. 137021004.
- [142] Robbins, J., Owen, S.J., Clark, B.W. and Voth, T.E. (2016), “An efficient and scalable approach for generating topologically optimized cellular structures for additive manufacturing”, *Additive Manufacturing*, Vol. 12, pp. 296-304.
- [143] Wang, D., Yang, Y., Liu, R., Xiao, D. and Sun, J. (2013), “Study on the designing rules and processability of porous structure based on selective laser melting (SLM)”, *Journal of Materials Processing Technology*, Vol. 213 No. 10, pp. 1734-1742.
- [144] Liu, X. and Rosen, D. (2010), “Ontology based knowledge modeling and reuse approach of supporting process planning in layer-based additive manufacturing”, *International Conference on Manufacturing Automation*.
- [145] Jin, Y., Du, J. and He, Y. (2017), “Optimization of process planning for reducing material consumption in additive manufacturing”, *Journal of Manufacturing Systems*, Vol. 44, pp. 65-78.

Chapter 2

An integrated design of 3D additively manufactured hybrid structures for cranioplasty

2.1. Introduction

Cranioplasty is the surgical procedure for correcting cranial deformities or defects arising from skull fracture, deformities, cancer and infections. The repair or regeneration of cranial defects involves the use of biomaterials, and several approaches, based on polymers and composites, can be distinguished [1-3].

The *in situ* application of bone cement such as poly(methyl methacrylate) (PMMA) represents the most common approach. This cement consists of a solid powder phase made of PMMA and a liquid monomer; by mixing these two phases a radical polymerization reaction occurs driven by benzoyl-peroxide and amines [2,4-6]. Such biomaterial is used for bone reconstruction from more than half a century, and the cranioplasty procedure consists of a single intra-operatively step [2,7], as the malleable paste is applied onto the cranial defect and it is easily shaped around the contours of the patient's skull defects [4,8]. Once polymerized, mechanical properties are in between those of cortical and spongy bone [9,10]. The PMMA skull prosthesis is commonly fixed through titanium screws and plates [11]. In order to prevent cranioplasty graft infections [4,12], gentamicin has been loaded into PMMA [13,14], but a reduction of mechanical properties has been shown [2,6]. The incorporation of silver [15] and gold [16] nanoparticles into PMMA bone cements has been suggested for antimicrobial and mechanical purposes. Recently, novel antibacterial agents, such as bioactive glass (BG) and copper doped tricalcium phosphate (Cu-TCP) particles, have been incorporated into surgical PMMA in order to prevent cranioplasty graft infections [2,17]. A low amount of Cu-TCP

(i.e., 2.5 wt%) showed an efficient antibacterial effect, while providing a mechanical reinforcement for the polymer matrix [17].

The *in situ* approach is considered convenient as it reduces the time from diagnosis to implantation, but heat and shrinkage due to the polymerization process as well as the release of unreacted monomers represent the main drawbacks. The most significant drawback of the *in situ* approach for large cranial defects based on PMMA is the heat developed as a consequence of the exothermic reaction. To overcome this issue, the *ex vivo* approach based on the molding strategy has been developed. The mold can be realised through a plaster impression previously taken with a gel or a wax over the skull defect, a silicone mold is then fabricated, and the PMMA skull prostheses is finally formed by pouring the cement into the mold [11,18].

Among the *ex vivo* approach, 3D scan of the cranial defect in conjunction with Additive Manufacturing (AM) technologies allow to manufacture the customized mold into which the PMMA paste is poured and formed [19-21]. Over the past few years, AM has replaced the computer-aided design (CAD)/computer-aided manufacturing (CAM) milling method for manufacturing the mold replicating the skull defect starting from X-ray computed tomography (CT) [22]. However, photogrammetry and Laser scanners are gaining popularity in the field of clinical 3D imaging tools as they are less invasive than X-ray CT [23,24]. The process by which 3D skull scans are analyzed and converted in suitable 3D virtual models is known as Reverse Engineering (RE) [1]. The combination of RE approach with AM has allowed the direct fabrication of the skull defect and, hence, the manufacturing of the mold. Ink-Jet Printing (IJP), Fused Deposition Modeling (FDM), Laser Sintering (LS), and Stereolithography (SLA) represent the main AM technologies employed for the fabrication of a synthetic replica of the skull defect [1]. A silicone mold has been manufactured using the positive shape of the cranial defect previously fabricated through IJP processing a photopolymerizable resin [25]. Using a similar strategy, the positive shape of the cranial defect has been additively manufactured through SLA and a composite skull prosthesis has been realised into an alginate mold [20,26]. The main advantage of SLA is the high accuracy in reproducing the solid

3D model [27]. A silicone mold has been manufactured from the positive shape of the cranial defect previously realised processing polyamide powders through LS [28]. Similarly, the mold has been fabricated around the positive shape of the acrylonitrile-butadiene-styrene cranial defect manufactured through FDM [4,8]. Instead, by using the FDM approach, an acrylonitrile-butadiene-styrene mold, directly reproducing the skull defect, has been produced, and paraffin oil has been spread over the mold walls to prevent the sticking of the PMMA prostheses [3].

The integrated approach combining 3D scanning, RE and AM [29-31] represents the most recent and advanced approach to directly fabricate skull prosthesis or scaffold. Biodegradable polymer based scaffolds for cranial bone regeneration are commonly manufactured by FDM. With this technology, a continuous thermoplastic filament (e.g. polyesters and their copolymers) is deposited from the melt state, the scaffold porosity and pore dimension are determined by process and geometrical parameters such as the strand distance and the layer stacking sequence [32]. In the case of non-degradable devices (i.e. prosthetic approach), skull growth clearly adds an additional concern in cranioplasty, thus biodegradable structures (i.e. scaffolds) for cranial bone tissue engineering are particularly important for paediatric patients [31]. Poly(ϵ -caprolactone) (PCL), polylactic acid (PLA) and poly(lactic-co-glycolic acid) (PLGA) represent the most common polyesters used to manufacture biodegradable scaffolds for cranial bone regeneration [31-35]. PLGA scaffolds, manufactured by FDM and implanted in the parietal skull defect, have shown evident angiogenesis within three weeks of *in vivo* observations in a mice model [36]. PCL is a degradable polyester easy to process using FDM as its melting temperature is low (60 °C) compared to the other polyesters, furthermore its mechanical properties are similar to dense spongy bone [36,37]. PCL has been processed by FDM, and scaffolds for cranial bone regeneration of critical-size defects have been investigated in the rabbit [38] and human [39] models.

The design of innovative 3D lattices and porous devices clearly spans from industrial to biomedical applications. Many progresses in 3D bioprinting of hydrogel-based biomaterials have also been recently discussed from the tissue engineering perspective. In this case, differently from the prosthetic

approach, the attention has been focused on hydrogel-based bioprinted scaffolds to develop functional tissues through the use of advanced fabrication methods covering multiple-dispenser, coaxial, and hybrid 3D printing processes [40].

Further progresses in the field of additive manufacturing were also related to the introduction of four-dimensional (4D) printing technology to develop tunable continuous-stable metamaterials with reversible thermo-mechanical memory operations [41]. Experimental and numerical tests were carried out to analyze a 3D printed tunable reversible mechanical metamaterial unit with bi-stable memory operations. Cold and hot programming were suitably combined, and the potential to mimic electronic memory devices as well as to design surface adaptive structures was demonstrated. In the biomedical field, the possibility to develop advanced devices (i.e., self-deployable stents) was stressed [41]. Several combinations of hard and soft components were adopted to fabricate dual-material lattice-based meta-structures through 4D printing FDM technology. As an example, an approach towards 4D printing tunable meta-sandwiches was already reported for applications concerning reversible energy absorption [42].

Even though many progresses have been made in the design of lattice structures, 3D printed scaffolds for tissue regeneration and advanced prosthesis [30,31,36,39,40,43-47], the aim of the current investigation was to design and fabricate customized hybrid devices as a further alternative for the repair of large cranial defects, integrating the reverse engineering approach with additive manufacturing. The hybrid device consisted of a 3D additive manufactured polyester porous structures infiltrated with PMMA/Cu-TCP (97.5/2.5 w/w) bone cement. Temperature profiles were first evaluated during setting also in the case of the hybrid devices. In addition, to the best of the authors' knowledge, none of the currently existing human head finite element models consider the impact-related features in the case of people using prosthetic devices for a large cranial defect. For this reason, a theoretical analysis was preliminarily performed on the entire head model trying to simulate a people with the customized hybrid device (PCL/PMMA/Cu-TCP) in severe impact conditions (i.e., a rigid sphere impacting the implant zone of the head).

2.2. Materials and Methods

2.2.1 Modified bone cement

Copper-doped tricalcium phosphate (Cu-TCP) particles were employed to modify a PMMA-based cement (Palacos, Heraeus, Wehrheim, Germany). Specifically, the precipitation technique was used to obtain Cu^{2+} -substituted TCP as previously described [2,17]. In brief, 0.5 mol/L solution of $\text{Cu}(\text{NO}_3)_2$ was mixed with 0.5 mol/L solution of $\text{Ca}(\text{NO}_3)_2$ and 0.5 mol/L solution $(\text{NH}_4)_2\text{HPO}_4$ was added. Ammonia solution was added to the solution for keeping the pH at 6.5–6.9. After 30 min, the formed precipitate was filtered and washed using distilled water.

The precipitate was then dried at 80 °C and calcined at 900 °C forming the whitlockite structure. PMMA cement was modified according to a previously reported procedure [17]. Cu-TCP particles were dispersed in the solid PMMA phase using ultrasonic dispersion. The liquid phase was then added and hand-mixed to the solid phase. Benefiting from the previous results, a specific formulation was considered for PMMA/Cu-TCP (97.5/2.5 w/w) [2,17].

2.2.2 Design and fabrication of 3D additive manufactured porous structures

3D porous structures with different lay-down patterns ($0^\circ/90^\circ$ and $0^\circ/45^\circ$) were fabricated by an additive manufacturing technique based on injection/extrusion methods (i.e., Fused Deposition Modeling), using a commercially available 3D printer (Creality3D Ender-3 PRO) and two different aliphatic polyesters (poly(ϵ -caprolactone) – PCL and polylactic acid – PLA). In brief, PCL (FacilanTM PCL 100 - density: 1.1 g/cm³, melting point: 58-60 °C) or PLA (FILOALFA – density: 1.24 g/cm³, melting point: 135°C) filaments (1.75 mm in diameter) were heated and the 3D polymeric structures were manufactured by injecting/extruding the material through a nozzle (inner diameter of 500 μm).

The filaments were deposited along specific directions between two successive layers according to the adopted lay-down pattern [2]. The filament distance (i.e., center-to-center distance) and layer thickness were set to 1000 μm and 400 μm , respectively. A printing speed of 15 mm/s was used.

2.2.3 Evaluation of temperature profile

The effect of the employed thermoplastic polyesters on the exothermal reaction occurring during cement setting was investigated by recording temperature profiles [2]. Specifically, cylindrical 3D printed PCL and PLA structures (diameter of 10 mm, height of about 5 mm) with a fully interconnected pore network (porosity of 50%) (Figure 2.1-left). Each 3D structure was equipped with a disposable k-type thermocouple (Figure 2.1-center).

Hollow cylindrical Teflon molds (inner diameter of 12 mm and height of 20 mm) were employed and equipped with k-type thermocouples (Figure 2.1-right). The k-type thermocouples connected to the National Instruments DAC interface and the LabView system were employed for temperature measurements. The mold was positioned onto a thermoblock system allowing the control of the base line temperature of the Teflon mold at 37°C [2].

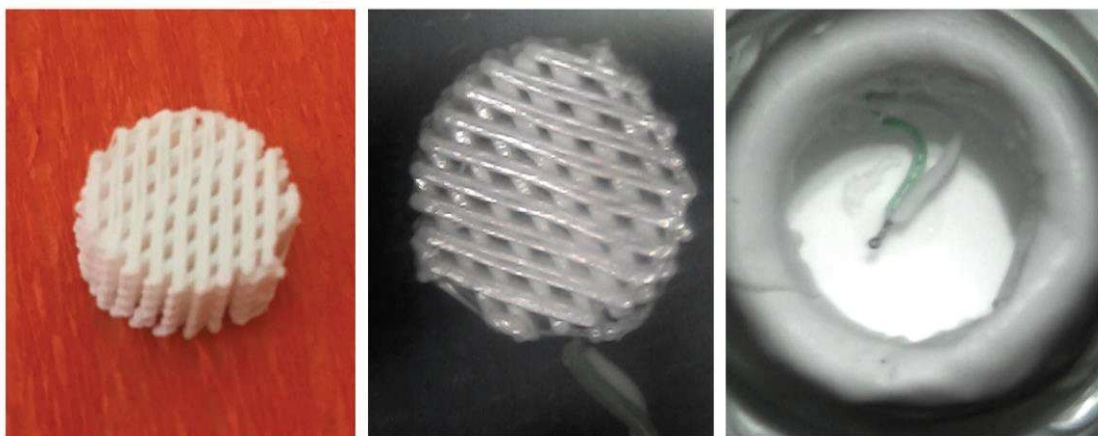


Figure 2.1. Typical image of a 3D printed porous structure (diameter of 10 mm, height of about 5 mm) (left); 3D porous structure incorporating a k-type thermocouple (center); hollow cylindrical Teflon mold equipped with k-type thermocouple (right).

PMMA and PMMA/Cu-TCP (97.5/2.5 w/w) cement pastes were poured into the Teflon molds equipped with the thermocouple (Figure 2.1-right). Heat was released during setting and temperature was recorded over time for 1000 s. Five specimens were considered for each kind of bone cement. PCL/PMMA and PLA/PMMA hybrid specimens were obtained by placing each 3D cylindrical porous structure into the Teflon mold and then pouring the bone cement pastes. A Teflon piston was manually used to gently press the cement into the mold for promoting the infiltration of PMMA bone cement into the pore network of the structure. Five specimens were considered for each kind of structure [2].

The measured peak temperatures were reported as mean value \pm standard deviation. Statistical analysis was performed by analysis of variance (ANOVA). Statistical significance was set at $p < 0.05$.

2.4. Design and fabrication of 3D customized hybrid devices for large cranial defects

Previous results obtained from image capture and analysis techniques were used to generate a 3D virtual model of a skull with a large cranial defect (Figure 2.2).

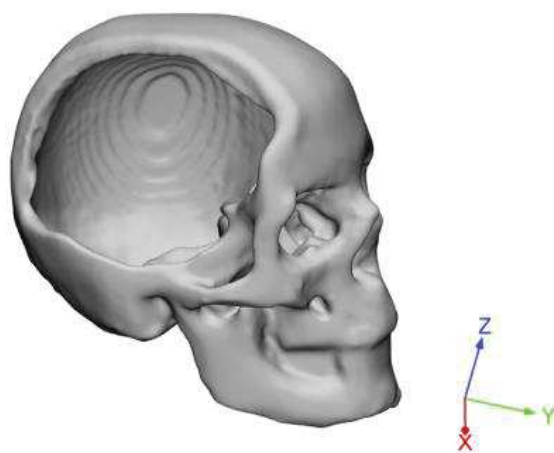


Figure 2.2. 3D reconstruction of a skull with a large cranial defect. The images were analyzed starting from a previous 3D scanning process [1,2].

SolidWorks®2017 (Dassault Systemes, Paris, France) computer-aided design (CAD) system was employed to create 3D customized porous models of devices for cranioplasty.

Starting from a non-porous geometrical model, a porous model was then created while maintaining constant a porosity of about 50% to allow the cement infiltration (Figure 2.3) [2].

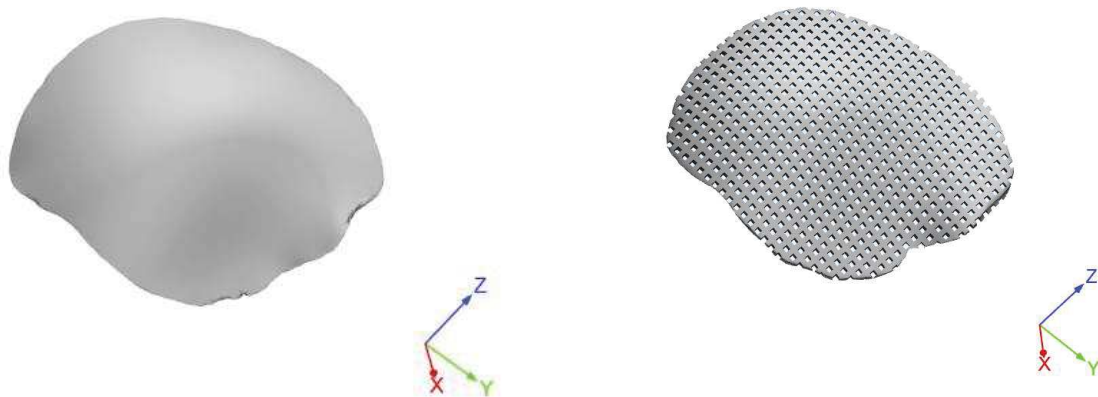


Figure 2.3. 3D geometrical models of a customized device for large cranial defect: non-porous model (left); model with interconnected pore network.

Customized devices consisting of PCL or PLA were also additive manufactured by FDM. As an example figure 2.4 reports an image of two models of customized PCL devices for large cranial defect.

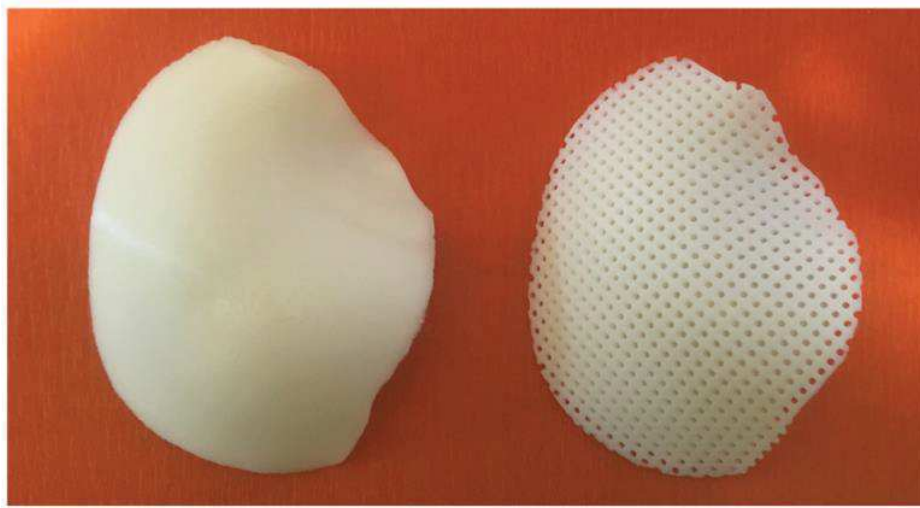


Figure 2.4. 3D additive manufactured devices for large cranial defect: non-porous model (left); model with interconnected pore network (right).

3D hybrid devices were physically obtained through cement infiltration (PMMA/Cu-TCP 97.5/2.5 w/w) in the fully interconnected pore network of the 3D additive manufactured structures. An external upper layer of bone cement was properly realized [2]. Thus, the additive manufactured hybrid structures were also geometrically modeled (Figure 2.5).



Figure 2.5. 3D geometrical models of a customized hybrid device for large cranial defect: top view evidencing the external cement layer (left); bottom view highlighting the cement infiltration in the fully interconnected pore network. Green color was chosen to identify the cement component of the hybrid device.

2.2.5 Theoretical impact analysis

The geometry of an adult human head was obtained from a previous study [1]. Benefiting from early studies [48,49], the main anatomical features were modeled (i.e, skull, falx, tentorium, subarachnoid space, scalp, cerebrum, cerebellum, brainstem), also taking into account their properties [2].

Scalp (16.7 MPa, 0.42), cerebral spinal fluid (CSF) (0.012 MPa, 0.49), tentorium (31.5 MPa, 0.45) and falx (31.5 MPa, 0.45) were assumed to be isotropic, homogeneous and elastic. The values reported in the brackets are the elastic modulus and Poisson's ratio for the different element of the model [2].

Brain was assumed to be viscoelastic considering the shear relaxation behavior with G_0 (1.66 kPa) and G_∞ (0.93 kPa) as the short-term and long-term shear modulus, respectively, and b (16.95 s^{-1}) as the decay coefficient [2,49,50]. A three-layer shell was employed to model the skull, the aim being to represent the external table, the intermediate porous layer and the inner table of human cranial bone. With regard to the cortical bone (i.e., inner and outer table) an elastic modulus of 15,000 MPa and a Poisson's ratio of 0.22 were considered, whereas values of 1,000 MPa and 0.24 were used for the cancellous bone [2,49].

The customized additive manufactured hybrid device consisting of PCL (380 MPa, 0.40) and the infiltrated PMMA/Cu-TCP (97.5/2.5 w/w) bone cement (3,200 MPa, 0.30) were the further components of the finite element analysis (FEA) model. Concerning the cement, the external upper layer and the part infiltrated into the interconnected pore network were modeled as a single block component [2].

The entire head model with the hybrid device for the large cranial defect was imported into HyperMesh[®] (HyperWorks[®], Altair Engineering Inc., Troy, MI, USA).

A 3D mesh was properly generated, adequate mesh size and mesh refinement techniques were used. Different contact types were considered for the several parts of the head [2]. Surface-to-surface contacts were used between the scalp and skull as well as between the scalp and the external cement

layer of the hybrid device. Tied surface-to-surface contacts were considered in the case of the other elements. Impact analysis was performed using Altair Radioss™ (Altair Engineering Inc., Troy, MI, USA), which is a structural analysis solver for highly non-linear problems under dynamic loadings. To simulate severe impact conditions, the head model was impacted on the region of the customized hybrid device by a 50 mm diameter rigid sphere (elastic modulus of 210,000 MPa, Poisson's ratio of 0.30, mass of 0.463 kg) moving at a speed of 7 m/s along the x-axis (opposite verse) (Figure 2.6) [2]. The impactor was in contact with the scalp surface. A friction coefficient of 0.3 was considered between the scalp and the impactor. The whole head was properly constrained. The von Mises stress distributions were evaluated for the different components of the model.

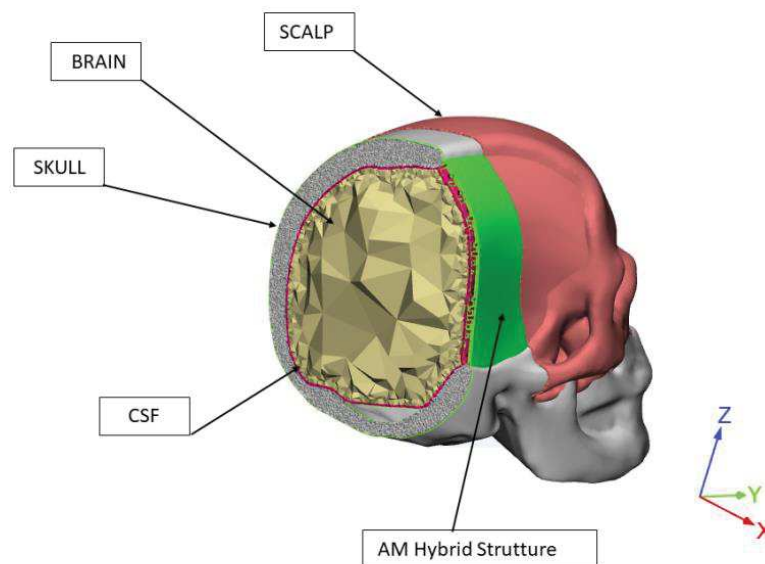


Figure 2.6. A simplified image reporting some components of the FEA model.

2.3. Results and Discussion

Figure 2.7 reports temperature peaks measured during setting of PMMA and PMMA/Cu-TCP bone cement. Mean peak temperature of plain PMMA cement ($98.9\text{ °C} \pm 7.0\text{ °C}$) was not significantly different than that of PMMA/Cu-TCP ($95.8\text{ °C} \pm 6.3\text{ °C}$). Irrespective of the type of bone cement,

mean peak temperature of the cement-infiltrated PLA structure (PLA/PMMA) was significantly lower than that of the plain cements ($p < 0.05$). Furthermore, no statistically significant differences were found between PLA/PMMA ($78.2 \text{ }^\circ\text{C} \pm 4.5 \text{ }^\circ\text{C}$) and PLA/PMMA/Cu-TCP ($77.0 \text{ }^\circ\text{C} \pm 4.9 \text{ }^\circ\text{C}$). Anyway, peak temperatures recorded for PCL structures infiltrated with bone cement ($p < 0.05$) were significantly lower than those found for the PLA ones [2]. However, in terms of mean peak temperature, no significant differences were observed between PCL/PMMA ($69.5 \text{ }^\circ\text{C} \pm 5.1 \text{ }^\circ\text{C}$) and PCL/PMMA/Cu-TCP ($67.8 \text{ }^\circ\text{C} \pm 4.9 \text{ }^\circ\text{C}$).

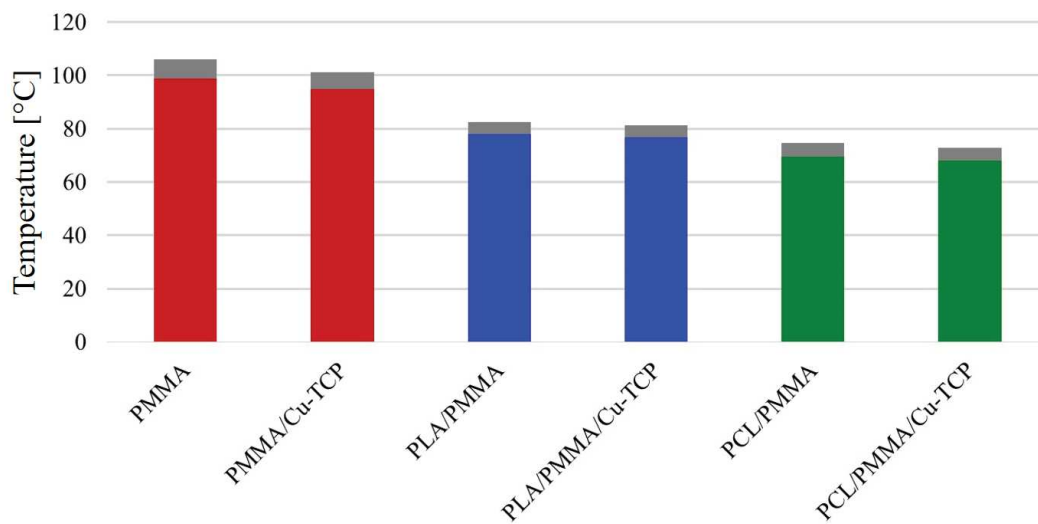


Figure 2.7. Temperature peaks measured during setting in the case of plain bone cements (PMMA, PMMA/Cu-TCP) and hybrid structures consisting of 3D PLA or PCL networks infiltrated with cement. Statistical analysis was performed by analysis of variance (ANOVA). Statistical significance was set at $p < 0.05$.

Figure 2.7 shows that peak temperature levels occurring in the setting of PMMA and PMMA/Cu-TCP cements are higher than $90 \text{ }^\circ\text{C}$. As PMMA cements are used in conjunction with porous polyester structures, a significant reduction in the temperature peak level can be observed.

This temperature reduction is partially due to the amount of the acrylic resin [2]. In fact, PLA and PCL structures have a fully interconnected porosity of 50%, therefore the polyester structures

infiltrated with PMMA presents a volume amount of acrylic resin which equals to the half of that of plain PMMA specimens. Hence, the heat developed through the polymerization phase of plain PMMA specimen is higher than that occurring in PLA/PMMA and PCL/PMMA. The further reduction in peak temperature observed for PCL/PMMA and PCL/PMMA/Cu-TCP can be ascribed to the peculiar thermal feature of this aliphatic polyester. PCL is a thermoplastic polymer with a melting temperature of about 60 °C, also showing a thermal regulating capability as PMMA polymerization is concerned [2,51].

Figure 2.8 reports the temperature profiles obtained for the plain bone cement as well as in the case of PLA and PCL structure infiltrated with PMMA. Although the PLA structures infiltrated with PMMA showed a temperature peak significantly lower ($p < 0.05$) than the plain bone cement, a similar temperature profile was observed. Indeed, looking at Figure 2.8 a different temperature profile can be distinguished for PCL structures infiltrated with PMMA during the cooling phase.

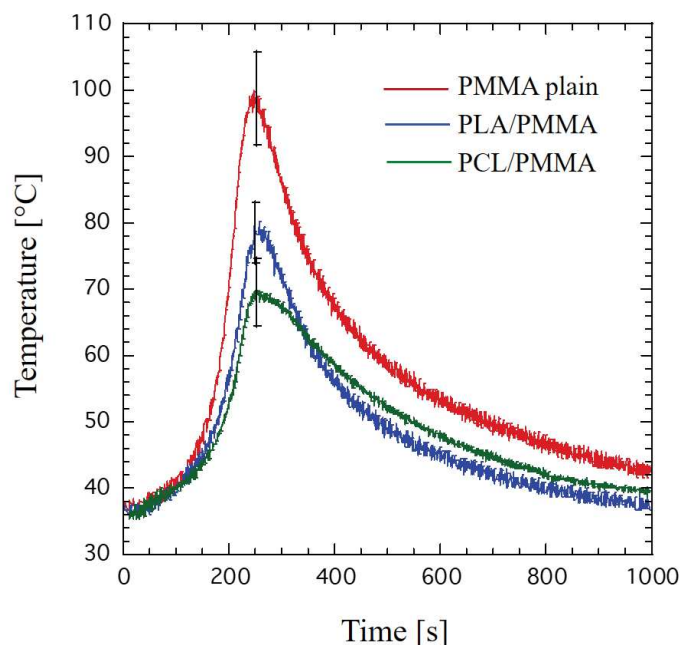


Figure 2.8. An example of temperature profiles: plain bone cement, PLA and PCL structures infiltrated with PMMA, evidencing some differences during the cooling phase.

The endothermic process, which is due to the phase change and should mainly occur at the PCL fiber surface, should compensate the exothermal polymerization reaction [2]. The effect is a further significant reduction in peak temperature (Figure 2.7). The heat absorbed by the PCL phase in the melting stage is then released in the cooling stage of PCL/PMMA (Figure 2.8). Even though the employed PLA has a melting point of 135 °C (i.e., higher than that of PCL), it has a glass transition temperature of about 55-60 °C, and it is well known that the glass–rubber transition occurs as the temperature is increased [2]. However, as a consequence, the cooling profile of PCL/PMMA is more spread than that of PLA/PMMA over the observed time period.

Contextually, an integrated approach involving the combination of RE and AM was considered to design virtual and physical models of customized devices for large cranial defects [2].

A skull model containing a large cranial defect was previously 3D printed by integrating the RE and AM approaches [1]. An inkjet printer was used to additively manufacture the 3D physical model of the skull (Figure 2.9).



Figure 2.9. Images of the 3D physical model of a skull with a large cranial defect, which was previously fabricated by inkjet printing, starting from image capture and analysis techniques [1,2]: top-front view (left) and lateral view (right).

Virtual models of the skull with the large defect and the additive manufactured prosthetic device were created. Starting from the shape and size of the large cranial defect, the geometry of the porous device was properly designed to be fitted in the large defect cavity.

The feasibility of the proposed technical solutions was preliminarily assessed through virtual and physical models (Figure 2.10), evidencing the potential to adapt and conform the device to the contours of the large cranial defect.

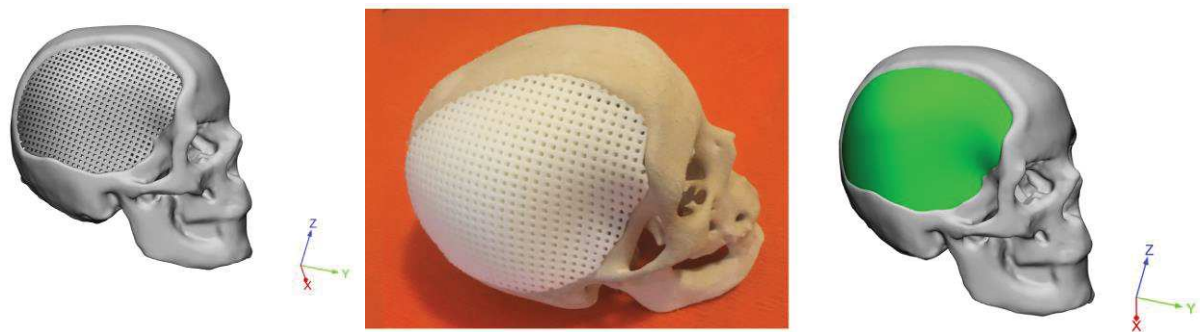


Figure 2.10. Feasibility of the reported technical solutions: images of virtual (left) and physical (center) models of skull with 3D additive manufactured PCL porous structure for large cranial defect 3D porous structure; image of virtual model of skull with 3D hybrid device (3D PCL porous structure infiltrated with PMMA/Cu-TCP 97.5/2.5 bone cement) for large cranial defect (right).

The mechanical and morphological properties of different kinds of bone cements [2,10,16,17] as well as of 3D printed PCL and PLA structures [43,44,47,52] were already investigated. The consistency between real and theoretical values of the fiber diameter and pore size was assessed through scanning electron microscopy and micro-computed tomography. In particular, the effects of the designed lay-down patterns (i.e., sequences of fiber stacking), as well as of the pore shape and size, on the

mechanical (e.g., modulus, maximum stress), mass transport and biological performances of 3D additive manufactured PCL structures were reported and also discussed from the tissue engineering perspective [2,43,44,47].

It has been frequently reported that traumatic brain injury is generally related to road traffic accidents, falls, sports, bullets, explosions and other kinds of external forces [2,49,53]. Road traffic accidents cause mortalities and most serious head injuries [2,49]. Moreover, measurements of the intracerebral local field potential are generally performed to monitor the brain activity and to further understand the information flow across the neural networks.

In this context, a nano/micro-scale porous surface topology was also considered to develop enhanced neural electrodes able to measure higher amplitudes with lower noise levels, if compared to the conventional brain electrodes [54].

However, head impact injury represents a critical societal challenge as it may be considered the leading cause of disability and death [2,49].

Accordingly, it results fundamental to understand the injury mechanisms of the head as a consequence of trauma events through a biomechanical analysis.

Basically, this should be important for healthy people and especially for people using prosthetic devices for large cranial defects. For this reason, over the past years most of researchers' attention has been focused on the development of protection strategies and FEA models for a better understanding of the biomechanical response of the entire head in severe impact conditions.

Besides traumatic brain injury, severe head injuries such as skull fracture obviously need further analyses. In this scenario, some scientific works have already reported experimental and theoretical studies on the skull and brain responses in several impact conditions (e.g., free falls, blunt and ballistic impacts), in many cases involving different kinds of impactors and tests on cadavers [48,49,55-60].

An advanced human head finite element model was also developed using a multi-block approach to predict skull response and brain pressure [49].

To the best of the authors' knowledge, none of the above mentioned human head models considered the impact-related features in the case of people using prosthetic devices for a large cranial defect. Benefiting from previous models and results [48,49,55-60], in the current research an entire head model was developed also taking into account the presence of the designed hybrid device for a large cranial defect as well as a direct impact on the implant region of the head in severe conditions [2]. A preliminary FEA provided information in terms of von Mises stress distributions in the different components of the model (Figures 2.11 and 2.12).

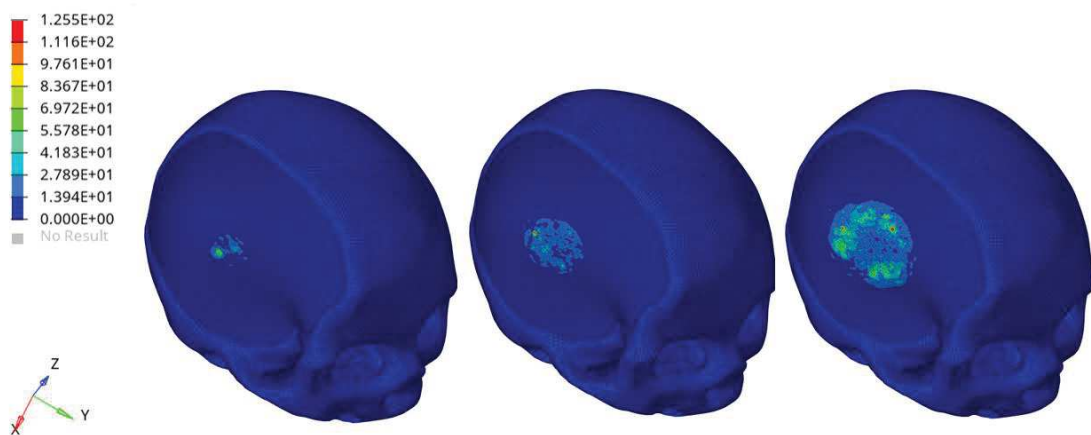


Figure 2.11. Biomechanical response as a result of the rigid sphere impacting the implant region of the head: von Mises stress (MPa) distributions for the external cement layer of the hybrid device at three different times after the initial impact (left). The figure is a guide for the eye to see the effect of the impact for the selected component. The color scale was chosen to allow for comparison among the models at different times.

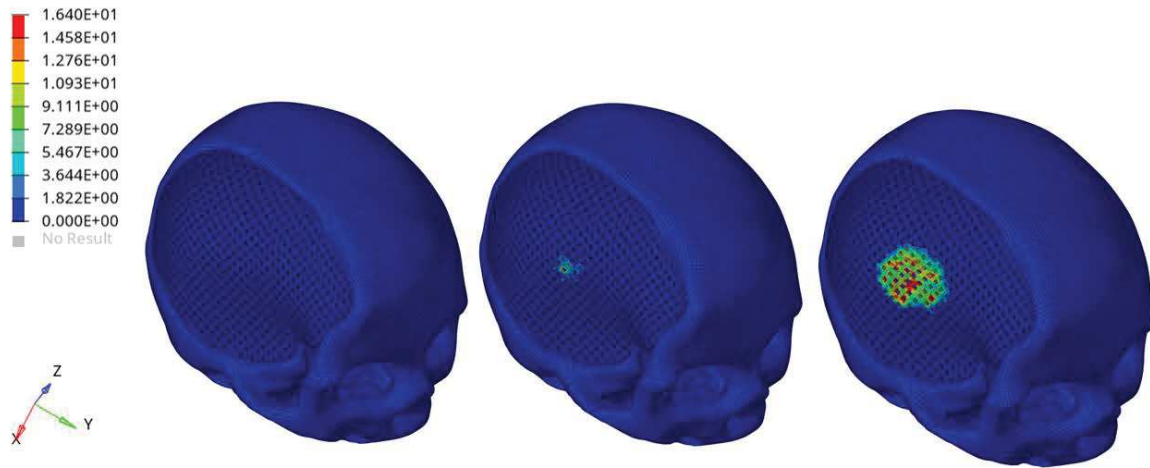


Figure 2.12. Biomechanical response as a result of the rigid sphere impacting the implant zone region of the head: von Mises stress (MPa) distributions for the 3D PCL structure underneath the external cement layer and infiltrated with the bone cement, at three different times after the initial impact (left). Bone cement was removed to visualize the effect of the impact for the selected component. The color scale was chosen to allow for comparison among the models at different times.

In figures 2.11 and 2.12, the color scale was chosen to allow for comparison among the models at different times. Stress results on the external cement layer was of the same order of magnitude of those reported for the skull obtained using a rigid hemispherical anvil (radius of 48 mm, density of 2700 kg/m³, elastic modulus of 70,000 MPa, Poisson's ratio of 0.33, mass of 1.234 kg) and speeds of 7.6, 7.3 and 7.1 m/s toward the head [49].

A specific number of elements clearly failed in the external cement layer of the hybrid device as a consequence of the impact of the rigid sphere (Figure 2.11), which represents a severe impact condition. However, the obtained FEA results also suggested that the impact did not significantly alter the mechanical stability of the 3D PCL structure infiltrated with the bone cement and underneath the external cement layer (Figure 2.12). The presence of the PCL porous structures embedded in the cement would also create a toughening effect, however increasing the ability of the hybrid device to absorb energy and deform before failure [2].

Moreover, a brief estimation of the minimum pressure for CSF and von Mises stress for the brain was also made. Even though the direct impact mainly caused the failure of some elements of the external cement layer, the analysis provided values of CSF minimum pressure and brain von Mises stress which should not lead to subdural haematomas (SDH) and diffuse axonal injuries (DAI), also considering the results computed with previous models as well as the corresponding injury risk curves for healthy people [61].

Although the current research provided an integrated approach to design 3D additively manufactured hybrid structures for large cranial defects, several limitations concerning the preliminary theoretical analysis need to be summarized: i) lack of validation of the model-predicted brain motion against the results already reported in the literature as well as of the inclusion of brain motion-related physics (e.g., bridging veins) [62-64]; ii) head-neck complex was not considered, even if neck is generally not taken into account when the impact time would be too short for it to affect the kinematic response of the head [48,49]; iii) physical features of the white matter (e.g., fiber orientation anisotropy) were missing.

Anyway, it is worth remembering that as the development of devices for large cranial defects is one of the most investigated and controversial topics in cranioplasty, contradictory opinions still remain about clinical procedures, materials and modeling features (e.g., elastic or viscoelastic behavior and material parameters for some components) [2].

For this reason, the present study may be also considered as a first step of a future research in which a complex model with more physical features will be analyzed.

2.4. Conclusions

Despite the limitations of the current research, the following conclusions were drawn:

1. Peak temperatures measured for hybrid PCL/PMMA ($69.5\text{ °C} \pm 5.1\text{ °C}$) and PCL/PMMA/Cu-TCP ($67.8\text{ °C} \pm 4.9\text{ °C}$) were lower than those found for the PLA-based ones.

2. An integrated design strategy was employed to develop 3D hybrid devices for large cranial defects, involving RE, AM and a modified PMMA bone cement (PMMA/Cu-TCP 97.5/2.5 w/w). The feasibility of the proposed technical solutions was validated through virtual and physical models.
3. A theoretical impact analysis was preliminarily carried out on the entire head model. Severe conditions were simulated considering a rigid sphere impacting the implant zone of the head for people with the customized PCL/PMMA/Cu-TCP device. FEA results suggested that the impact caused the failure of some elements of the external cement layer, without significantly altering the mechanical of the underneath PCL structure infiltrated with the cement.

However, even though mechanical and morphological analyses were already performed on the 3D additive manufactured structures, strong limitations are clearly related to FEA which can make an overall conclusion about the designed 3D hybrid devices surely difficult as further experimental tests must be carried out (e.g., several impact conditions, cadavers, analysis of the 3D network-cement interface, *in vivo* studies) and compared to the results obtained from simulations [2]. The achieved findings should probably help to improve predictions of the impact of the proposed hybrid devices in cranioplasty research as well as in clinical practice. Anyway, the current research can contribute to provide a further insight into the development of alternative devices for the repair of large cranial defects and may be also considered as the first step of a future complex research, aiming at the evaluation of the *in vitro* and *in vivo* performances of such devices.

2.5. References

- [1] De Santis, R.; Gloria, A.; Ambrosio, L. Materials and technologies for craniofacial tissue repair and regeneration. *Top. Med.* 2010, 16, 1-6.
- [2] De Santis, R.; Russo, T.; Rau, J.V.; Papallo, I.; Martorelli, M.; Gloria, A. Design of 3D Additively Manufactured Hybrid Structures for Cranioplasty. *Materials* 2021, 14, 181.

- [3] Unterhofer, C.; Wipplinger, C.; Verius, M.; Recheis, W.; Thomé, C.; Ortler, M. Reconstruction of large cranial defects with poly-methyl-methacrylate (PMMA) using a rapid prototyping model and a new technique for intraoperative implant modeling. *Neurol Neurochir Pol.* 2017, 51(3), 214-220.
- [4] Lee, S.C.; Wu, C.T.; Lee, S.T.; Chen, P.J. Cranioplasty using polymethyl methacrylate prostheses. *J Clin Neurosci.* 2009,16(1), 56-63.
- [5] Harris, D.A.; Fong, A.J.; Buchanan, E.P.; Monson, L.; Khechoyan, D.; Lam, S. History of synthetic materials in alloplastic cranioplasty. *Neurosurgical Focus.* 2014, 36(4), E20.
- [6] De Santis, R.; Mollica, F.; Ambrosio, L.; Nicolais, L.; Ronca, D. Dynamic mechanical behavior of PMMA based bone cements in wet environment. *J. Mater. Sci.: Mater. Med.* 2003, 14(7), 583-594.
- [7] Spence, W.T. Form-fitting plastic cranioplasty. *J. Neurosurg.* 1954, 11(3), 219-225.
- [8] Bloch, O.; McDermott, M.W. In situ cranioplasty for hyperostosing meningiomas of the cranial vault. *Can. J. Neurol. Sci.* 2011, 38(1), 59-64.
- [9] McElhaney, J.H.; Fogle, J.L.; Melvin, J.W.; Haynes, R.R.; Roberts, V.L.; Alem, N.M. Mechanical properties on cranial bone. *J. Biomech.* 1970, 3(5), 495-511.
- [10] Ronca, D.; Gloria A.; De Santis, R.; Russo, T.; D'Amora, U.; Chierchia, M.; et al. Critical analysis on dynamic-mechanical performance of spongy bone: the effect of an acrylic cement. *Hard Tissue.* 2014, 3(1), 9-16.
- [11] Caro-Osorio, E.; De la Garza-Ramos, R.; Martínez-Sánchez, S.R; Olazarán-Salinas, F. Cranioplasty with polymethylmethacrylate prostheses fabricated by hand using original bone flaps: Technical note and surgical outcomes. *Surg Neurol Int.* 2013, 8, 136.
- [12] Matsuno, A.; Tanaka, H.; Iwamuro, H.; Takanashi, S.; Miyawaki, S.; Nakashima, M.; Nakaguchi, H.; Nagashima, T. Analyses of the factors influencing bone graft infection after delayed cranioplasty. *Acta Neurochir.* 2006, 148, 535–540.

- [13] Minelli, E.B.; Della Bora, T.; Benini, A. Different microbial biofilm formation on polymethylmethacrylate (PMMA) bone cement loaded with gentamicin and vancomycin. *Anaerobe* 2011, 17 (6), 380-383.
- [14] Worm, P.V.; do Nascimento, T.L.; do Couto Nicola, F.; Sanches, E.F.; dos Santos Moreira, C.F.; et al. Polymethylmethacrylate imbedded with antibiotics cranioplasty: An infection solution for moderate and large defects reconstruction? *Surg Neurol Int.* 2016, 7 (Suppl 28), S746–S751.
- [15] Oei, J.D.; Zhao, W.W.; Chu, L.; DeSilva, M.N.; Ghimire, A.; Rawls, H.R.; et al. Antimicrobial acrylic materials with in situ generated silver nanoparticles. *J Biomed Mater Res B.* 2012, 100(2), 409-415.
- [16] Russo, T.; Gloria, A.; De Santis, R.; D'Amora, U.; Balato, G.; Vollaro, A.; et al. Preliminary focus on the mechanical and antibacterial activity of a PMMA-based bone cement loaded with gold nanoparticles. *Bioact Mater.* 2017, 2(3), 156-161.
- [17] Russo, T.; De Santis, R.; Gloria, A.; Barbaro, K.; Altigeri, A.; Fadeeva, I. V.; Rau, J. V. Modification of PMMA Cements for Cranioplasty with Bioactive Glass and Copper Doped Tricalcium Phosphate Particles. *Polymers* 2020, 12(1), 37.
- [18] Jaber, J.; Gambrell, K.; Tiwana, P.; Madden, C; Finn, R. Long-term clinical outcome analysis of poly-methyl-methacrylate cranioplasty for large skull defects. *J. Oral Maxillofac. Surg.* 2013, 71(2), e81-88.
- [19] Saringer, W.; Nöbauer-Huhmann, I.; Knosp, E. Cranioplasty with individual carbon fibre reinforced polymere (CFRP) medical grade implants based on CAD/CAM technique. *Acta Neurochir.* 2002, 144 (11), 1193-1203.
- [20] Peltola, M.J.; Vallittu, P.K.; Vuorinen, V.; Aho, A.A.; Puntala, A.; Aitasalo, K.M. Novel composite implant in craniofacial bone reconstruction. *Eur Arch Otorhinolaryngol.* 2012, 269(2), 623-628.

- [21] Msallem, B.; Beiglboeck, F.; Honigmann, P.; Jaquiéry, C.; Thieringer, F. Craniofacial reconstruction by a cost-efficient template-based process using 3d printing. *Plast Reconstr Surg Glob Open*. 2017, 5(11), e1582.
- [22] Van Putten, M.C. Jr; Yamada, S.; Alloplastic cranial implants made from computed tomographic scan-generated casts. *J Prosthet Dent*. 1992, 68(1), 103-108.
- [23] Arridge, S., Moss, J.P.; Linney, A.D; James, D.R. Three dimensional digitization of the face and skull. *J. Maxillofac. Surg*. 1985, 13, 136-143.
- [24] Mertens, C.; Wessel, E.; Berger, M.; Ristow, O.; Hoffmann, J.; Kansy, K.; Freudlsperger, C.; Bächli, H.; Engel, M. The value of three-dimensional photogrammetry in isolated sagittal synostosis: Impact of age and surgical technique on intracranial volume and cephalic index— a retrospective cohort study. *Craniofacial Surg* 2017, 45(12), 2010-2016.
- [25] Cheng, C.H.; Chuang, H.Y.; Lin, H.L., Liu, C.L.; Yao, C.H. Surgical results of cranioplasty using three-dimensional printing technology. *Clin Neurol Neurosurg*. 2018, 168, 118-123.
- [26] Dean, D.; Min, K.J. ; Bond, A. Computer aided design of large-format prefabricated cranial plates. *J. Craniofac. Surg*. 2003, 14(6), 819-832.
- [27] De Santis, R., D'Amora, U.; Russo, T.; Ronca, A.; Gloria, A.; Ambrosio, L. 3D fibre deposition and stereolithography techniques for the design of multifunctional nanocomposite magnetic scaffolds. *J. Mater. Sci. Mater. Med*. 2015, 26(10), 250.
- [28] Maricevich, J.P.; Cezar-Junior, A.B.; de Oliveira-Junior, E.X.; Silva, J.A.; da Silva, J.V.; Nunes, A.A.; et al. Functional and aesthetic evaluation after cranial reconstruction with polymethyl methacrylate prostheses using low-cost 3D printing templates in patients with cranial defects secondary to decompressive craniectomies: A prospective study. *Surg Neurol Int*. 2019, 117, 443-452.
- [29] Chim, H. ; Schantz, J.T. New frontiers in calvarial reconstruction: integrating computer-assisted design and tissue engineering in cranioplasty. *Plast Reconstr Surg*. 2005, 116(6), 1726-1741.

- [30] Espalin, D.; Arcaute, K.; Rodriguez, D.; Medina, F.; Posner, M. ; Wicker, R. Fused deposition modeling of patient-specific polymethylmethacrylate implants. *Rapid Prototyp J.* 2010, 16(3), 164-173.
- [31] Hassan, M.N.; Yassin, M.A.; Suliman, S.; Lie, S.A.; Gjengedal, H.; Mustafa, K. The Bone Regeneration Capacity of 3D-Printed Templates in Calvarial Defect Models: A Systematic Review and Meta-Analysis. *Acta Biomater.* 2019, 91, 1-23.
- [32] Gloria, A.; De Santis, R.; Ambrosio, L. Polymer-based composite scaffolds for tissue engineering. *J. Appl. Biomater. Biomec.* 2010, 8(2), 57-67.
- [33] Sinikovic, B.; Schumann, P.; Winkler, M.; Kuestermeyer, J.; Tavassol, F.; von See, C; et al. Calvaria bone chamber—a new model for intravital assessment of osseous angiogenesis. *J. Biomed. Mater. Res. A.* 2011, 99(2), 151-157.
- [34] Gephart, M.G.H.; Woodard, J.I.; Arrigo, R.T.; Lorenz, H.P.; Schendel, S.A.; Edwards, M.S.B.; et al. 2013. Using bioabsorbable fixation systems in the treatment of pediatric skull deformities leads to good outcomes and low morbidity. *Childs Nerv Syst* 2013, 29(2), 297-301.
- [35] Chao, M.T.; Jiang, S.; Smith, D.; DeCesare, G.E.; Cooper, G.M.; Pollack, I.F., et al. Demineralized bone matrix and resorbable mesh bilaminar cranioplasty: a novel method for reconstruction of large-scale defects in the pediatric calvaria. *Plast Reconstr Surg.* 2019, 123(3), 976-982.
- [36] De Santis, R.; Gloria, A.; Russo, T.; D'Amora, U.; Zeppetelli, S.; Tampieri, A.; et al. A route toward the development of 3D magnetic scaffolds with tailored mechanical and morphological properties for hard tissue regeneration: Preliminary study. *Virtual and Physical Prototyping* 2011, 6(4), 189-195.
- [37] Russo, L.; Gloria, A.; Russo, T.; D'Amora, U.; Taraballi, F.; De Santis, R.; et al. Glucosamine grafting on poly (ϵ -caprolactone): a novel glycosylated polyester as a substrate for tissue engineering. *RSC Adv.* 2013,3(18), 6286-6289.

- [38] Schantz, J.T.; Teoh, S.H.; Lim, T.C.; Endres, M.; Lam, C.X.; Hutmacher, D.W. Repair of calvarial defects with customized tissue-engineered bone grafts I. Evaluation of osteogenesis in a three-dimensional culture system. *Tissue eng.* 2003, 9(4, Supplement 1), 113-126.
- [39] Schantz, J.T.; Hutmacher, D.W.; Lam, C.X.; Brinkmann, M.; Wong, K.M.; Lim, T.C.; et al. Repair of calvarial defects with customised tissue-engineered bone grafts II. Evaluation of cellular efficiency and efficacy in vivo. *Tissue eng.* 2003, 9(4, Supplement 1), 127-139.
- [40] Askari, M.; Naniz, M.A.; Kouhi, M.; Saberi, A.; Zolfagharian, A.; Bodaghi M. Recent progress in extrusion 3D bioprinting of hydrogel biomaterials for tissue regeneration: a comprehensive review with focus on advanced fabrication techniques. *Biomater Sci* 2020 Nov 13. Online ahead of print.
- [41] Bodaghi, M.; Liao, W.H. 4D printed tunable mechanical metamaterials with shape memory operations. *Smart Mater. Struct.* 2019, 28, 045019.
- [42] Bodaghi, M.; Zolfagharian, A.; Serjouei, A.; et al. Reversible Energy Absorbing Meta-Sandwiches by 4D FDM Printing. *Int J Mech Sci.* 2020,173, 105451.
- [43] Domingos, M.; Chiellini, F.; Gloria, A.; Ambrosio, L.; Bartolo, P.; Chiellini, E. Effect of process parameters on the morphological and mechanical properties of 3D Bioextruded poly(ϵ -caprolactone) scaffolds. *Rapid Prototyping Journal* 2012, 18, 56-67.
- [44] Domingos, M.; Intranuovo, F.; Russo, T.; Santis, R.D.; Gloria, A.; Ambrosio, L.; Ciurana, J.; Bartolo, P. The first systematic analysis of 3D rapid prototyped poly(ϵ -caprolactone) scaffolds manufactured through BioCell printing: The effect of pore size and geometry on compressive mechanical behaviour and in vitro hMSC viability. *Biofabrication* 2013, 5, 045004.
- [45] Gonçalves F.A.M.M.; Fonseca A.C.; Domingos M.; Gloria A.; Serra A.C.; Coelho J.F.J. The potential of unsaturated polyesters in biomedicine and tissue engineering: Synthesis, structure-properties relationships and additive manufacturing. *Prog. Polym. Sci.* 2017, 68, 1–34.
- [46] Moxon, S.R.; Ferreira, M.J.; Santos, P.; Popa, B.; Gloria, A.; Katsarava, R.; Tugushi, D.; Serra, A.C.; Hooper, N.M.; Kimber, S.J.; Fonseca, A.C.; Domingos, M.A.N. A Preliminary Evaluation of

- the Pro-Chondrogenic Potential of 3D-Bioprinted Poly(ester Urea) Scaffolds. *Polymers* 2020, 12, 1478.
- [47] Rocco, N.; Papallo, I.; Nava, M.B.; Catanuto, C.; Accurso, A.; Onofrio, I.; et al. Additive manufacturing and technical strategies for improving outcomes in breast reconstructive surgery. *ACTA IMEKO* 2020, 9(4), 74-79.
- [48] Caroline, Deck and Willinger Rémy. Head injury prediction tool for protective systems optimisation. Proceedings of the 7th European LS-DYNA Conference, 2009.
- [49] Zhihua, C.; Yun, X.; Zheng, B; Haojie, M. Creating a human head finite element model using a multi-block approach for predicting skull response and brain pressure. *Comput Methods Biomech Biomed Engin.* 2019, 22(2), 169-179.
- [50] Takhounts, E.G.; Ridella, S.A.; Hasija, V.; Tannous, R.E.; Campbell, J.Q.; Malone, D.; Danelson, K.; Stitzel, J.; Rowson, S.; Duma, S. Investigation of traumatic brain injuries using the next generation of simulated injury monitor (SIMon) finite element head model. *Stapp Car Crash J.* 2008, 52, 1–31.
- [51] De Santis, R.; Ambrogi, V.; Carfagna, C.; Ambrosio, L.; Nicolais, L. Effect of microencapsulated phase change materials on the thermo-mechanical properties of poly(methyl-methacrylate) based biomaterials. *J Mater Sci Mater Med.* 2006, 17(12), 1219-1226.
- [52] Lanzotti, A.; Martorelli, M.; Maietta, S.; Gerbino, S.; Penta, F.; Gloria, A. A comparison between mechanical properties of specimens 3D printed with virgin and recycled PLA. *Procedia CIRP* 2019, 79, 143-146.
- [53] Tse, K.M.; Lim, S.P.; Tan, V.; Lee, H. A review of head injury and finite element head models. *Am J Eng Technol Soc.* 2014, 1(5), 28–52.
- [54] Lee, S.H.; Lee, K.-S.; Sorcar, S.; Razzaq, A.; Lee, M.-G.; In, S.-I. Novel Porous Brain Electrodes for Augmented Local Field Potential Signal Detection. *Materials* 2019, 12, 542.
- [55] Yoganandan, N.; Pintar, F.A.; Sances Jr, A.; Walsh, P.R.; Ewing, C.L.; Thomas, D.J.; Snyder, R.G. Biomechanics of skull fracture. *J Neurotrauma.* 1995, 12(4), 659–668.

- [56] Yoganandan, N.; Zhang, J.; Pintar, F.A. Force and acceleration corridors from lateral head impact. *Traffic Injury Prevention*. 2004, 5(4), 368–373.
- [57] Raymond, D.; Van Ee, C.; Crawford, G.; Bir, C. 2009. Tolerance of the skull to blunt ballistic temporo-parietal impact. *J Biomech*. 42(15), 2479–2485.
- [58] Sahoo, D.; Robbe, C.; Deck, C.; Meyer, F.; Papy, A.; Willinger, R. Head injury assessment of non-lethal projectile impacts: A combined experimental/computational method. *Injury*. 2016, 47(11), 2424–2441.
- [59] Zhang, L.; Yang, K.H.; Dwarampudi, R.; Omori, K.; Li, T.; Chang, K.; Hardy, W.N.; Khalil, T.B.; King, A.I. Recent advances in brain injury research: A new human head model development and validation. *Stapp Car Crash J*. 2001, 45, 369–394.
- [60] Mao, H.; Gao, H.; Cao, L.; Genthikatti, V.; Yang, K.H. Development of high-quality hexahedral human brain meshes using feature-based multi-block approach. *Comput Method Biomech Biomed Eng*. 2013,16(3), 271–279.
- [61] Deck, C.; Willinger, R. Improved head injury criteria based on head FE model. *International Journal of Crashworthiness* 2008, 13(6), 667-678.
- [62] Hardy, W.N.; Foster, C.D.; Mason, M.J.; Yang, K.H.; King, A.I.; Tashman S. Investigation of head injury mechanisms using neutral density technology and high-speed biplanar X-Ray. *Stapp Car Crash J*. 2001, 45, 337–368.
- [63] Hardy, W.N.; Mason, M.J.; Foster, C.D.; Shah, C.S.; Kopacz, J.M.; Yang, K.H.; King A.I.; Bishop, J.; Bey, M.; Anderst, W.; Tashman, S. A study of the response of the human cadaver head to impact. *Stapp Car Crash J*. 2007, 51, 17–80.
- [64] Miller, L.E.; Urban, J.E.; Stitzel, J.D. Validation performance comparison for finite element models of the human brain. *Comput Methods Biomech Biomed Eng*. 2017, 20(12), 1273–1288.

Chapter 3

An approach towards the design of technical solutions in skull base reconstruction after endoscopic endonasal surgery

3.1. Introduction

The skull base is considered one of the most complex areas of the human body. A great variety of lesions can arise from such area or successively involve it.

From a surgical point of view, novel craniofacial approaches have been developed to access the entire skull base [1-9].

The recent progresses in terms of technologies, diagnostic imaging techniques and intraoperative neuronavigation systems have contributed to a progressive reduction of the surgical invasiveness.

Currently, the endonasal endoscopic route can represent a suitable approach in the case of skull base lesions [10-12], and the several surgical and technological advances have led to a revolution in skull base surgery [13].

The use of an endoscope has allowed to obtain several benefits for the patients [14]. Anyway, the skull base reconstruction represents the main issue of this method, due to a higher risk of postoperative cerebrospinal fluid (CSF) leakage, if compared to the conventional transcranial approach [15].

Thus, an efficient watertight closure is crucial to isolate the intracranial cavity for the restoration of the natural intra and extradural compartment division, the aim being to prevent postoperative CSF leakage and other complications [16-18].

Different devices may be adopted in the reconstruction, involving autologous grafts and non-autologous materials, individually or combined in a multilayer strategies, as well as further technical solutions [19-23].

The development of novel closure techniques as well as the availability of several reconstructive materials and surgical approaches may provide a great contribution in reducing postoperative CSF leakage [22-26].

In this scenario, further efforts are needed for the development of innovative strategies and devices for reducing CSF leak rates after the endoscopic skull base surgery.

In addition, benefiting from the development of advanced technologies [27] and methodologies of analysis [28-31] in different fields, novel systems can be clearly designed.

The current research has been driven toward the engineering of materials [32,33] and biomedical devices with enhanced and tailored functional properties [34,35].

Novel devices can be developed in the form of injectable or solid systems, according to the specific application and the surgical approach.

With regard to the skull base reconstruction after endoscopic endonasal surgery, intriguing strategies would involve advances in the design of injectable semi-interpenetrating polymer networks (semi-IPNs) and composites, reverse engineering and 3D additive manufactured devices with well defined architectures and mechanical properties [34,35].

In the current study, novel approaches and devices were developed to prevent the postoperative CSF leakage in skull base reconstruction after endoscopic endonasal surgery.

The design strategy involved the use of an injectable tool as filling system and a “solid” customized device as closure system for skull base defects.

3.2. Materials and Methods

The semi-IPNs were prepared by promoting the polymer network formation. Natural and synthetic polymers were employed and also properly modified [2]. Micro/nanoparticles were also used as

reinforcement. The selection of the system components was made with the aim of promoting a clinical translation of the injectable devices as dura mater substitutes and sealant systems able to reduce the risk of CSF leakage [2].

A rheometer (Bohlin Gemini; Malvern Instruments, Malvern, UK) equipped with parallel-plate geometry was used to evaluate the viscoelastic properties of the materials at 37 °C. To determine the linear viscoelastic region, strain sweep tests were carried out at a fixed oscillation frequency. Small amplitude oscillatory shear tests were performed, and the frequency varied from 0.01 to 2 Hz. The storage modulus (G') and the loss modulus (G'') were evaluated as follows:

$$G' = \frac{\tau_0}{\gamma_0} \cos \delta \quad (3.1)$$

$$G'' = \frac{\tau_0}{\gamma_0} \sin \delta \quad (3.2)$$

with δ representing the phase shift between the input and output signals, whereas γ_0 and τ_0 represent the strain and stress amplitudes, respectively [2]. Different clinical needles were considered, and the effect of the injection on the viscoelastic properties was analysed, as it plays a crucial role in the design of injectable systems. Steady shear measurements were carried out, and viscosity as a function of shear rate was evaluated at 37 °C. The shear rate ranged from 0.01 to 10 s⁻¹.

To simulate clinical practice, injectability tests were also performed using an INSTRON 5566 testing machine. By contrast, image capture and analysis techniques were used to generate 3D virtual models of the skull base defects [2]. In particular, 3D reconstruction of the skull base region and defects was performed using computed tomography (CT) and a dedicated software.

The model of a region of the skull base and customised devices for the defects were manufactured by fused deposition modelling using a 3D printer. In particular, Z-Glass filament was used to manufacture models of a skull base region, whereas a very durable and flexible material certified for

medical use (BioFlex, FILOALFA) was employed for the fabrication of customised closure devices for the skull base defects [2].

3.3. Results and Discussion

Starting from some basic concepts and principles, novel strategies may be proposed towards the design of injectable systems and additively manufactured devices for skull base reconstruction after endoscopic endonasal surgery. Recent literature stresses the important role of reverse engineering [2,36-39], computer-aided design (CAD), and finite element analysis [2,40-43], as well as the potential of pushing the research toward the development of design strategies and methodologies of analysis in different fields of application [2,44-47]. The strategy related to the design of injectable semi-IPNs and composites with tailored properties has benefited from specific rheological/mechanical and injectability studies [48]. Injectable devices can also be developed through the combination of conventional methods and additive manufacturing techniques. Some examples of rheological results obtained from analyses performed on semi-IPNs consisting of different materials are reported below. The materials are not specified, the aim being only to stress the importance and the role of the viscoelastic properties and the flow behaviour in the design of the proposed systems, as it is widely reported [2,48] that the potential to tailor their rheological characteristics clearly depends on the employed material combinations. An example, one of the mechanical spectra achieved for the developed semi-IPNs is reported in Figure 3.1.

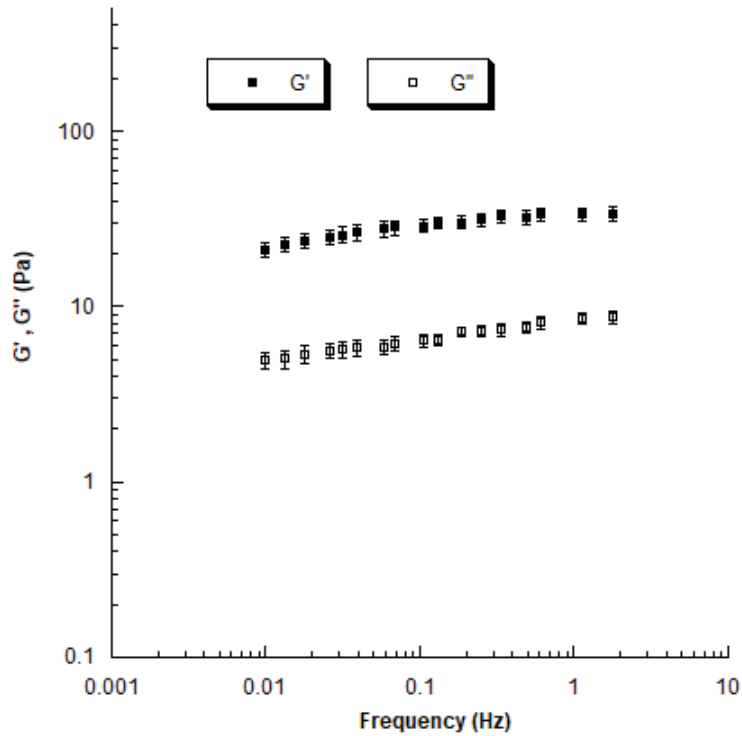


Figure 3.1. Example of storage modulus (G') and loss modulus (G'') as function of frequency for the developed semi-IPNs. Data are reported as mean value, error bar represents the standard deviation.

The G' values were always higher than the G'' values in the analysed frequency range (Figure 3.2). Furthermore, the presence of micro/nanoparticles generally improved both viscoelastic moduli, until a threshold limit value was reached for the particle concentration [2].

Figure 3.2 reports typical values of the viscosity as a function of the shear rate obtained for some engineered semi-IPNs.

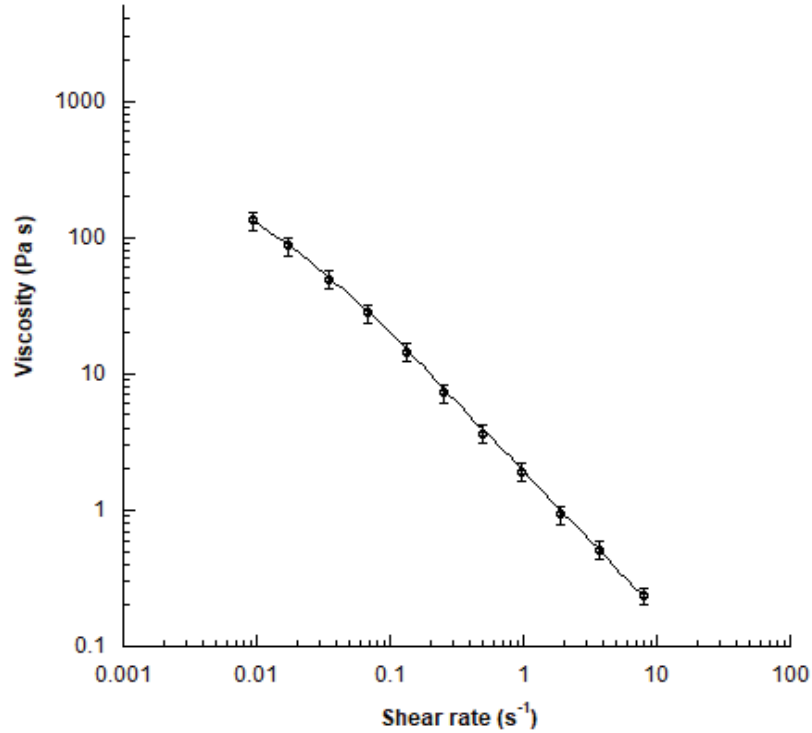


Figure 3.2. Example of viscosity as function of shear rate for the developed semi-IPNs. Data are reported as mean value, error bar represents the standard deviation.

The results showed that the viscosity decreased with the increasing shear rate (shear thinning behaviour), thus suggesting the possibility of injecting the developed materials. Load–displacement curves were obtained from injectability tests. At low displacements, the curves obtained for the semiIPNs showed a linear region until the load reached a maximum value. Successively, the load sharply dropped to a plateau value as the displacement further increased. At the end of the plateau-like region, the material was completely injected [2]. The obtained values for the maximum and plateau loads were in the range of 6.6 – 3.7 N and 2.0 – 0.9 N, respectively, depending on the clinical needle employed and the material composition. By contrast, additive manufacturing techniques offer the opportunity of developing customised devices with complex geometry. Additive manufactured devices with several architectural features can be fabricated by the 3D fibre deposition technique/fused deposition modelling (FDM) [2,34,35]. Starting from CT analysis [2], the surgical approach and the creation of a bone defect (i.e., cavity) were planned (Figures 3.3 and 3.4).

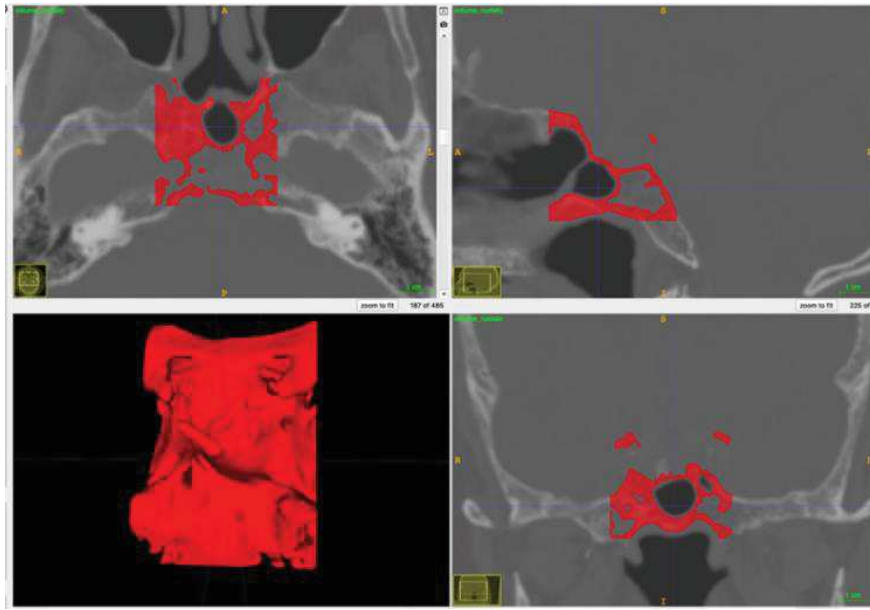


Figure 3.3. Results from image capture and analysis - skull base region.

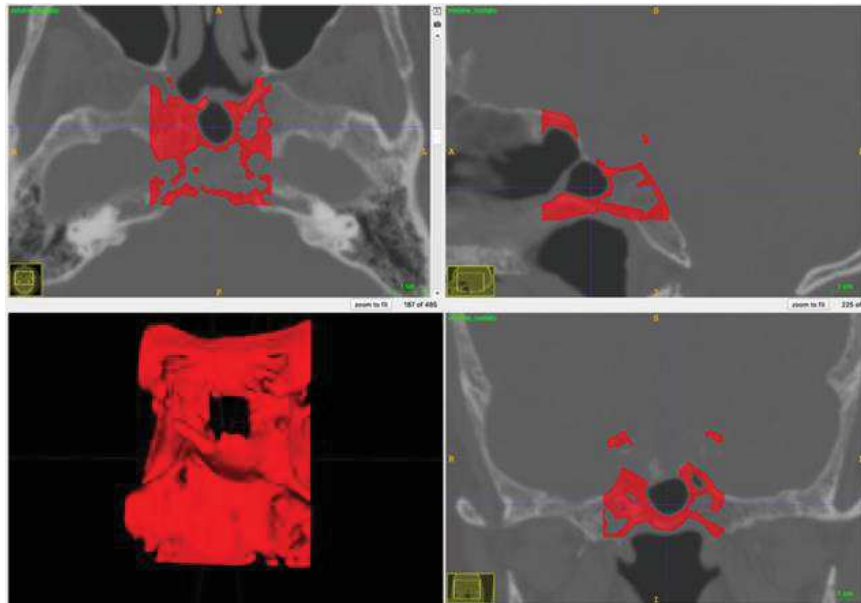


Figure 3.4. Results from image capture and analysis: planning of surgical approach and preparation of a cavity as skull base defect.

Virtual models of a region of the skull base without and with the defect (Figures 3.5 and 3.6), as well as of the customised closure device (Figure 3.7) were created.

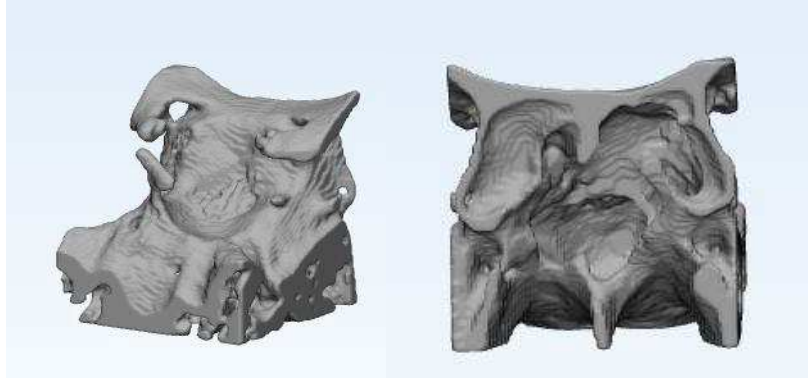


Figure 3.5. 3D reconstruction of a skull base region.

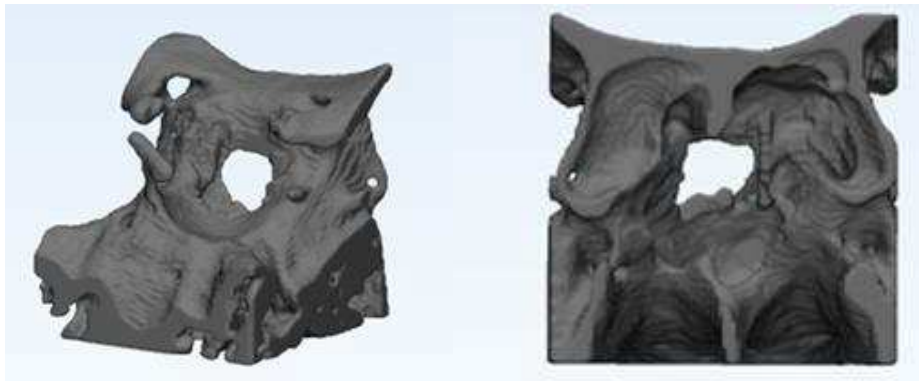


Figure 3.6. 3D reconstruction of a skull base region with the created defect.



Figure 3.7. 3D model of the customized device as closure system for the skull base defect.

Initially starting from the shape and size of the defect, the geometry of the closure device was appropriately designed to be fitted in the cavity to prevent CSF leakage [2].

The feasibility of the proposed technical solutions was first assessed through virtual models (Figure 3.8).

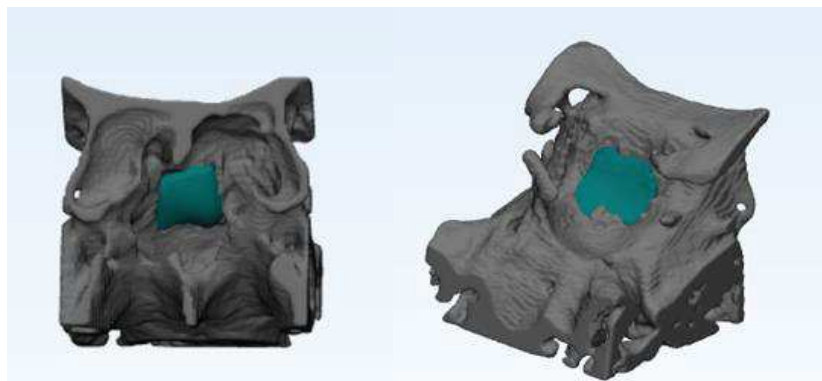


Figure 3.8. 3D model of the device closing the skull base defect - different views. Feasibility assessment of the proposed technical solutions.

Additive manufactured models of a skull base region with the defect were developed using Z-Glass filament (Figure 3.9).



Figure 3.9. 3D Additive manufactured model of a skull base region with the created defect – different views.

3D customised devices with appropriate flexibility were also manufactured by FDM, using BioFlex filament, as a closure system for the created skull base defect (Figure 3.10).



Figure 3.10. 3D Additive manufactured model of the closure device – different views.

In comparison with conventional fabrication methods, additive manufacturing techniques allow strict control of the structural features and, consequently, of the properties of the devices, satisfying all the requirements [2,34,35]. The customised closure devices were suitably developed to provide high flexibility and relatively high strength, according to the specific application.

The physical models were used to simulate clinical practice, and the feasibility of the proposed approach was consequently demonstrated (Figure 3.11).



Figure 3.11. 3D physical model of the device closing the skull base defect – different views.

Feasibility assessment of the proposed technical solutions.

3.4. Conclusions

An insight into the development of novel strategies and devices for skull base defects was provided by integrating rheological/mechanical concepts, image capture and analysis techniques, the CAD approach, and additive manufacturing. Specifically, a systematic study of the design of multifunctional systems in the form of injectable tools and ‘solid’ customised devices was reported in the current research. The focus was set on the importance of viscoelastic properties and the flow behaviour of materials in the case of injectable systems, as well as on the potential to start from the geometry of skull base defects to design additive manufactured closure devices with tailored properties (i.e. flexibility, strength) for the skull base reconstruction after endoscopic endonasal surgery [2]. 3D virtual and physical models allowed the possibility of planning the surgery, as well as assessing the feasibility of the proposed technical solutions.

3.5. References

- [1] R. Fahlbusch, W. Schott, Pterional surgery of meningiomas of the tuberculum sellae and planum sphenoidale: surgical results with special consideration of ophthalmological and endocrinological outcomes, *Journal of neurosurgery* (2002) 96(2) pp.235-243.
- [2] D. Solari, I. Papallo, L. Ugga, L. M. Cavallo, I. Onofrio, R. Cuocolo, G. Improta, A. Brunetti, M. Martorelli, A. Gloria, P. Cappabianca, T. Russo, Novel concepts and strategies in skull base reconstruction after endoscopic endonasal surgery, *ACTA IMEKO*, Volume 9, Number 4, (2020) pp. 67-73.
- [3] T. Kawase, R. Shiobara, S. Toya, Anterior transpetrosal-transtentorial approach for sphenopetroclival meningiomas: surgical method and results in 10 patients, *Neurosurgery* 28(6) (1991) pp. 869-875, discussion pp. 875-866.
- [4] D.A. Lang, G. Neil-Dwyer, F. Iannotti, The suboccipital transcondylar approach to the clivus and cranio-cervical junction for ventrally placed pathology at and above the foramen magnum, *Acta Neurochirurgica* 125(1-4) (1993) pp. 132-137.

- [5] J.D. MacDonald, P. Antonelli, A.L. Day, The anterior subtemporal, medial transpetrosal approach to the upper basilar artery and ponto-mesencephalic junction, *Neurosurgery* (1998) 43(1) pp. 84-89.
- [6] E. Miller, H.A. Crockard, Transoral transclival removal of anteriorly placed meningiomas at the foramen magnum, *Neurosurgery* 20(6) (1987) pp. 966-968.
- [7] M. Nakamura, M. Samii, Surgical management of a meningioma in the retrosellar region, *Acta neurochirurgica* 145(3) (2003) pp. 215-219, discussion pp. 219-220.
- [8] R. Reisch, M. Bettag, A. Perneczky, Transoral transclival removal of anteriorly placed cavernous malformations of the brainstem, *Surgical Neurology* 56(2) (2001) pp. 106-115 discussion pp. 115-106.
- [9] V. Seifert, A. Raabe, M. Zimmermann, Conservative (labyrinth-preserving) transpetrosal approach to the clivus and petroclival region--indications, complications, results and lessons learned, *Acta Neurochirurgica* 145(8) (2003) pp. 631-642 , discussion p. 642.
- [10] P. Cappabianca, L.M. Cavallo, F. Esposito, O. De Divitiis, A. Messina, E. De Divitiis, Extended endoscopic endonasal approach to the midline skull base: the evolving role of transsphenoidal surgery, *Adv Tech Stand Neurosurg* 33 (2008) pp. 151-199.
- [11] G. Zada, D.F. Kelly, P. Cohan, C. Wang, R. Swerdloff, Endonasal transsphenoidal approach for pituitary adenomas and other sellar lesions: an assessment of efficacy, safety, and patient impressions, *J Neurosurg* 98(2) (2003) pp. 350-358.
- [12] L.M. Cavallo, P. Cappabianca, A. Messina, et al., The extended endoscopic endonasal approach to the clivus and cranio-vertebral junction: anatomical study, *Childs Nerv Syst* 23(6) (2007) pp 665-671.
- [13] D. Solari, C. Chiaramonte, A. Di Somma, et al., Endoscopic anatomy of the skull base explored through the nose, *World Neurosurg* 82(6 Suppl) (2014) pp. S164-S170.
- [14] P. Cappabianca, L.M. Cavallo, Solari D, V. Stagno, F. Esposito, M. de Angelis, Endoscopic endonasal surgery for pituitary adenomas, *World Neurosurg* (2014) 82(6 Suppl) pp. S3-S11.

- [15] F. Esposito, J.R. Dusick, N. Fatemi, D.F. Kelly, Graded repair of cranial base defects and cerebrospinal fluid leaks in transsphenoidal surgery, *Neurosurgery* 60(4 Suppl 2) (2007) pp.295-303, discussion pp. 303-304.
- [16] R.L. Carrau, C.H. Snyderman, A.B. Kassam, The management of cerebrospinal fluid leaks in patients at risk for high-pressure hydrocephalus, *Laryngoscope* 115(2) (2005) pp. 205-212.
- [17] M. de Angelis, P. Cappabianca, Gutta cavat lapidem: the reconstruction of the skull base after endoscopic endonasal surgery, *World Neurosurg* 83(2) (2015) pp. 136-137.
- [18] M. Turri-Zanoni, J. Zocchi, A. Lambertoni, et al., Endoscopic Endonasal Reconstruction of Anterior Skull Base Defects: What Factors Really Affect the Outcomes? *World Neurosurg* 116 (2018) pp. e436-e443.
- [19] M.R. Patel, R.N. Shah, C.H. Snyderman, et al., Pericranial flap for endoscopic anterior skull-base reconstruction: clinical outcomes and radioanatomic analysis of preoperative planning, *Neurosurgery* 66(3) (2010) pp. 506-512, discussion p. 512.
- [20] H. Hasegawa, M. Shin, K. Kondo, N. Saito, Reconstruction of Dural Defects in Endoscopic Transnasal Approaches for Intradural Lesions Using Multilayered Fascia with a Pressure-Control Spinal Drainage System, *World Neurosurg* 114 (2018) pp. e1316-e1324.
- [21] M.R. Patel, R.J. Taylor, T.G. Hackman, et al., Beyond the nasoseptal flap: outcomes and pearls with secondary flaps in endoscopic endonasal skull base reconstruction, *Laryngoscope* 124(4) (2014) pp. 846-852.
- [22] G. Hadad, L. Bassagasteguy, R.L. Carrau, et al., A novel reconstructive technique after endoscopic expanded endonasal approaches: vascular pedicle nasoseptal flap, *Laryngoscope* 116(10) (2006) pp.1882-1886.
- [23] B.D. Thorp, S.B. Sreenath, C.S. Ebert, A.M. Zanation, Endoscopic skull base reconstruction: a review and clinical case series of 152 vascularized flaps used for surgical skull base defects in the setting of intraoperative cerebrospinal fluid leak, *Neurosurg Focus* 37(4) (2014) E4.

- [24] A. Kassam, R.L. Carrau, C.H. Snyderman, P. Gardner, A. Mintz, Evolution of reconstructive techniques following endoscopic expanded endonasal approaches, *Neurosurg Focus* 19(1): (2005) E8.
- [25] A. Conger, F. Zhao, X.Wang, et al., Evolution of the graded repair of CSF leaks and skull base defects in endonasal endoscopic tumor surgery: trends in repair failure and meningitis rates in 509 patients. *J Neurosurg* 130(3) (2018) pp. 861-875.
- [26] L.M. Cavallo, D. Solari, T. Somma, P. Cappabianca, The 3F (Fat, Flap, and Flash) Technique For Skull Base Reconstruction After Endoscopic Endonasal Suprasellar Approach, *World Neurosurg* 126 (2019) pp.439-446.
- [27] F. Bonavolontà, A. Tedesco, R. Schiano Lo Moriello, A. Tufano, Enabling wireless technologies for industry 4.0: State of the art, In: *Proc. of IEEE International Workshop on Measurement and Networking, M & N 2017, Naples, 27-29 September 2017*, pp. 1-5.
- [28] F. Bonavolontà, M. D'Arco, G. Ianniello, A. Liccardo, R. Schiano Lo Moriello, L. Ferrigno, G. Miele, On the suitability of compressive sampling for the measurement of electrical power quality, In *Proc. Of Instrumentation and Measurement Technology Conference (I2MTC), Minneapolis, 6-9 May 2013* pp. 126-131.
- [29] L. Angrisani, A. Arpaia, F. Bonavolontà, M. Conti, A. Liccardo, LoRa protocol performance assessment in critical noise conditions, in *Proc. of IEEE International Forum on Research and Technologies for Society and Industry (RTSI), Modena, Italy, 11-13 September 2017*.
- [30] A. Landi, A. Liccardo, N. Polese. Remote laboratory activities to support experimental session for undergraduate measurements courses, in *Proc. of IEEE Instrumentation and Measurement Technology Conference (IMTC), Sorrento, Italy, 24-27 April 2006*, pp. 851-856.
- [31] L. Angrisani, F. Bonavolontà, R. Schiano Lo Moriello, A. Andreone, R. Casini, G. Papari, D. Accardo, First steps towards an innovative compressive sampling based-THz imaging system for early crack detection on aerospace plates, In *Proc. of 2014 IEEE Metrology for Aerospace (MetroAeroSpace), Benevento, 29-30 May 2014*, p. 488-493.

- [32] L. Russo, A. Gloria, T. Russo, U. D'Amora, F. Taraballi, R. De Santis, L. Ambrosio, F. Nicotra, L. Cipolla, Glucosamine grafting on poly(ϵ -caprolactone): a novel glycated polyester as a substrate for tissue engineering, *RSC Advances* 3 (2013) pp. 6286-6289.
- [33] L. Russo, T. Russo, C. Battocchio, F. Taraballi, A. Gloria, U. D'Amora, R. De Santis, G. Polzonetti, F. Nicotra, L. Ambrosio, L. Cipolla, Galactose grafting on poly(ϵ -caprolactone) substrates for tissue engineering: a preliminary study, *Carbohydrate Research* 405 (2015) pp. 39-46.
- [34] R. De Santis, U. D'Amora, T. Russo, A. Ronca, A. Gloria, L. Ambrosio, 3D fibre deposition and stereolithography techniques for the design of multifunctional nanocomposite magnetic scaffolds, *J Mater Sci Mater Med* 26(10) (2015) 250.
- [35] M. Domingos, A. Gloria, J. Coelho, P. Bartolo, J. Ciurana, Three-dimensional printed bone scaffolds: The role of nano/micro-hydroxyapatite particles on the adhesion and differentiation of human mesenchymal stem cells, *Proc. Inst. Mech. Eng. H*. 231 (2017) pp. 555-564.
- [36] M. Martorelli, P. Ausiello, R. Morrone, A new method to assess the accuracy of a Cone Beam Computed Tomography scanner by using a non-contact reverse engineering technique, *Journal of Dentistry* 42 (2014) pp. 460-465.
- [37] M. Martorelli, C. Pensa, D. Speranza, Digital Photogrammetry for Documentation of Maritime Heritage, *Journal of Maritime Archaeology* 9 (2014) pp.81-93.
- [38] M. Cali, D. Speranza, M. Martorelli, Dynamic spinnaker performance through digital photogrammetry, numerical analysis and experimental tests, in: *Advances on Mechanics, Design Engineering and Manufacturing. Lecture Notes in Mechanical Engineering*. B. Eynard, V. Nigrelli, S. Oliveri, G. Peris-Fajarnes, S. Rizzuti (editors). Springer, Switzerland, 2017, ISBN 978-3-319-45781-9, pp. 585-595.
- [39] V. Pagliarulo, F. Farroni, P. Ferraro, A. Lanzotti, M. Martorelli, P. Memmolo, D. Speranza, F. Timpone, Combining ESPI with laser scanning for 3D characterization of racing tyres sections, *Optics and Lasers in Engineering* 104 (2018) pp. 71-77.

- [40] P. Ausiello, S. Ciaramella, M. Martorelli, A. Lanzotti, A. Gloria, D.C. Watts, CAD-FE modeling and analysis of class II restorations incorporating resin-composite, glass ionomer and glass ceramic materials, *Dental Materials* 33(12) (2017) pp. 1456-1465.
- [41] P. Ausiello, S. Ciaramella, M. Martorelli, A. Lanzotti, F. Zarone, D.C. Watts, A. Gloria, Mechanical behavior of endodontically restored canine teeth: Effects of ferrule, post material and shape, *Dental Materials* 33(12) (2017) pp. 1466-1472.
- [42] F. Caputo, A. De Luca, A. Greco, S. Maietta, M. Bellucci, FE simulation of a SHM system for a large radio-telescope, *International Review on Modelling and Simulations* 11(1) (2018) pp. 5-14.
- [43] A. Gloria, S. Maietta, M. Martorelli, A. Lanzotti, D.C. Watts, P. Ausiello, FE analysis of conceptual hybrid composite endodontic post designs in anterior teeth, *Dental Materials* 34(7) (2018) pp. 1063-1071.
- [44] L. Gallucci, C. Menna, L. Angrisani, D. Asprone, R. Schiano Lo Moriello, F. Bonavolontà, F. Fabbrocino, An embedded wireless sensor network with wireless power transmission capability for the structural health monitoring of reinforced concrete structures, *Sensors* 17 (2017) 2566.
- [45] M. Giordano, P. Ausiello, M. Martorelli, R. Sorrentino, Reliability of computer designed surgical guides in six implant rehabilitations with two years follow-up, *Dental Materials* 28(9) (2012) pp. e168-e177.
- [46] R. Fontanella, D. Accardo, R.S. Lo Moriello, L. Angrisani, D. De Simone, MEMS gyros temperature calibration through artificial neural networks, *Sensors and Actuators A: Physical* 279 (2018) pp. 553- 565.
- [47] L. Angrisani, F. Bonavolontà, A. Liccardo, R. Schiano Lo Moriello, L. Ferrigno, M. Laracca, G. Miele, Multi-channel Simultaneous Data Acquisition Through a Compressive Sampling-Based Approach, *Measurement* 52 (2014) pp. 156-172.
- [48] X. Xin, A. Borzacchiello, P.A. Netti, L. Ambrosio, L. Nicolais, Hyaluronic-acid-based semi-interpenetrating materials, *J Biomater Sci Polym Ed.* 15(9) (2004) pp. 1223-1236.

Chapter 4

Design strategies for the development of customized prosthetic devices with tailored properties for skull base reconstruction after extended endoscopic endonasal surgery

4.1. Introduction

The endoscopic endonasal approaches are often carried out in the case of the surgical treatment of multiple skull base pathologies. The possibility to prevent postoperative CSF leaks represents one of the major challenges as discussed in the previous chapter.

In this scenario, recent efforts have been devoted to the design and fabrication of novel and tailored prosthetic devices for reconstructive purposes.

The aim of the current research was to develop further technical solutions. Several design concepts were generated and explored.

4.2. Materials and Methods

Design process and fabrication

The surgical approach was planned as the skull based defects were designed starting the results obtained from a computed tomography (CT) scanner system. Specifically, image capture and analysis techniques were employed to generate 3D virtual models of skull base region and defects. In brief, DICOM image reconstruction and segmentation were carried out and image data sets were processed via ScanIP[®] (3.2, Simpleware Ltd., Exeter, UK). Procedure related to image segmentation and filtering were employed [1-4] and 3D tessellated models of the skull base region were created [1,2].

Moreover, blending operations were performed through cross sections and surfaces were obtained from tessellated models. Such operations were done using SolidWorks®2017 (Dassault Systemes, Paris, France) computer-aided design (CAD) system, where the ScanTo3D® add-in also allowed the management of the tessellated geometry.

Geometric models of the planned skull base defects were employed to create 3D customized models of the prosthetic device for preventing postoperative CSF leaks.

Different prosthetic models were designed consisting of a more rigid central part and flexible regions (edges) to satisfy at the same time two design criteria: mechanical/functional stability and easy introduction through nasal passages (i.e. tight cavities).

The design process involved creativity and innovation to develop technical solutions.

Four concepts of customized models were first built-up for the prosthetic device considering thin flexible edges with different thickness (Figure 4.1):

Model A (2.0 mm thick edges),

Model B (1.5 mm thick edges),

Model C (1.0 mm thick edges),

Model D (0.5 mm thick edges).

Handles for *in situ* positioning at the insertion point were designed in the back region of the stiffer central part (Figure 4.1).

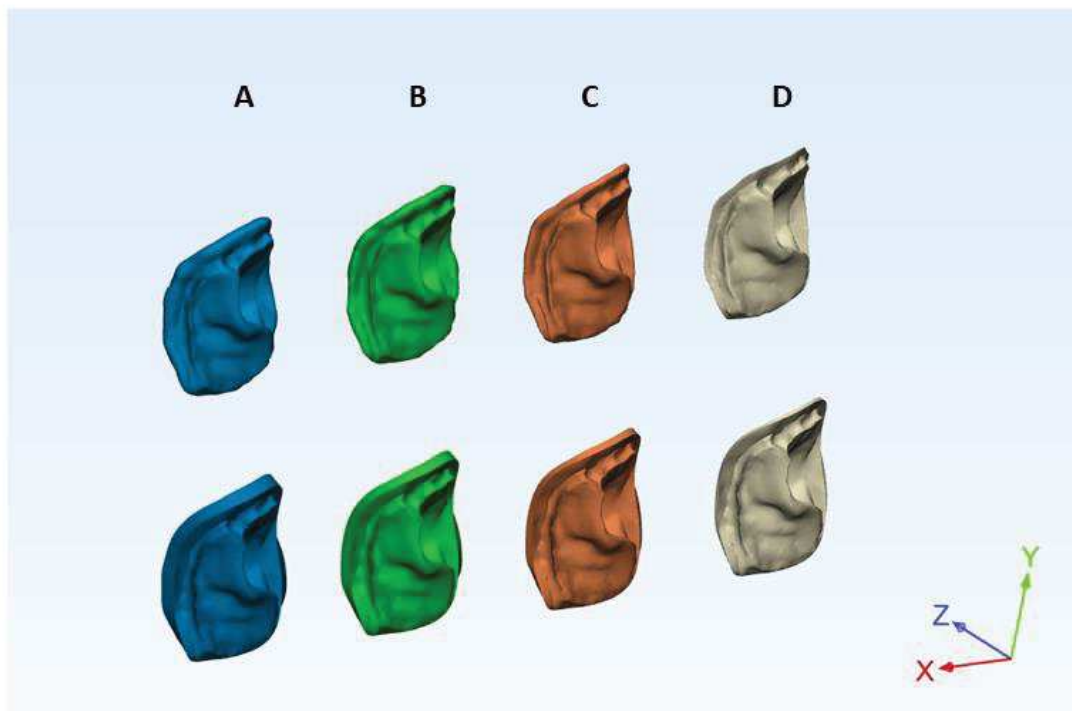


Figure 4.1. Design concepts - customized models of prosthetic devices with flexible edges of different thickness: A) 2.0 mm; B) 1.5 mm; C) 1.0 mm; D) 0.5 mm.

The IGES format was employed and the geometric models of the prosthetic devices were imported into HyperMesh[®] (HyperWorks[®] - 14.0, Altair Engineering Inc., Troy, Michigan, USA), a finite element (FE) pre-processor allowing to manage the generation of the complex models, starting with the import of a computer-aided design (CAD) geometry to exporting ready-to-run solver file.

The 3D mesh was created and each model was divided into 3D solid CTETRA elements with four grid points, suitable mesh size and refinement techniques were adopted.

A durable and flexible material certified for medical use (BioFlex, FILOALFA) [9,10], belonging to the group of thermoplastic elastomers was selected. A Young's modulus of 35 MPa and a Poisson's ratio of 0.40 were considered to model the prosthetic device.

Total number of grids (structural), elements, degrees of freedom were properly defined for each analyzed models. Finite element analysis (FEA) was carried out on the different models to provide

information on the compliance and, hence, on the flexibility under the same loading condition. Each model was located in a system of coordinates (Figure 4.2) and the lower part was constrained using “freeze” type as contact condition. A vertical load of 10 N was applied to a region on the upper surface. Static analyses were performed with a non-failure condition (Figure 4.2).

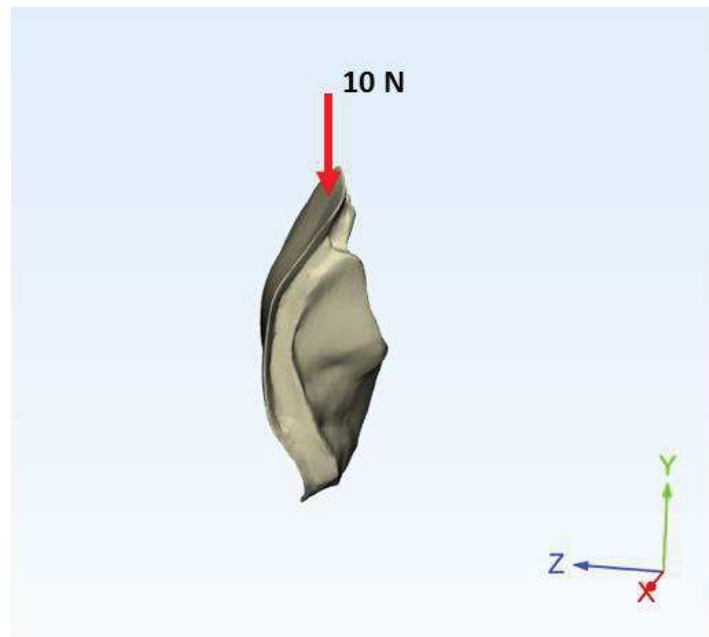


Figure 4.2. Schematic representation of the loading condition employed for FEA.

The von Mises and maximum principal stress and strain distributions were analyzed. The compliance was then evaluated for the different models. As reported in the literature [5-8], the compliance (C) is calculated using the vectors of applied loads (\mathbf{f}) and nodal displacements (\mathbf{u}) and the stiffness matrix (\mathbf{K}), as well as the strain ($\boldsymbol{\epsilon}$) and stress ($\boldsymbol{\sigma}$) vectors.

Starting from Models A to D, a further model (Model E) was finally developed considering a shell-core configuration for the central part of the device. The external shell was considered as non-design space, whereas the inner core was selected as design space, which was properly optimized from a topological point of view for the given loading condition, boundary conditions and constraints, using a material volume fraction of 0.50.

The optimized model (Model E) was finally manufactured by fused deposition modeling (FDM) using a commercially available 3D printer (Crealty3D Ender-3 PRO) and BioFlex (FILOALFA) filaments.



Figure 4.3. Images of the additively manufactured prosthetic device.

4.3. Results and Discussion

Virtual models of a skull base region with the defect as well as of the prosthetic device were created. Starting from the shape and size of the defect, the geometry of the closure device was suitably designed to be fitted in the cavity in order to prevent CSF leakage. The feasibility of the proposed technical solutions was preliminarily assessed through virtual models (Figure 4.4).

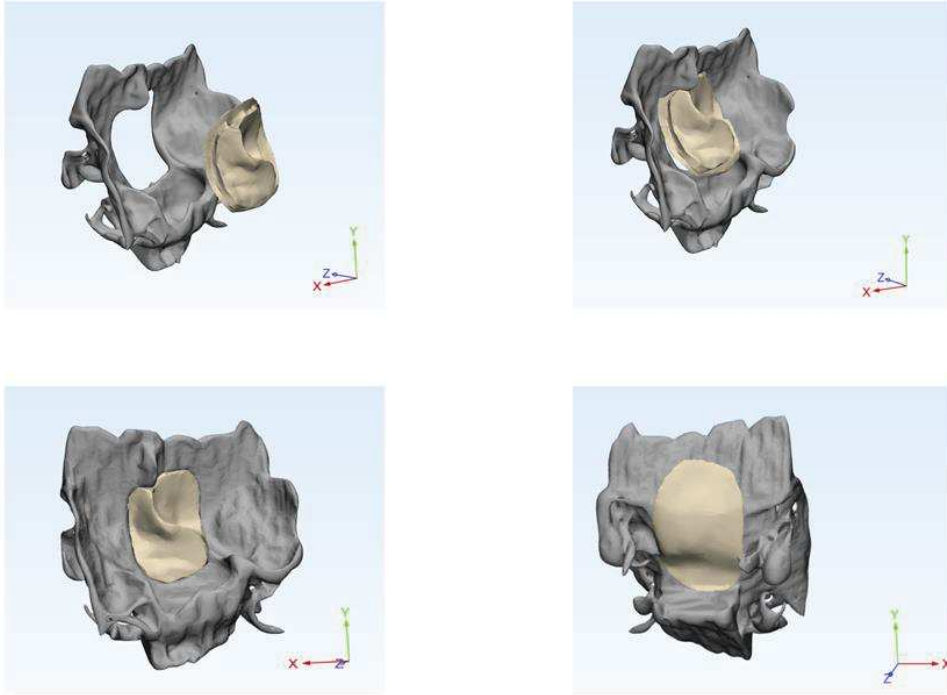


Figure 4.4. 3D model of the prosthetic device closing the skull base defect - different stages and views. Preliminary feasibility assessment of the conceived technical solutions.

FEA provided important information in terms of stress and strain distributions as well as of compliance for the different models under the same loading condition.

The von Mises stress and strain obtained from FEA are reported for all models in Figures 4.5-4.8.

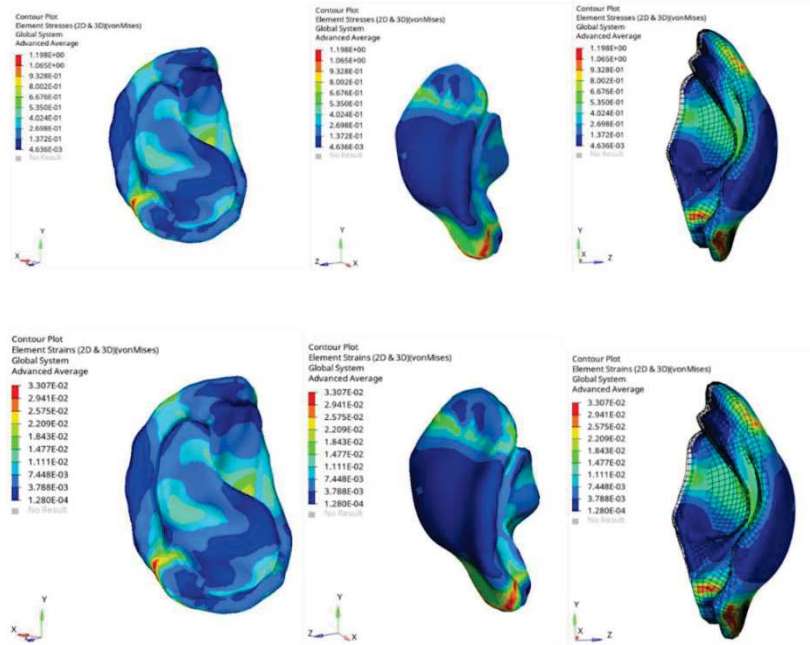


Figure 4.5. Results from FEA on model A: von Mises stress (MPa) and strain distributions. Both upper right and lower right images report the deformed and undeformed configurations as a guide for the eye to visualize the effect of the loading condition.

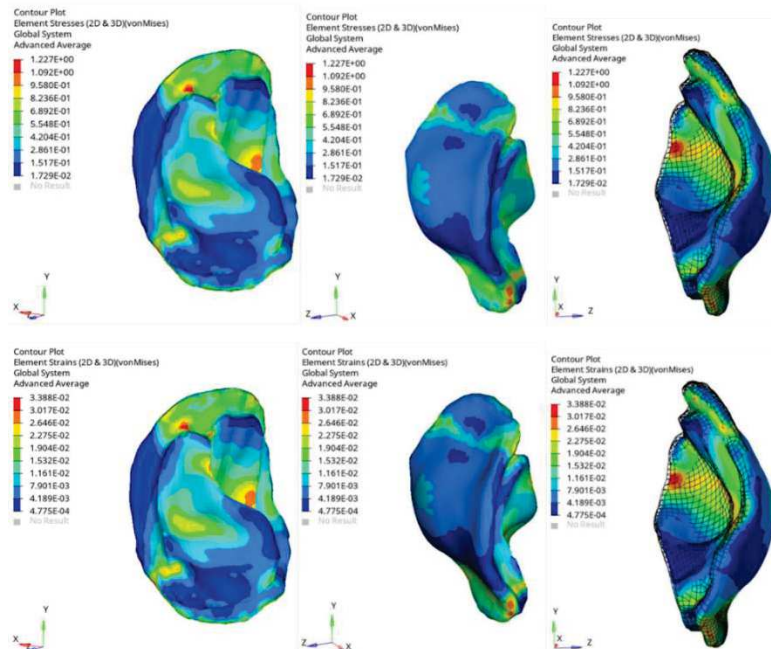


Figure 4.6. Results from FEA on model B: von Mises stress (MPa) and strain distributions. Both upper right and lower right images report the deformed and undeformed configurations as a guide for the eye to visualize the effect of the loading condition.

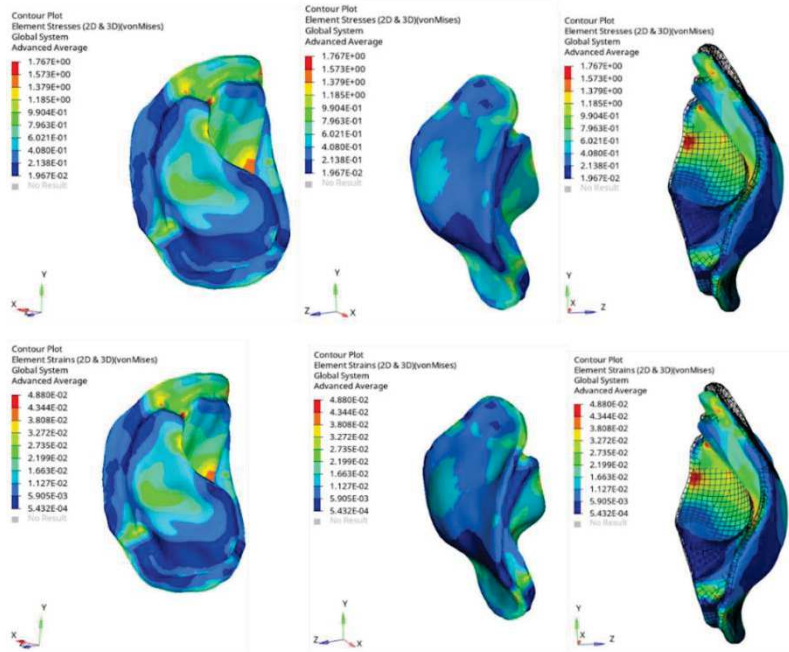


Figure 4.7. Results from FEA on model C: von Mises stress (MPa) and strain distributions. Both upper right and lower right images report the deformed and undeformed configurations as a guide for the eye to visualize the effect of the loading condition.

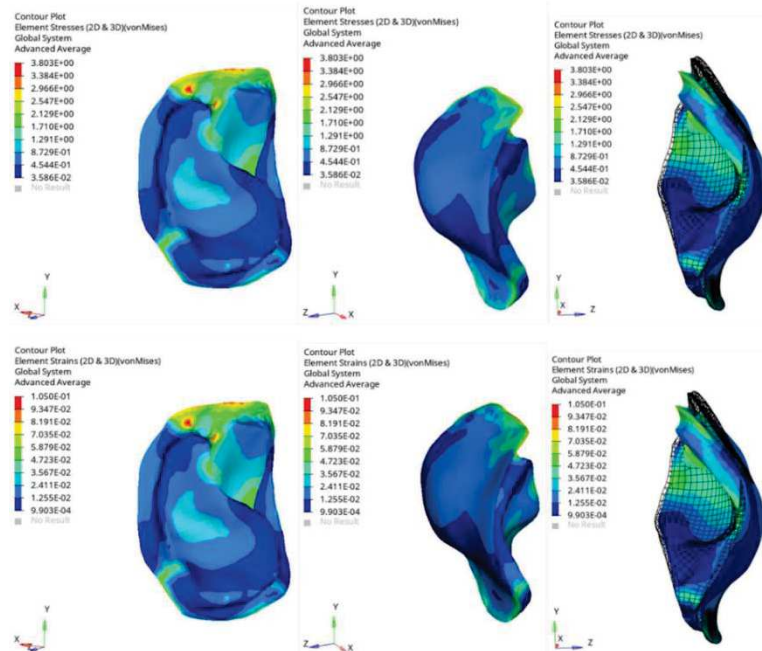


Figure 4.8. Results from FEA on model D: von Mises stress (MPa) and strain distributions. Both upper right and lower right images report the deformed and undeformed configurations as a guide for the eye to visualize the effect of the loading condition.

The obtained results evidenced that as the thickness of the flexible edges decreased from 2.0 to 0.5 mm, the values of von Mises stress and strain increased from 1.2 to 3.8 MPa and from 0.03 to 0.10, respectively. Analogously, similar trends were also found for maximum principal stress and strain distributions (Figures 4.9-4.12).

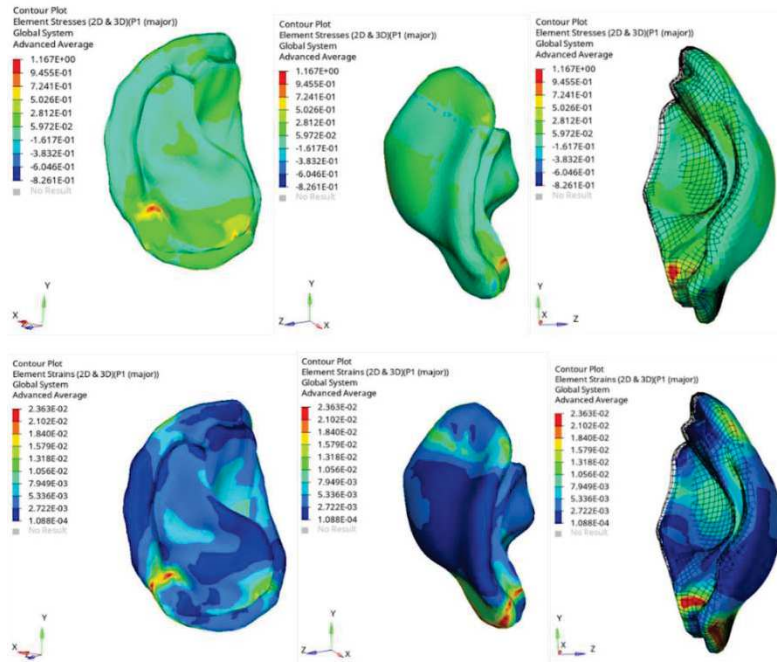


Figure 4.9. Results from FEA on model A: maximum principal stress (MPa) and strain distributions. Both upper right and lower right images report the deformed and undeformed configurations as a guide for the eye to visualize the effect of the loading condition.

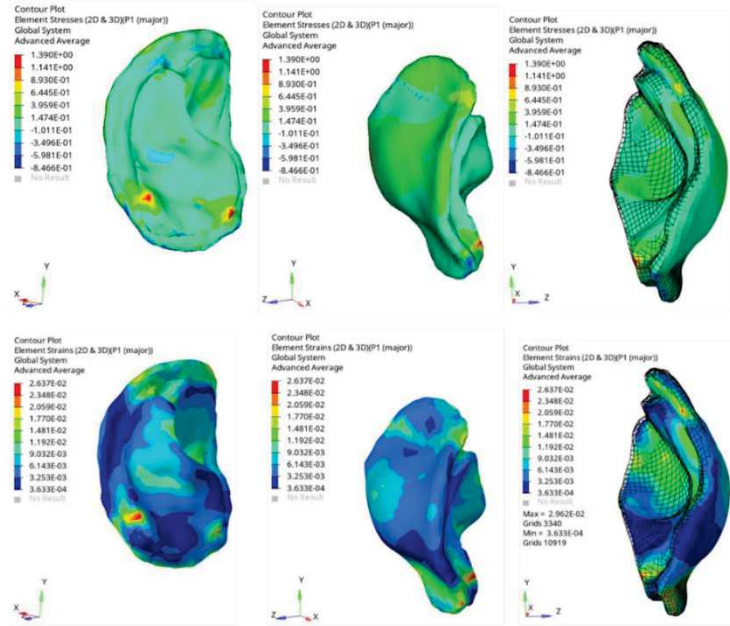


Figure 4.10. Results from FEA on model B: maximum principal stress (MPa) and strain distributions. Both upper right and lower right images report the deformed and undeformed configurations as a guide for the eye to visualize the effect of the loading condition.

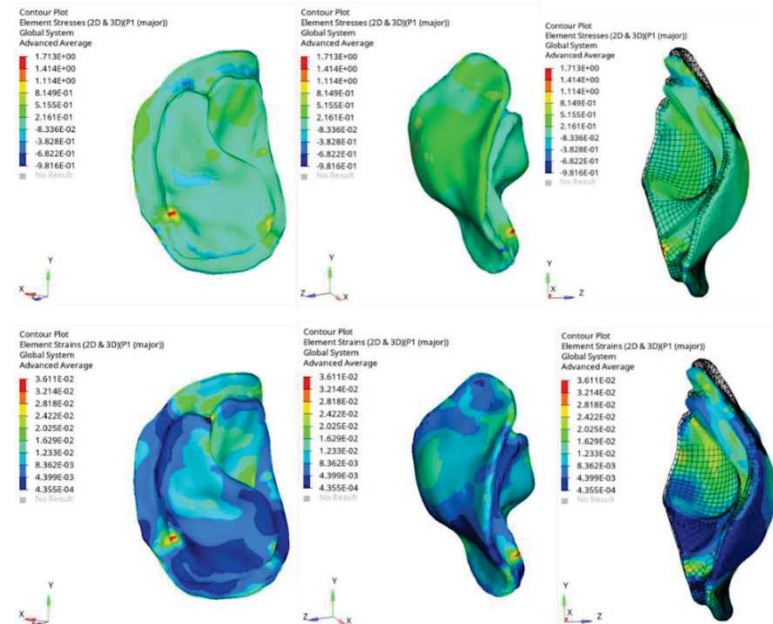


Figure 4.11. Results from FEA on model C: maximum principal stress (MPa) and strain distributions. Both upper right and lower right images report the deformed and undeformed configurations as a guide for the eye to visualize the effect of the loading condition.

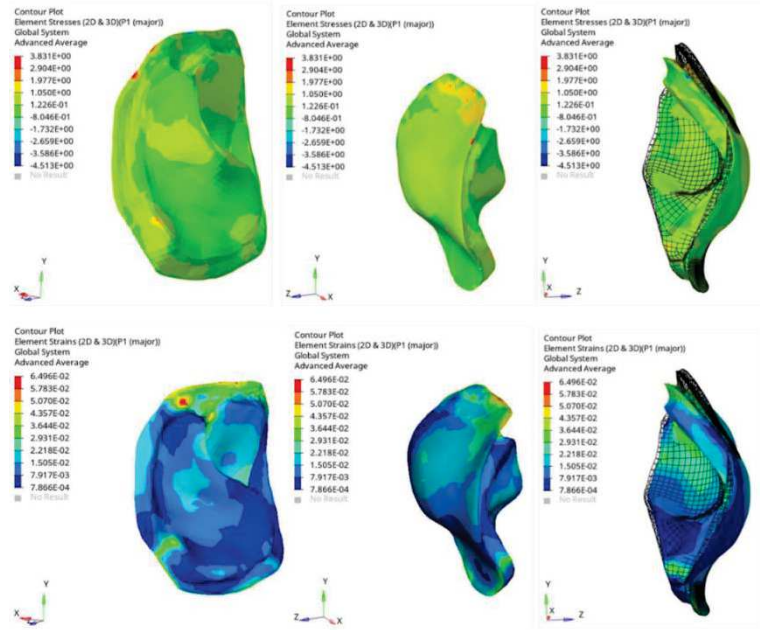


Figure 4.12. Results from FEA on model D: maximum principal stress (MPa) and strain distributions. Both upper right and lower right images report the deformed and undeformed configurations as a guide for the eye to visualize the effect of the loading condition.

Thus, the lower was the thickness of the flexible edges, the greater were the stress and strain values. Furthermore, as the thickness of the edges decreased from 2.0 to 0.5 mm, an increase of compliance values was found (i.e. 1.2 mJ - model A, 1.7 mJ - model B, 2.3 mJ – model C, 4.3 mJ model D). Anyway, it is worth noting the higher the compliance of the device, the greater the flexibility and the more easily it can be strained.

As consequence, model D was designed to possess better flexibility than the other proposed models. However, benefiting from the obtained results, design concept tools were also employed to further increase the compliance of the proposed model, while maintaining an appropriate mechanical stability.

Accordingly, starting from model D a creative solution design for a new model E involved a shell-core configuration for the central part of the device. In particular, the external shell was considered

as non-design space, whereas the inner core was selected as design space, which was properly optimized in terms of material distribution.

In this context, the compliance represents an important feature of the proposed design and was selected as the objective function to be maximized during the optimization process. A design constraint was considered placing a restriction on the problem in order to limit the values that the compliance (i.e. response function) of the device had to take and that must be satisfied for the design acceptability.

Specifically, a typical formulation of topology optimization problems was used focusing on material distribution for the design space as well as on the equivalent density of each element as a design variable. Basically, the objective was to maximize the compliance with a constraint on the material volume fraction, which was set to 0.50.

Results from FEA on the new concept device (model E) are shown in Figures 4.13 and 4.14 reporting the von Misses and maximum principal stress and strain distributions.

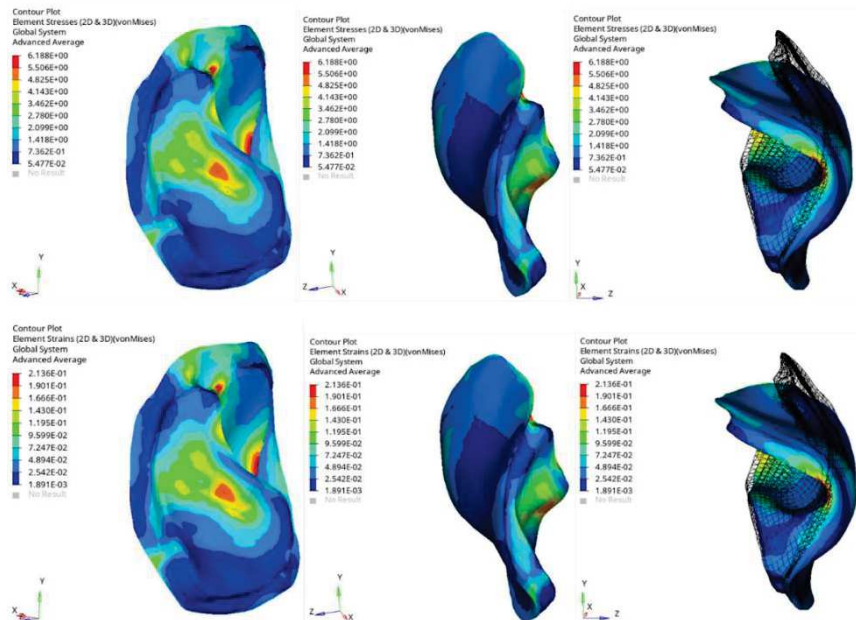


Figure 4.13. Results from FEA on the optimized model (E): von Mises stress (MPa) and strain distributions. Both upper right and lower right images report the deformed and undeformed configurations as a guide for the eye to visualize the effect of the loading condition.

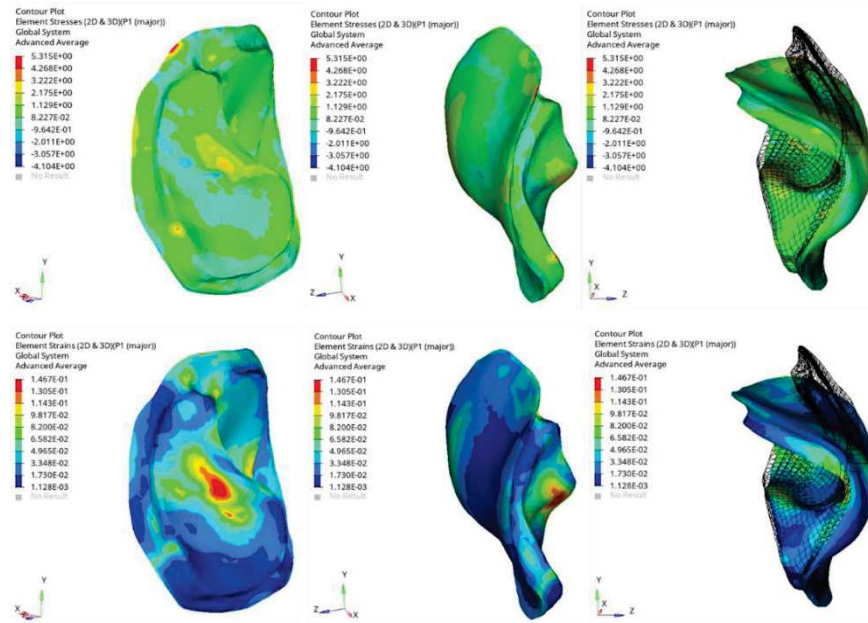


Figure 4.14. Results from FEA on the optimized model (E): maximum principal stress (MPa) and strain distributions. Both upper right and lower right images report the deformed and undeformed configurations as a guide for the eye to visualize the effect of the loading condition.

If compared to model D, greater values of von Mises stress (6.2 MPa) and strain (0.21) were achieved for model E. Similar considerations may be clearly made for the maximum principal stress and strain. In addition, the optimization led to a significant increase of compliance (14.1 mJ for model E) without altering the external shape and size of the model D as well as the edge thickness (0.5 mm), however maintaining an appropriate mechanical stability to fulfil the required function.

It is frequently reported that endoscopic endonasal approaches are increasingly performed in the case of the surgical treatment of multiple skull base pathologies. Preventing postoperative CSF leaks still represents a major challenge, especially in extended approaches.

In this context, recent efforts have been devoted to the development of advanced and tailored prosthetic devices for reconstructive purposes.

For this reason, a previous work [11] already reported a proof of concept based on 3D printing and intraoperative neuronavigation tailoring for skull base reconstruction after extended endoscopic

endonasal surgery. The authors developed such prosthetic devices based on preoperative and intraoperative CT scans. The navigation transfer allowed to obtain accurate data for tailoring the pre-printed prosthetic devices, which were also successfully implanted [11].

The functional material gradient was introduced between the rigid (core) and flexible (edge) regions using a multimaterial 3D printer and two photopolymers with different Young's modulus (VeroWhitePlus RGD835, Stratasys – approximately 1 GPa, TangoPlus FLX930, Stratasys – approximately 1 MPa) [11].

Anyway, even though many light-activated polymers and composites are employed for biomedical applications (e.g., dental restorative materials), it is worth remembering that in general many concerns still remain due to the difficulties to optimize the curing process. The performance of such materials strongly depends upon the light curing process [12,13]. The depth of cure and degree of conversion influence the mechanical properties. Thus, the use of non-optimized process conditions negatively affect the mechanical performances of the developed devices, also potentially leading to the release of toxic agents [12,13].

Unlike the previous work [11], in the current research an integrated design strategy was reported to develop customized devices for extended skull base defects using a commercially available 3D printer and a single biocompatible material (BioFlex, FILOALFA) as well as a one-step fabrication process. In particular, the combination of a widely employed additive manufacturing technique based on material injection/extrusion methods (i.e., fused deposition modeling) with reverse engineering and design optimization strategies allowed for the development of a customized prosthetic device consisting of a more rigid central part and flexible regions (edges).

Different design concepts (A-D) were first generated and explored. FEA was carried out to highlight the potential of tailoring the properties of the device, however satisfying at the same time two fundamental design criteria (i.e., mechanical/functional stability and easy introduction through nasal passages).

The optimal design solution (model E) was then achieved by means of an appropriate strategy which led to a shell-core configuration for the central part through the optimization of the core material layout within a defined design space, for a given loading condition, boundary conditions and constraints, with the aim of improving the performance of the device in terms of compliance.

4.4. Conclusions

The tailored flexibility of the model E was the result of a synergistic contribution of the edges with the optimized material arrangement for the core of the central part of the device.

In brief, starting from model D, the adopted design optimization process allowed: i) to further increase the compliance of the device improving the introduction through tight cavities (i.e., easy intranasal maneuverability), however maintaining an appropriate mechanical stability to fulfil the required function; ii) to reduce the amount of used material and the fabrication time.

4.5. References

- [1] Ausiello P, Franciosa P, Martorelli M, Watts DC. Mechanical behavior of post-restored upper canine teeth: a 3D FE analysis. *Dent Mater* 2011;27:1285–94.
- [2] Ausiello P, Ciaramella S, Martorelli M, Lanzotti A, Zarone F, Watts DC, et al. Mechanical behavior of endodontically restored canine teeth: effects of ferrule, post material and shape. *Dent Mater* 2017;33(12):1466–72.
- [3] Rodrigues FP, Li J, Silikas N, Ballester RY, Watts DC. Sequential software processing of micro-XCT dental-images for 3D-FE analysis. *Dent Mater* 2009;25(6):47–55.
- [4] Gloria A, Maietta S, Martorelli M, Lanzotti A, Watts DC, Ausiello P. FE analysis of conceptual hybrid composite endodontic post designs in anterior teeth. *Dent Mater* 2018; 34: 1063–1071.
- [5] Bendsoe M P, Sigmund O. *Topology Optimization: Theory, Methods and Applications*, Springer-Verlag, Berlin, Germany, 2003

- [6] Reist TA, Andrysek J, Cleghorn WL. Topology Optimization of an Injection Moldable Prosthetic Knee Joint, *Computer-Aided Design and Applications* 2010, 7(2), 247-256.
- [7] Zhang W, Yang J, Xu Y, Gao T. Topology optimization of thermoelastic structures: mean compliance minimization or elastic strain energy minimization. *Struct Multidisc Optim* 2014, 49, 417–429.
- [8] Panesar A, Abdi M, Hickman D, et al. Strategies for functionally graded lattice structures derived using topology optimisation for additive manufacturing. *Addit Manuf* 2018; 19: 81–94.
- [9] Haryńska, A.; Gubanska, I.; Kucinska-Lipka, J.; Janik, H. Fabrication and Characterization of Flexible Medical-Grade TPU Filament for Fused Deposition Modeling 3DP Technology. *Polymers* 2018, 10, 1304.
- [10] Filoalfa–Bioflex Filament. Available online: <https://www.filoalfa3d.com/en/filaments-175mm/296-bioflexpla-shore-27d-white-o-175-mm-8050327032385.html> (accessed on November 24, 2020).
- [11] Essayed WI, Unadkat P, Hosny A, Frisken S, Rassi MS, Mukundan S, Weaver JC, Al-Mefty O, Golby AJ, Dunn IF. 3D printing and intraoperative neuronavigation tailoring for skull base reconstruction after extended endoscopic endonasal surgery: proof of concept. *J Neurosurg.* 2018;130(1):248-255.
- [12] De Santis R, Gloria A, Prisco D, Amendola E, Puppulin L, Pezzotti G, Rengo S, Ambrosio L, Nicolais L. Fast curing of restorative materials through the soft light energy release. *Dent Mater* 2010;26(9):891-900.
- [13] Gloria A, Martorelli M, Gerbino S, Tagliaferri F, Kräusel V, Lanzotti A. Functional analyses to assess the effect of the curing process on the properties of light activated composites. *Production Engineering*, 2019, 13(2), 239-246.

Chapter 5

Design of solid-lattice hybrid structures with optimized properties for biomedical applications

5.1 Introduction

Titanium alloys (e.g., Ti6Al4V) have been often considered to develop orthopedic and dental implants, benefiting from their excellent biocompatibility, good corrosion resistance, and high strength [1-4].

As an example, total hip replacement generally involves the use of cementless femoral stems, which are proximally inserted in the medullary canal of the femur. The stem must be firmly attached to the bone in order to ensure the physiological stress transfer to the bone during daily activities. In this scenario, Ti6Al4V (elastic modulus of 114 GPa) has been frequently selected to fabricate cementless stems [1–4], also causing several complications. In particular, stress shielding effects, bone atrophy and implant loosening are related to devices fabricated using a material with an elastic modulus which is much higher than that of the cortical bone (i.e., 10–30 GPa) [1,4,5].

Finite element (FE) models may be successfully used to study the biomechanical behavior of natural tissues and implants [6].

The great need of increasing and to optimising the implant life, as a consequence of population ageing, diffusion of extreme sports, revision surgery and costs of implant replacement, has led to the development of long-lasting implants, also using materials with mechanical properties which are close to those of human tissues [1-4].

Composite and porous implants were also designed with the aim to overcome the above reported drawbacks [7–11]. The use of novel materials and designs through the integration of porous

structures, several geometrical profiles and functionally graded materials allowed for the development of strategies to reduce the implant stiffness [12-14].

Contextually, 3D porous devices with controlled geometry and architecture were designed, also trying to promote the possibility of tissue ingrowth, which should stabilize the implant [1]. In recent years, some studies have also reported novel designs of porous and semi-porous stems for reducing the stiffness of the stems [6,15,16,17]. It has been frequently reported how the use of low stiffness porous stems provides lower stress shielding and bone resorption in comparison to the dense stems [18].

Several cellular structures were analyzed to obtain a wide range of mechanical properties. Concerning torsional, bending and compression, excellent mechanical performances were found for diamond and body-centered-cubic (BCC) [6,14,19]. For this reason, the diamond and BCC types were further employed to generate porous and semi-porous femoral stems, which were then properly analyzed.

Several investigations have reported that porous cellular microstructures possess a fatigue strength which is a fraction to that of the effective yield strength (about $0.3\sigma_{ys}$) of the cellular microstructure [13–19].

A recent study on a novel design, analysis and 3D printing of Ti6Al4V alloy bio-inspired porous femoral stem was performed using a wide range of porosity for the inner core [6].

Accordingly, the aim of the current study was to provide further insight into the design of solid-lattice hybrid structures with optimized properties for biomedical applications. A cementless femoral stem was considered as a case study.

5.2. Materials and Methods

SolidWorks®2017 (Dassault Systemes, Paris, France) computer-aided design (CAD) system was used to create 3D models of a hip stem. A total hip replacement using an alumina head a Ti6Al4V stem was considered. A Young's modulus of 114 GPa and a Poisson's ratio of 0.33 were used for Ti6Al4V alloy [1].

As reported in a previous work, the bodyweight was assumed as 800 N and a wide range of physiological loads was considered [6].

3D models of the femur with implant were also designed. With regard to the femur bone, cortical bone and cancellous bone were considered. A Young's modulus of 17 GPa and a Poisson's ratio of 0.30 were used for cortical bone, whereas values of 0.52 GPa and 0.29 were considered for cancellous bone [20].

The entire model of the femur with the implant was imported into HyperMesh® (HyperWorks®, Altair Engineering Inc., Troy, MI, USA). A 3D mesh was suitably generated, adequate mesh size and mesh refinement techniques were employed. Finite element analysis (FEA) was performed on the models. The von Mises stress distributions were evaluated in the different component of the model. The stem compliance was evaluated for the starting model. As reported in the literature, the compliance (C) is evaluated using the vectors of applied loads (\mathbf{f}) and nodal displacements (\mathbf{u}) and the stiffness matrix (\mathbf{K}), as well as the strain ($\boldsymbol{\epsilon}$) and stress ($\boldsymbol{\sigma}$) vectors.

The starting model was properly optimized from a topological point of view for the given boundary conditions, constraints and loading condition, focusing on the compliance and a material mass fraction of 0.40 and 0.70.

An integrated approach involving classical and lattice topology optimization was used to generate different technical solutions.

A specific lattice type was individuated consisting of beams with a fixed radius to length ratio, constant radius (i.e., 0.1 mm) or variable radius and tapered formulation with circular cross sections (i.e., two different radii at the nodes, with values spanning in a range from 0.02 to 0.2 mm).

The topological optimization problems were solved using a density method known as the solid isotropic material with penalization (SIMP).

A preliminary (classical) topology optimization was integrated with lattice topology optimization. With regard to the lattice topology optimization, the penalty factor (p) was also set at 1.0, 1.25 and 1.8, also exploring high, medium and low values of porosity.

5.3. Results and Discussion

The increasing applications of additive manufacturing technologies in industrial production have currently led to product reimagination from a new standpoint.

Additive manufacturing allows to create complex shapes and to enhance the performance of critical components in different fields, spanning from aerospace and automotive to biomedical applications. In general, the performances of the as-built parts can be an obstacle in terms of satisfaction of the parts' functional requirements. Concerning the manufacturing process, the relationship among the process parameters, microstructure and mechanical properties is also crucial in different areas and involves innovative and traditional fabrication techniques [1,2,21,22].

In this context, selective laser melting is widely analyzed to develop metal components and lattice structures as functional lightweight devices with tailored and improved properties [1]. Ti6Al4V lattice components were manufactured by selective laser melting and then analyzed in terms of compressive properties, surface roughness, microhardness, and dimensional accuracy [5]. A further theoretical-experimental analysis was also performed on selective laser melted Ti6Al4V lattice structures [1].

In general, the design cycle starts from a drawing (i.e., a sketch to report a concept) and ends with a manufacturing drawing. Thus, one of the great challenges is how to translate the initial drawing into a manufacturable design. Many trade-offs are involved in a typical design cycle (e.g., appearance versus function, cost versus easy manufacturability). However, every trade-off clearly modifies the design.

Over the past few years, many efforts have been devoted to develop strategies for finding the design which is best suited to the requirements (i.e., “optimum” design)

Simulation-driven design tools have an important part in achieving this with design optimization subject to the capabilities of additive manufacturing technologies. Simulation-driven design is related to the design strategy which relies on simulation approaches to guide the designer towards the conceptualization phase. In this phase, better and innovative solutions are proposed, instead of a mere verification of an already existing concept. The process leads to fewer and sophisticated prototypes

as well as to quality improvement together with time and cost reduction, enhancing the product development efficiency. Consequently, the number of fabricated prototypes for physical testing can also be reduced.

Topology optimization may be clearly considered as a tool to implement this process, providing functional parts and devices, which may most efficiently be fabricated using additive manufacturing techniques. In particular, topology optimization represents a method which is able to optimize the material layout within a defined design space, for a given set of loads, constraints and boundary conditions, with the aim of improving the performance of the device.

In particular, a typical formulation of topology optimization problems was considered with a special focus on material distribution for the design space and on the equivalent density of each element as a design variable. In the classical topology optimization, the elements with high density are replaced by full dense matter, whereas the elements with low density are replaced by void. The mid-density elements may be interpreted as matter or void and the aim should be to limit their amount. Differently from a classical topology optimization approach, in the lattice topology optimization the elements with intermediate density are replaced by lattice structure.

Accordingly, in the current study a further insight into the design and analysis of solid-lattice hybrid structures was reported for biomedical applications. A cementless femoral stem was selected as a case study.

As an example, at a fixed loading condition (i.e., contact forces on the hip joint as 250-300% of the bodyweight) the results obtained from a preliminary topology optimization (mass fraction of 0.40 and 0.70) for the analyzed femoral stem is reported in Figure 5.1, in terms of contour plot of element densities.

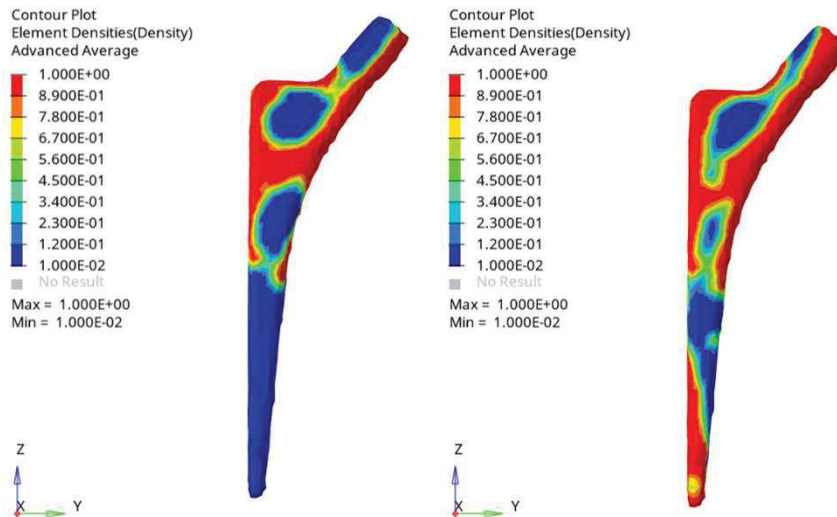


Figure 5.1. Preliminary topology optimization (mass fraction of 0.40-left and 0.70-right): contour plot of element densities.

In terms of element densities, values closest to 1 are related to important elements from a structural point of view, whereas small density elements may be considered not structurally relevant.

In order to avoid a reduction of the number of low density elements, which does not generally preserve the integrity of the external shape of the stem, the classical topology optimization was integrated with a further lattice topology optimization process.

Starting from the results in terms of element densities (Figure 5.1), a lattice topology with specific parameters was defined. The beams represent the elements giving stiffness to the structure, the nodes are the locations where the beams are jointed.

Specifically, a defined lattice type with a tapered beam formulation was selected and the penalty factor (p) was set to 1.0, 1.25 and 1.8 (Figures 5.2 and 5.3).

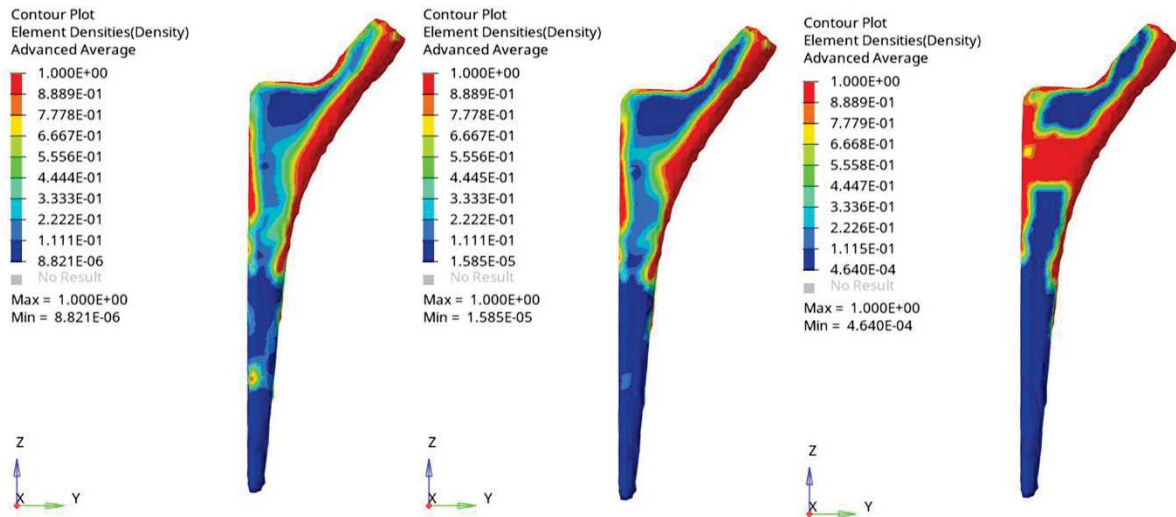


Figure 5.2. Lattice topology optimization process (mass fraction of 0.40): contour plot of element densities for $p=1.0$ (left), $p=1.25$ (center) and $p=1.8$ (right).

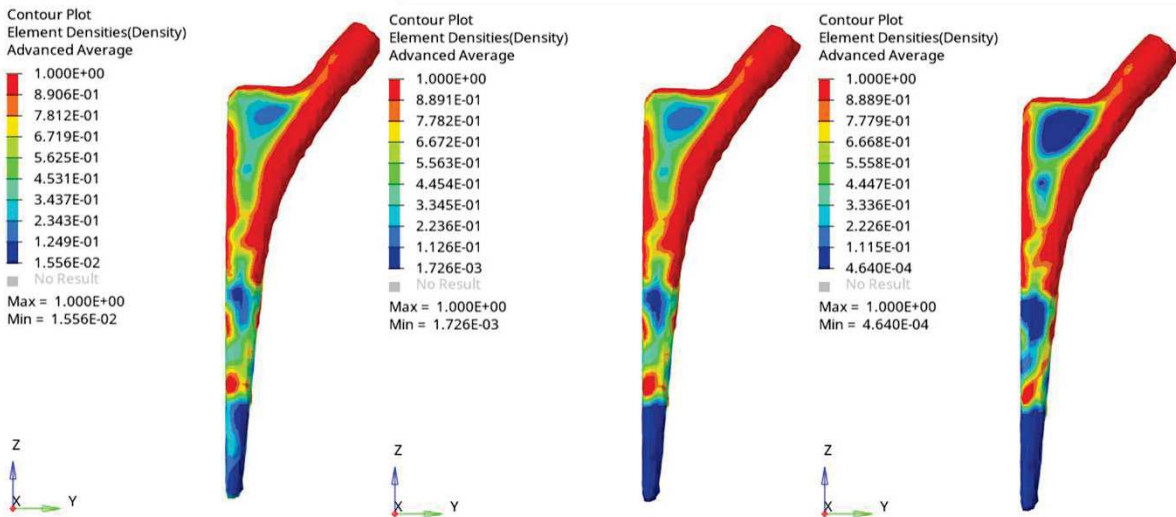


Figure 5.3. Lattice topology optimization process (mass fraction of 0.70): contour plot of element densities for $p=1.0$ (left), $p=1.25$ (center) and $p=1.8$ (right).

The results from the further lattice topology optimization led to different technical solutions (Figures 5.4 and 5.5).

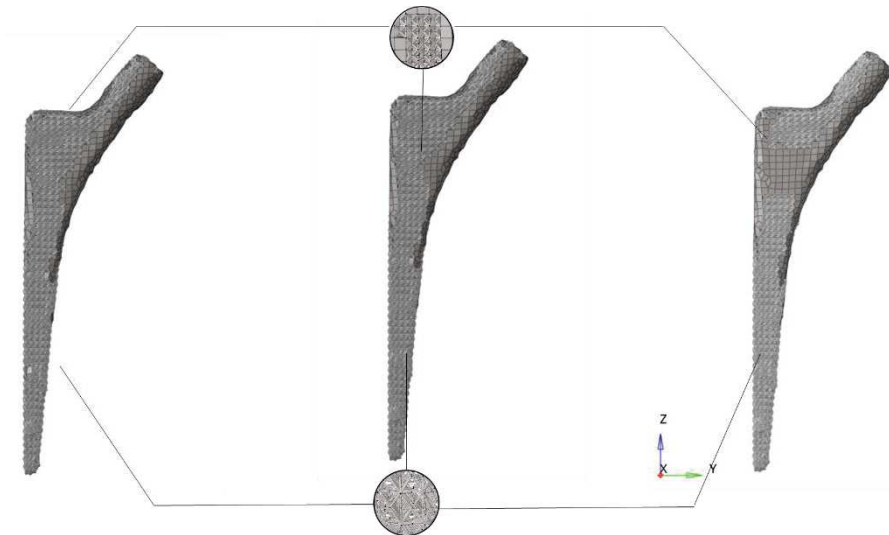


Figure 5.4. Lattice topology optimization (mass fraction of 0.40): example of the generated solid-lattice hybrid structure for $p=1.0$ (left), $p=1.25$ (center) and $p=1.8$ (right).

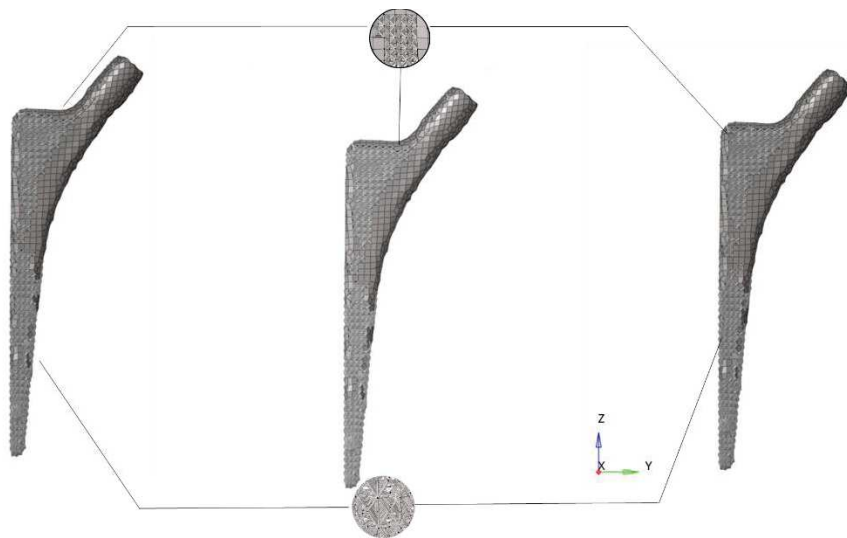


Figure 5.5. Lattice topology optimization (mass fraction of 0.70): example of the generated solid-lattice hybrid structure for $p=1.0$ (left), $p=1.25$ (center) and $p=1.8$ (right).

Even though the mass fraction was fixed (0.40 and 0.70), the solutions obtained for the three cases ($p=1.0, 1.25, 1.8$) provided some differences in terms of material distribution/layout within the design space.

Differently from the above reported case, when the radius of beam of the lattice was constant and equal to 0.1 mm, at a fixed value of the radius to length ratio, no differences were found in terms of material distribution/layout and compliance value at varying values of the penalty factor (1.0, 1.25, 1.8) (Figures 5.6).

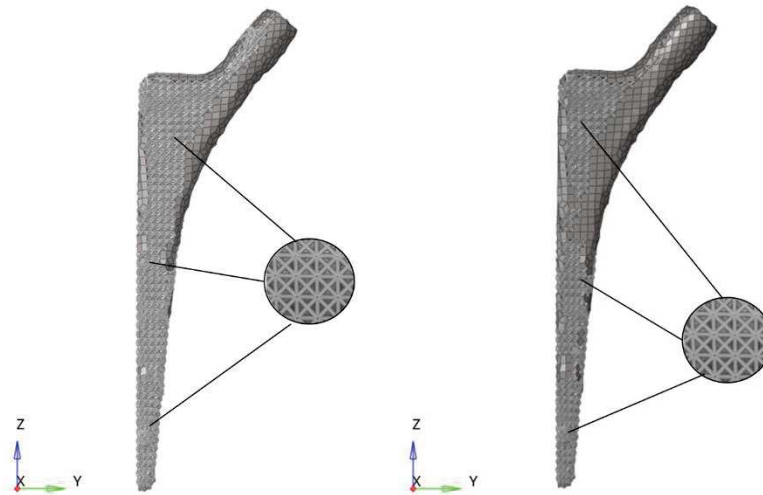


Figure 5.6. Lattice topology optimization (mass fraction of 0.40-left and 0.70-right): an example of the generated solid-lattice hybrid structure in the case of a constant beam radius (0.1 mm) and a fixed radius to length ratio.

However, with regard to the FE re-analysis, considering the von Mises stress distributions in the case of mass fraction of 0.70, the solid-lattice hybrid structures generated using the tapered beam formulation generally showed maximum values (e.g., 671.3 and 71.8 MPa) in the lattice part, which were higher than those obtained using a constant radius (i.e., 0.1 mm) and a fixed radius to length ratio for the beam. Specifically, in such latter case maximum stress values of 100.4 MPa and 45.8 MPa were found in the solid and lattice part, respectively.

On the other hand, in the case of topology optimization where the constraint on mass fraction was set to 0.40, in the lattice part of the hybrid structure the tapered beam formulation led to stress values which were much more higher than those achieved for the corresponding case at a mass fraction of

0.70. However, the generated solid-lattice hybrid structures using a constant radius of 0.1 mm and a fixed radius to length ratio for the beam showed a maximum stress value of 131.0 MPa for the solid part, whereas 280.0 MPa was achieved in the lattice part.

5.4. Conclusions

The current research provided a further investigation toward the re-design of device for biomedical applications. Briefly, a design strategy of cementless femoral stems with optimized properties was reported. Classical and lattice topology optimization were properly explored and integrated, with some focus on the step related to a lattice size optimization, trying to determine the effect of the “formulation” of each beam forming the lattice structure. At a fixed mass fraction (0.70 and 0.40), a constant radius and a fixed radius to length for the beam, variable radius and tapered formulation with circular cross sections were also explored at varying values of the penalty factor.

Anyway, even if many cases were theoretically explored, only few examples were reported in the current investigation with the aim to focus on a strategy for the development of lightweight devices with optimized properties. The same methodology may clearly revised and in many cases extended taking into account the manufacturability constraints according to the selected technology.

In this scenario, design for manufacturability (often known as design for manufacturing), which represents the general engineering practice of designing devices in a way which are easy to manufacture, will be properly considered.

Even though this concept exists in the different engineering disciplines, its implementation clearly differs depending upon the selected manufacturing technology. Several formulations of the design problem may be possible and should be introduced in the different features of the fabrication process. Based on the objectives of the problem, the design formulation may consist of a single problem or a sequential problem according to the selected manufacturing process. In general, due to the problem complexity, further solution approaches may be also considered.

The lattice type with its geometrical features and cell parameters could be “in conflict” with the selected manufacturing technology (e.g., selective laser melting, electron beam melting), as restrictions could exist in terms of both the minimum size of a cell in a lattice structure and the size of the device. The designer should solve the given problems creating feasible solutions rather than exploring novel perspectives on the analyzed problems. For this reason, strategies have to be adopted in order to redefine the problem exploration space for the design innovation. Thus, among the technical solutions which are best suited to the requirements, the “optimum” design should be found taking into consideration the manufacturing constraints due to the adopted technology.

The current research may be also considered as the first step of a future complex study, also aiming at the strict correlation between the stress shielding in the femur and the several solid-lattice hybrid structures which may be generated and explored, in order to provide re-design guidelines.

5.5. References

- [1] Maietta, S., Gloria, A., Improta, G., Richetta, M., De Santis, R., Martorelli, M.: A Further Analysis on Ti6Al4V Lattice Structures Manufactured by Selective Laser Melting. *Journal of Healthcare Engineering* 2019, 3212594 (2019).
- [2] Zhu, M., Xu, G., Zhou, M., Yuan, Q., Tian, J., Hu, H.: Effects of tempering on the microstructure and properties of a high-strength bainite rail steel with good toughness. *Metals* 8(7), 484(2018).
- [3] Campanelli, S., Contuzzi, N., Ludovico, A., Caiazzo, F., Cardaropoli, F., Sergi, V.: Manufacturing and characterization of Ti6Al4V lattice components manufactured by selective laser melting. *Materials* 7(6), 4803–4822 (2014).
- [4] Bandyopadhyay, A., Espana, F., Balla, V. K., Bose, S., Ohgami, Y., Davies, N. M.: Influence of porosity on mechanical properties and in vivo response of Ti6Al4V implants. *Acta Biomaterialia* 6(4), 1640–1648 (2010).
- [5] Spoerke, E. D., Murray, N. G., Brinson, L. C., Li, H., Dunand, D. C., Stupp, S. I.: A bioactive titanium foam scaffold for bone repair. *Acta Biomaterialia* 1(5), 523–533 (2005).

- [6] Mehboob, H., Mehboob, A., Chang, S.-H., Ramesh, S., Sharuzi, W., Harun, W., Kadirgama, K.: A novel design, analysis and 3D printing of Ti-6Al-4V alloy bio-inspired porous femoral stem. *Journal of Materials Science: Materials in Medicine* 31(9), (2020).
- [7] Mehboob, H., Chang, S.-H.: Application of composites to orthopedic prostheses for effective bone healing. A review. *Compos Struct* 118, 328–341(2014).
- [8] Sridhar, I., Adie, P.P., Ghista, D.N. Optimal design of customised hip prosthesis using fiber reinforced polymer composites. *Mater Des* 31(27), 67–75. (2010).
- [9] Rezaei, F., Hassani, K., Solhjoei, N., Karimi, A.: Carbon/PEEK composite materials as an alternative for stainless steel/titanium hip prosthesis: a finite element study. *Australas Phys Eng Sci Med* 38(5), 69–80. (2015).
- [10] Oshkour, A.A., Abu Osman, N.A., Yau, Y.H., Tarlochan, F., Abas, W.A.: Design of new generation femoral prostheses using functionally graded materials: a finite element analysis. *Proc Inst Mech Eng H* 227, 3–17 (2013).
- [11] Ramos, A., Completo, A., Relvas, C., Simoes, J.A.: Design process of a novel cemented hip femoral stem concept. *Mater Des.* 33, 313–321.(2012).
- [12] Limmahakhun, S., Oloyede, A., Sithiseripratip, K., Xiao, Y., Yan, C.: 3D-printed cellular structures for bone biomimetic implants. *Addit Manuf.* 15, 93–101 (2017).
- [13] Kadirgama, K., Harun, W.S.W., Tarlochan, F., Samykano, M., Ramasamy, D., Azir, M.Z., et al.: Statistical and optimize of lattice structures with selective laser melting (SLM) of Ti6Al4V material. *Int J Adv Manuf Technol* 97, 495–510. (2018).
- [14] Mehboob, H., Tarlochan, F., Mehboob, A., Chang, S.H. Finite element modelling and characterization of 3D cellular microstructures for the design of a cementless biomimetic porous hip stem. *Mater Des.* 149, 101–12, (2018).
- [15] Gonzalez, F.J.Q., Nuno, N.: Finite element modelling approaches for well-ordered porous metallic materials for orthopaedic applications: cost effectiveness and geometrical considerations. *Comput Methods Biomech Biomed Eng.* 19, 845–85, (2016).

- [16] Kim, C-H., Lee, S.J., Aditya, K., Kim, H.Y., Yoon, K.S., Yoon, P.W.: Incidence of a stem sitting proud of a proximally coated cementless tapered wedge stem. *J Orthop Transl* 19, 118–125 (2019).
- [17] Dong, G., Tang, Y., Li, D., Zhao, Y.F.: Design and optimization of solid lattice hybrid structures fabricated by additive manufacturing, *Additive Manufacturing* 33, 101116 (2020).
- [18] Arabnejad, S., Johnston, B., Tanzer, M., Pasini, D.: Fully porous 3D printed titanium femoral stem to reduce stress-shielding following total hip arthroplasty. *J Orthop Res* 35, 1774–83 (2017).
- [19] Wang, L., Kang, J.F., Sun, C.N., Li, D.C., Cao, Y., Jin, Z.M.: Mapping porous microstructures to yield desired mechanical properties for application in 3D printed bone scaffolds and orthopaedic implants. *Mater Des.* 8, 133-62 (2017).
- [20] Chethan, K. N., Shyamasunder Bhat, N., Zuber, M., Satish Shenoy, B.: Finite Element Analysis of Different Hip Implant Designs along with Femur under Static Loading Conditions. *J Biomed Phys Eng* 9(5), 507-516 (2019).
- [21] Fiorese, E., Bonollo, F., Battaglia, E.: A tool for predicting the effect of the plunger motion profile on the static properties of aluminium high pressure die cast components. *Metals* 8(10), 798 (2018).
- [22] Jeon, G., Kim, K., Moon, J.-H., Lee, C., Kim, W.J., Kim, S.: Effect of Al 6061 alloy compositions on mechanical properties of the automotive steering knuckle made by novel casting process. *Metals* 8(10), 857 (2018).



UNIONE EUROPEA
Fondo Sociale Europeo



*Ministero dell'Università
e della Ricerca*



Dottorando	Ida Papallo
Tutor	Giovanni Improta
Coordinatore	Alberto Cuocolo
Corso di Dottorato	Scienze Biomorfologiche e Chirurgiche
Ciclo	XXXIII
Codice borsa e n.	DOT1318209-BORSA3
CUP	E62G17000000006
Titolo Progetto	METODOLOGIE E TECNOLOGIE AVANZATE A SUPPORTO DELLE SCIENZE BIOMEDICHE

La borsa di dottorato è stata cofinanziata con risorse del
Programma Operativo Nazionale Ricerca e Innovazione 2014-2020 (CCI 2014IT16M2OP005), Fondo
Sociale Europeo, Azione I.1 “Dottorati Innovativi con caratterizzazione Industriale”